

Thermal transport in strongly correlated electron systems

Dissertation

zur Erlangung des akademischen Grades

Doctor rerum naturalium

(Dr. rer. nat.)

vorgelegt

der Fakultät Mathematik und Naturwissenschaften
der Technischen Universität Dresden

von

Adriana Mercedes Sánchez Lotero

geboren am 26. August 1971 in Armenia, Kolumbien

MAX-PLANCK-INSTITUT FÜR CHEMISCHE PHYSIK FESTER STOFFE
DRESDEN, 2005

Gutachter:

Prof. Dr. Frank Steglich

Prof. Dr. Joachim Wosnitza

Dr. Andre Strydom

Tag der mündlichen Prüfung: 08. Juli 2005

Contents

| | |
|--------------------------------------------------------------|-----------|
| Abstract | i |
| 1 Introduction | 1 |
| 2 Experimental Methods | 5 |
| 2.1 Definitions | 5 |
| 2.2 Experimental set-up | 7 |
| 2.2.1 Sample holder | 7 |
| 2.2.2 Dilution refrigerator | 7 |
| 2.2.3 AC Transport Option | 9 |
| 2.3 Measurement and data analysis | 10 |
| 3 Theoretical concepts | 17 |
| 3.1 Thermal Transport | 17 |
| 3.1.1 Thermopower | 18 |
| 3.1.2 Thermal conductivity | 19 |
| 3.2 Kondo insulators | 25 |
| 3.3 Fermi-Liquid State | 26 |
| 3.4 Heavy-fermion metal | 27 |
| 3.5 Non-Fermi-liquid behavior | 29 |
| 3.5.1 Quantum critical point (QCP) theories | 29 |
| 3.5.2 The single-impurity multichannel Kondo model | 32 |
| 4 U₂Ru₂Sn | 35 |
| 4.1 Introduction | 35 |
| 4.2 Physical properties | 38 |

| | | |
|----------|-----------------------------------------------------------------------------------------------|-----------|
| 4.3 | Results and discussion | 42 |
| 4.3.1 | Thermopower | 42 |
| 4.3.2 | Thermal conductivity | 44 |
| 4.4 | Outlook | 47 |
| 5 | $\text{Yb}_4(\text{As}_{0.7}\text{P}_{0.3})_3$ | 49 |
| 5.1 | Introduction | 49 |
| 5.2 | Physical properties | 51 |
| 5.2.1 | Physical properties at $B = 0$ | 51 |
| 5.2.2 | Physical properties under magnetic field | 57 |
| 5.2.3 | Thermal conductivity of Yb_4As_3 | 58 |
| 5.3 | Results and analysis | 59 |
| 5.4 | Outlook | 63 |
| 6 | $\text{YbRh}_2(\text{Si}_{1-x}\text{Ge}_x)_2$ with $x = 0, 0.05$ | 65 |
| 6.1 | Introduction | 65 |
| 6.2 | Physical properties | 67 |
| 6.3 | Results and discussion | 71 |
| 6.3.1 | Thermopower | 71 |
| 6.3.2 | Thermal Conductivity | 72 |
| 6.4 | Outlook | 78 |
| 7 | T^2 phonon thermal conductivity | 81 |
| 7.1 | ThAsSe | 81 |
| 7.1.1 | Introduction | 81 |
| 7.1.2 | Physical properties | 82 |
| 7.1.3 | Results and discussion | 85 |
| 7.2 | $\text{Ba}_8\text{Ga}_{16}\text{Ge}_{30}$ | 87 |
| 7.2.1 | Introduction | 87 |
| 7.2.2 | Physical properties of $\text{Ba}_8\text{Ga}_{16}\text{Ge}_{30}$ | 89 |
| 7.2.3 | Results and discussion | 91 |
| 7.3 | Outlook | 94 |
| 8 | Summary | 95 |

| | |
|-----------------------------|------------|
| Bibliography | 99 |
| List of symbols | 127 |
| Acknowledgements | 133 |
| List of publications | 135 |
| Author's declaration | 137 |
| Versicherung | 139 |

Abstract

In this thesis thermal-conductivity κ and thermopower S measurements have been performed on the Kondo insulator $\text{U}_2\text{Ru}_2\text{Sn}$, the quasi-one-dimensional spin system $\text{Yb}_4(\text{As}_{0.7}\text{P}_{0.3})_3$, the heavy-fermion compound $\text{YbRh}_2(\text{Si}_{1-x}\text{Ge}_x)_2$ ($x = 0, 0.05$), the diamagnet ThAsSe and the clathrate $\text{Ba}_8\text{Ga}_{16}\text{Ge}_{30}$.

$\text{U}_2\text{Ru}_2\text{Sn}$ has been classified as the first tetragonal uranium-based Kondo insulator. Specific heat and magnetic susceptibility, as well as NMR provide evidence for the opening of an energy gap of approximately 160 K. Thermal-conductivity and thermopower measurements were performed on $\text{U}_2\text{Ru}_2\text{Sn}$ along and perpendicular to the tetragonal c axis, in the temperature range between 100 mK and 1 K, in zero field and in a magnetic field of 6 T. Below 400 mK, the phonon contribution to $\kappa(T)$ shows a T^2 behavior for both directions that can be attributed to phonons scattered from electrons. $S(T)$ presents a linear behavior in the whole temperature range. S is positive along the c axis and negative perpendicular to the c axis. Using a one-band model the effective mass m^* is estimated to be $2m_0$ along and $16m_0$ perpendicular to the c axis, where m_0 is the free-electron mass. This indicates that $\text{U}_2\text{Ru}_2\text{Sn}$ has a highly anisotropic residual density of states within the pseudogap.

The $\text{Yb}_4(\text{As}_{0.7}\text{P}_{0.3})_3$ is a quasi-one-dimensional $S = 1/2$ Heisenberg antiferromagnet. $\text{Yb}_4(\text{As}_{0.7}\text{P}_{0.3})_3$ was studied by thermal-conductivity measurements at low temperatures. κ was measured in the temperature range between 150 mK and 7 K and in applied magnetic fields up to 8 T. $\kappa(T)$ is found to follow the relation $aT + bT^2$ between 0.4 and 3 K at zero magnetic field. This dependence is attributed to the dominating role of magnons: The magnons act as heat carriers at the lowest temperatures (aT term) and as scatterers for the phonons at higher temperatures (bT^2 term). Below 0.4 K, the thermal conductivity drops below

the $aT + bT^2$ law, in agreement with the deviation from the magnon-related γT term in the specific heat due to spin-glass freezing. Above 1 K, the thermal conductivity decreases with increasing magnetic field, the opening of a gap in the magnon-excitation spectrum and the scattering of the phonons by magnetic solitons are possible explanations of this behavior.

The heavy-fermion compound YbRh_2Si_2 is a weak-antiferromagnet with $T_N \approx 70$ mK. It shows pronounced non-Fermi-liquid behavior related to a nearby antiferromagnetic quantum critical point. Thermopower and thermal-conductivity measurements were performed on $\text{YbRh}_2(\text{Si}_{1-x}\text{Ge}_x)_2$ ($x = 0, 0.05$) between 200 mK and 7 K. One aim of this study is to check the predictions of a model proposed for heavy-fermion compounds close to an antiferromagnetic quantum critical point. The model predicts an anomalous logarithmic temperature dependence in the thermopower, which is indeed observed in $\text{YbRh}_2(\text{Si}_{1-x}\text{Ge}_x)_2$ ($x = 0, 0.05$) in a certain range of temperature. κ shows striking deviations for the behavior expected for a simple metal, e.g. the Wiedemann-Franz law does not appear to be fulfilled.

The structurally disordered diamagnetic compound ThAsSe shows a glass-like behavior observed in specific-heat measurements. Resistivity measurements reveal Kondo-like behavior followed by non-Fermi-liquid behavior upon cooling. This behavior is independent of magnetic field and pressure. A Kondo effect derived from a structural two-level system is a possible explanation of the behavior in this compound. Thermal-conductivity measurements were performed on ThAsSe in the temperature range between 300 mK and 1 K, in zero field and in a magnetic field of 6 T. The phonon contribution to $\kappa(T)$ shows a $T^{1.9}$ behavior that can be attributed to phonons scattered from tunneling states.

The clathrate $\text{Ba}_8\text{Ga}_{16}\text{Ge}_{30}$ prepared with an excess of Ga presents p -type transport properties with temperature dependences typical for heavily doped semiconductors. Thermal-conductivity measurements were performed on single crystals of p -type $\text{Ba}_8\text{Ga}_{16}\text{Ge}_{30}$ in the temperature range between 200 mK and 7 K. Below 1.5 K, the phonon contribution to $\kappa(T)$ shows a $T^{1.5}$ behavior that can be attributed to phonons scattered from electrons instead of the commonly expected scattering of phonons from guest-atom tunneling states.

Chapter 1

Introduction

The last two decades have seen a growth of interest in strongly correlated electron systems — materials where the electron-interaction energies dominate the electron kinetic energies, becoming so large that they qualitatively transform the physics of the medium. The picture of an electron gas without interaction, which describes reasonably well simple metals, is no more applicable. In general, specific magnetic properties arise, especially when electrons become localized. Examples of strongly correlated systems include cuprate superconductors, heavy-electron compounds, Kondo insulators, Fermi and non-Fermi-liquid compounds, quasi-one-dimensional materials, etc [1].

Furthermore, strongly interacting electrons are the key ingredient for many unusual optical, electrical, and magnetic properties of technologically promising materials such as high-temperature superconductors, colossal magneto-resistance materials or Kondo insulators. Among other things, possible future applications for these classes of materials may range from magnetic data recording to significantly faster computers, loss-free transport and storage of electrical energy, new means of transport based on magnetic levitation, medical imaging, better speech quality in mobile communication, generation of electric energy, portable refrigerators and hyperfine detectors in scientific research and material testing [2–4].

A powerful tool for studying strongly correlated electron systems are thermal-transport measurements, which are important for the determination of the basic scattering mechanism in these systems. The thermal conductivity is a useful tool

in order to probe dissipation and scattering of any propagating excitation in a solid, while, thermopower measurements provide a sensitive probe of low-energy excitations in metallic systems [5, 6].

In this thesis a number of compounds which present strong electronic correlations have been investigated. The main aim of this work is to study the features that thermal conductivity and thermopower present in different kinds of strongly correlated electron materials at low temperatures.

Thermal-conductivity measurements can be used to probe magnetic excitations in low-dimensional magnetic materials, where magnetic interactions along one direction or plane of the crystallographic structure are much larger than in the transverse direction. It has been found that magnetic excitations in such materials provide an unusual transport channel of heat. The huge anisotropy seen in the thermal conductivity in the direction parallel and perpendicular to the chains or ladders indicates that magnetic excitations of these quasi-one-dimensional systems do play an important role in heat transport [7].

An exciting question is whether the theoretical understanding of electrons with strong correlations can be verified experimentally. This is the case for ThAsSe which apparently represents an experimental realization of a two-channel Kondo effect [8]. Thermal-conductivity measurements could help to explain the main mechanism by which heat is conducted and by which the heat flow is limited in this compound.

Another recent topic is the study of the thermal-transport properties of metallic heavy-fermion systems near a magnetic quantum critical point. A problem of interest is to understand the behavior of the thermal conductivity and thermopower of compounds that show non-Fermi-liquid behavior. In particular, it is an interesting task to study whether the Wiedemann-Franz law can still describe the behavior in those compounds. The Wiedemann-Franz law is a robust signature of a Fermi liquid and, until a very recent study on a high- T_c superconductors [9], no materials have been reported to violate it.

Studies of thermal-transport properties could help to clarify the origin of the energy-gap formation in Kondo insulators. This is due to the fact that thermal conductivity and thermopower are sensitive to the opening of the energy gap in these compounds. Kondo insulators are not only an interesting research topic

but might also find an application as thermoelectric materials. This is due to the huge thermopower observed in the temperature range where the gap opens [10, 11].

Studies of thermoelectric phenomena in strongly correlated electron systems are not only of fundamental interest in condensed-matter physics, but could also have great technological implications. Using thermoelectric effects of solids it is possible to generate electric energy from heat. This process is not accompanied with any pollution. Therefore thermoelectric materials are clean means for waste heat utilization, power generation for deep-space missions, and so on. The materials which have been studied as promising candidates for thermoelectric applications are mostly semiconducting alloys and compounds. Materials such as $\text{Bi}_2\text{Te}_3/\text{Sb}_2\text{Te}_3$ and Si-Ge, which are currently favored for room-temperature applications, belong to this category. Another class of materials with potentially useful thermoelectric properties are Ce and La filled skutterudites such as $\text{LaFe}_3\text{CoSb}_{12}$ and $\text{CeFe}_3\text{CoSb}_{12}$. Recently, it has been claimed that the best thermoelectric materials could be correlated metals and semiconductors (i.e., rare-earth intermetallic compounds) [4]. The search for new thermoelectric materials with high efficiency has recently focused on novel compounds with a complex crystal structure such as clathrates, mainly due to their remarkably low lattice thermal conductivity [12].

This thesis is divided into eight chapters. After a general introduction in this chapter the experimental part will be outlined in chapter 2. Both the experimental technique and the equipment are described there. Chapter 3 gives the basic theories that will help to understand and to analyze the experimental results. Chapters 4 to 7 cover the main content of the thesis, each chapter dealing with another topic. In chapter 4, thermal-transport properties of the Kondo insulator $\text{U}_2\text{Ru}_2\text{Sn}$ are investigated. Chapter 5 presents thermal-conductivity measurements of the quasi-one-dimensional $S = 1/2$ Heisenberg antiferromagnet $\text{Yb}_4(\text{As}_{0.7}\text{P}_{0.3})_3$ at low temperature and in applied magnetic fields. Chapter 6 is dedicated to the thermal transport of the antiferromagnetic heavy-fermion compound $\text{YbRh}_2(\text{Si}_{1-x}\text{Ge}_x)_2$, which is close to an antiferromagnetic quantum critical point. Chapter 7 is dedicated to the study of the thermal conductivity of the structurally disordered compound ThAsSe and the *p*-type clathrate

$\text{Ba}_8\text{Ga}_{16}\text{Ge}_{30}$. Finally, in chapter 8 the general conclusions will be given.

Chapter 2

Experimental Methods

The thermal-transport behavior of the different compounds studied in this thesis has been investigated by measuring thermal conductivity κ , thermopower S and electrical resistivity ρ as a function of temperature T and magnetic field B . In this chapter, the concepts and methods of measurement will be given. Thermal conductivity and thermopower were measured simultaneously by means of a steady-state method. The experiments were performed at low temperature ($T < 7$ K) in dilution refrigerators. Measurements of the electrical resistivity were performed in the Physical Properties Measurement System (PPMS) of Quantum Design, using the AC Transport Option in the range of temperature between 0.35 and 7 K.

2.1 Definitions

To define and estimate the thermal conductivity and the thermopower, consider a metal bar along which the temperature varies slowly in space. By supplying heat to one end of the bar, at the rate as it flows away, one can produce a steady state. Thermal conductivity is related to the ratio between a uniform flow of thermal energy and a temperature gradient on the bar [13]. The thermopower concerns the direct generation of an electrical field by thermal means. This phenomenon arises because electrons at the hot end of a conductor can find states of lower energy at the cold end, setting up an electric field or a potential difference between the two ends [14].

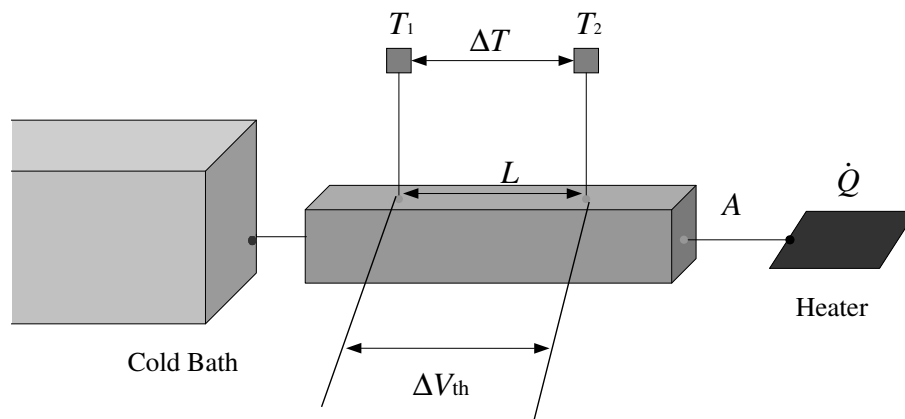


Figure 2.1: Scheme of the experimental arrangement for measuring thermal conductivity and thermopower.

In the simplest steady-state (experimental) arrangement, illustrated schematically in Fig. 2.1, heat is supplied at one end of the sample of uniform cross section A at a known rate \dot{Q} and is removed at the other end. Thermometers are attached at two places along the sample separated by a distance L , and the temperature difference ΔT and the thermal voltage ΔV_{th} between them is measured. The thermal conductivity κ and the thermopower S are then derived from the relations

$$\dot{Q} = \kappa A \frac{\Delta T}{L} \quad (2.1)$$

and

$$S = \frac{\Delta V_{th}}{\Delta T}. \quad (2.2)$$

For κ measurements, if ΔT is not too large ($\frac{\Delta T}{T} < 0.1$), the derived value of κ will be that corresponding to the mean temperature $T = \frac{T_1 + T_2}{2}$ between the thermometers even if κ is a rapidly varying function of temperature. The steady-state method can be used if it is certain that nearly all the heat supplied by the heater does indeed travel through the sample to the colder end [5].

For S , equation 2.2 is just valid if a small temperature difference ($\frac{\Delta T}{T} < 0.1$) is maintained between the two ends [15].

2.2 Experimental set-up

2.2.1 Sample holder

In Fig. 2.2 the sample holder is shown. Thermal links between the sample and the heater, the RuO₂ thermometers and the cold bath were established with high-purity Au wires ($\phi \approx 25 \mu\text{m}$ or $50 \mu\text{m}$) spot welded to the sample. The spot-welded contacts were stabilized mechanically using silver paint. In some cases, the sample was directly glued to the cold bath using silver paint. The thermometers were glued to silver foil and the heater was wrapped into silver foil. NbTi superconducting wires were used in the electrical wiring since superconducting wires, much below the critical temperature T_c , have very low thermal conductivity and do not contribute to the thermopower. The entire set-up was suspended with the help of fine Nylon wires in a Vespel frame. Application of a heat load to generate ΔT of the order of a few percent (1 % to 5 %) rapidly lead to equilibrium even at the lowest T (≈ 100 mK) investigated. Four thermometers were attached to the sample holder for the determination of ΔT ; two of them were calibrated from 100 mK up to 1.2 K and the second pair was calibrated from 1 K to 7 K. The four thermometers were calibrated in situ in different magnetic fields (1 T, 2 T, 4 T, 6 T, 8 T). The thermal voltage ΔV_{th} was measured using a Keithley 2001 multimeter with the help of a Keithley 1801 nanovolt preamplifier. The resistance of the thermometers was measured with an AVS-47 resistance bridge from RV-Elektronikka OY. The power dissipated at the heater was generated using a Keithley 236 current source and measured using a Keithley 2182 nanovoltmeter.

Typically, the investigated samples had dimensions of $1.5 \text{ mm} \times 0.5 \text{ mm} \times 0.2 \text{ mm}$.

2.2.2 Dilution refrigerator

Most of the measurements performed in the framework of this thesis were carried out using a dilution refrigerator (³He-⁴He refrigerator). This kind of refrigerator uses the thermodynamic properties of a ³He-⁴He mixture to cool down the system. When a mixture of the two stable isotopes of helium is cooled below a critical temperature it separates into two phases. The lighter “concentrated phase” is rich

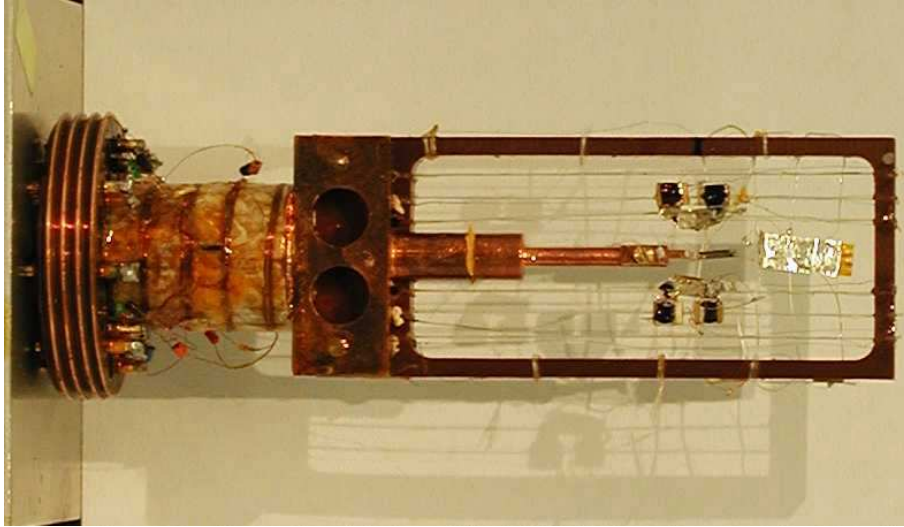


Figure 2.2: Experimental set up. A sample of U_2Ru_2Sn is glued to the cold finger with silver paint, the heater is located at the other end of the sample. The black squares at both sides of the sample are RuO_2 thermometers.

in 3He and the heavier “diluted phase” is rich in 4He . Since the enthalpy of the 3He in the two phases is different, it is possible to obtain cooling by “evaporating” the 3He from the concentrated phase into the diluted phase. The 4He which makes up the majority of the diluted phase is inert, and the 3He “gas” moves through the liquid 4He without interacting with it. This gas is formed in the mixing chamber at the phase boundary, and the cooling obtained by this process is used to cool the sample. A detailed discussion of the principles of a dilution refrigerator has, for example, been given in Ref. 16.

Two dilution refrigerators were used in this thesis. The first one is the so-called “mini fridge” (home made). In this cryostat, the sample holder was mounted on a decoupling platform which allows to regulate the bath temperature between 0.07 K and 7 K in a magnetic field up to 8 T. Several changes were performed on the cryostat to improve its base temperature from 150 mK to 70 mK and to reach a higher reliability: The old wiring which was soldered to several thermalization stages in the inner vacuum chamber was changed into one band of superconducting wires which has just two soldering points, one at the 1 K pot and the other one at the mixing chamber. The amount of 3He - 4He mixture was increased. In order to reduce the background signal in the thermopower measurements, a vacuum

tube for the thermal voltage wires, which originally passed through the He bath, was installed. Using this “mini fridge” the following samples of this thesis were measured: $\text{YbRh}_2(\text{Si}_{1-x}\text{Ge}_x)_2$ ($x = 0, 0.05$), $\text{Yb}_4(\text{As}_{0.7}\text{P}_{0.3})_3$ and $\text{Ba}_8\text{Ga}_{16}\text{Ge}_{30}$. Due to a leak in the inner vacuum chamber which, after various attempts, could not be fixed the use of another cryostat was necessary.

The second cryostat is a Kelvinox 100 (Oxford Instruments). This cryostat is situated at the Institut für Festkörperphysik at Dresden University of Technology and was made available for this study by Professor Joachim Wosnitza. The base temperature was 60 mK with the sample holder in a magnetic field up to 6 T. The sample holder was mounted 23 cm below the mixing chamber in the center of the magnet. There is no decoupling platform in this cryostat; thus measurements could be performed below 1 K only. The following samples of this thesis were measured using this cryostat: $\text{YbRh}_2(\text{Si}_{1-x}\text{Ge}_x)_2$ ($x = 0, 0.05$), $\text{U}_2\text{Ru}_2\text{Sn}$ and ThAsSe .

In both cryostats, for measuring thermopower a pair of copper wires ($\phi \approx 100 \mu\text{m}$) was installed in the cryostat without interruption and soldering points from the preamplifier at room temperature down to the mixing chamber, where a pair of superconducting wires continues down to the sample holder. In order to prevent the generation of parasitic thermal voltages at the copper/superconductor transition, the wires were screwed to small copper blocks which, by using GE varnish, were brought in good thermal contact with the mixing chamber but were electrically insulated from it. All wires from the sample holder to room temperature were thermally anchored at various points on the refrigerator.

On the mixing chamber decoupling platform a germanium thermometer and a heater were installed in order to measure and control the temperature of the cryostat. The temperature stabilization occurs by a combination of an AVS-47 resistance bridge and a PID-temperature controller TS-530, both from RV-Elektroniikka OY.

2.2.3 AC Transport Option

The Quantum Design AC Transport Option of the Physical Property Measurement System (PPMS) permits measurements of electrical-transport properties in

the temperature range from 0.35 to 400 K and in applied magnetic fields up to 14 T. The system measures the electrical resistivity ρ by using a standard four-point AC technique, passing an AC bias current I and measuring the potential drop V across the sample. The resistivity ρ is calculated from

$$\rho = \frac{V}{I} \frac{A}{L} \quad (2.3)$$

where A and L are the sample cross section and the distance between the voltage contacts, respectively (see Fig 2.1). The sample contacts for measuring ρ are the same contacts used for measuring the thermal conductivity. Using the AC transport option the following samples were measured: $\text{YbRh}_2(\text{Si}_{1-x}\text{Ge}_x)_2$ ($x = 0, 0.05$), $\text{U}_2\text{Ru}_2\text{Sn}$, and $\text{Ba}_8\text{Ga}_{16}\text{Ge}_{30}$.

2.3 Measurement and data analysis

To determine κ and S from the measurements, relations 2.1 and 2.2 are used. \dot{Q} is the power generated by the heater which is related to its resistance R and the applied current I by $\dot{Q} = RI^2$. ΔT is the temperature difference across the sample, $\Delta T = T_2 - T_1$, where T_2 is the temperature at the warm end and T_1 is the temperature at the cold end. Replacing \dot{Q} and ΔT in equations 2.1 and 2.2, the relations

$$\kappa = \frac{RI^2}{T_2 - T_1} \frac{L}{A} \quad (2.4)$$

and

$$S = \frac{\Delta V_{th}}{T_2 - T_1} \quad (2.5)$$

are obtained.

The experiment was performed as follows: After setting the temperature of the cryostat (bath temperature), a set of currents was applied to the heater to generate different gradients of temperature. For each current, the sample's temperature profile was stabilized and T_1 , T_2 and ΔV_{th} were measured, keeping the bath temperature stable. After the last current setting and measurement the next bath temperature was set.

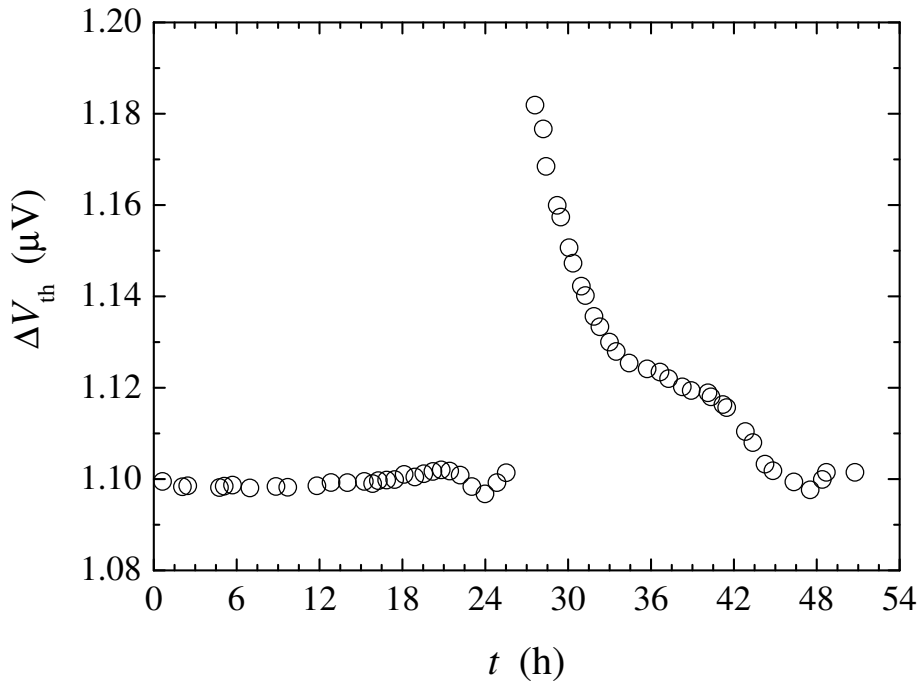


Figure 2.3: Background signal of ΔV_{th} as a function of time t . These data were measured in the Kelvinox 100. For the “mini fridge”, the background was larger and the time dependency was stronger. The jump is generated when ^4He is transferred to the cryostat.

For each bath temperature, four heater currents (I_0 , I_1 , I_2 and I_3) were applied; two of them had value zero (I_0 and I_3). The first zero-current measurement was performed after a well stabilized bath temperature was reached and the second one after the last measurement with a non-zero current was performed.

The zero-current measurements provide information about the stability of the system during a complete measurement at a given bath temperature: ΔT and ΔV_{th} ought to be the same for I_0 and I_3 , if the system is thermally stable. In addition, in an “ideal” system, ΔT and ΔV_{th} ought to be zero at $I_0 = I_3 = 0$. The fact that always finite background signals are measured is due to weak thermal links on the sample holder and inhomogeneities in the wiring. The background signal of ΔV_{th} was found to depend strongly on time t ; in fact it depends on the ^4He level in the cryostat (see Fig. 2.3 and more information in [17]).

Before calculating κ and S , it is important to subtract background signals from the measured data. Figure 2.4 shows ΔV_{th} as a function of t for four

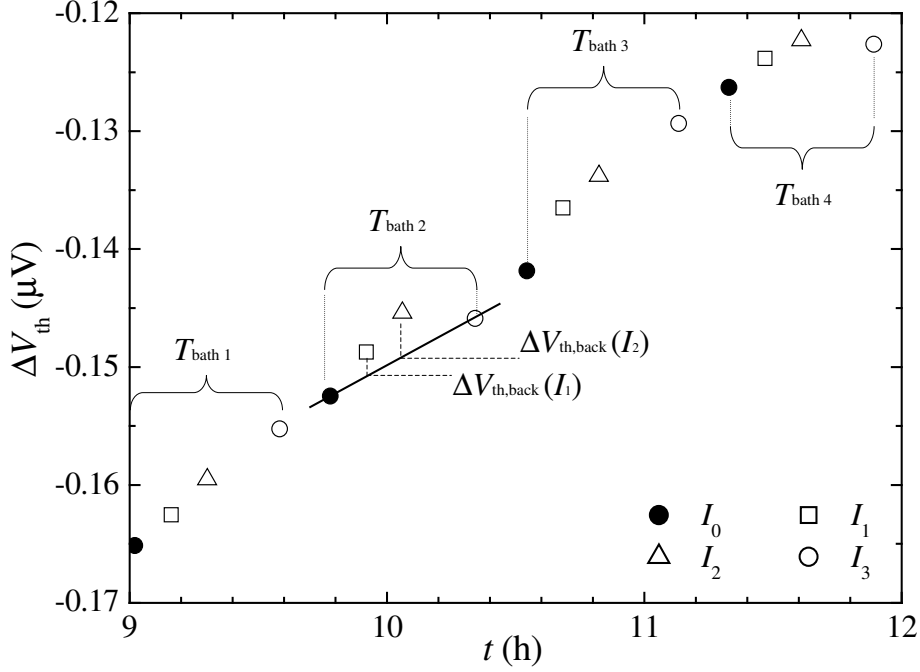


Figure 2.4: Thermal voltage ΔV_{th} as a function of time t for four different currents. Each set of 4 points was measured at constant bath temperature. The solid line is a linear-in- t fit between the I_0 and I_3 data.

different current settings. Each set of four points was measured at a constant bath temperature. The solid line is a linear-in- t fit for the two zero-current settings of the second bath temperature T_{bath2} . Using the fit, it is possible to estimate the background $\Delta V_{th,back}$ for the non-zero-current data of the same bath-temperature setting.

To estimate the background signal of ΔT it is necessary to consider that, at a given bath-temperature setting, for each non-zero applied current the average temperature T of the sample increases. In Fig. 2.5, ΔT is plotted as a function of $\ln(T)$ for four different current settings. The leftmost point of each curve corresponds to the first bath-temperature setting T_{bath1} . The curves for the currents I_1 and I_2 are shifted to higher temperature with respect to the curves for the currents I_0 and I_3 . The estimated background signal ΔT_{back} is, for each current and average temperature, determined from the $\Delta T(I_0)$ and $\Delta T(I_3)$ data by interpolation in temperature (cf. Fig. 2.5).

In order to calculate κ and S it is necessary to obtain the background-corrected

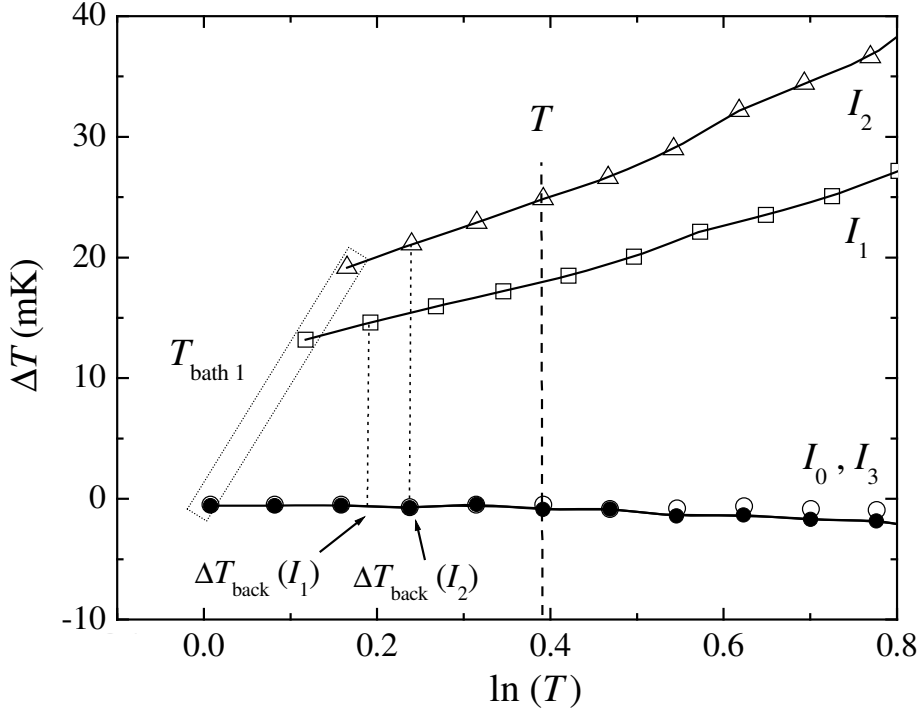


Figure 2.5: Temperature gradient ΔT as a function of $\ln(T)$ for four different currents. T is the average sample temperature. The solid lines are interpolations for each current.

ΔT and ΔV_{th} values for the different current settings at the same average sample temperatures, e.g. at a select average temperature $T(I_2)$, interpolation-in- T is also necessary for obtaining $\Delta T(I_1)$, $\Delta V_{th}(I_1)$ and I_1 at $T(I_2)$. Then, to extract κ and S for each average sample temperature, a plot of I^2 versus the background-corrected ΔT values and a plot of ΔV_{th} versus ΔT , both background-corrected, are made. If the condition for κ and S are fulfilled ($\frac{\Delta T}{T} < 0.1$), the plots should represent lines the slopes of which are κ and S , according to equations 2.4 and 2.5.

A polycrystalline sample of lead (Pb 5N) was used to test the system. Pb is superconducting below the critical temperature T_c of 7.19 K. In superconductors much below T_c , the electronic contribution to κ is suppressed and other contributions to κ , e.g. the lattice contribution, become more important. According to various theories [18, 19], this phonon-dominated regime is expected at temperatures $\frac{T}{T_c} < 0.15$ where, on account of the energy gap in the electronic excitation

spectrum of the superconductor, not only the electronic transport contribution has vanished but also the scattering of phonons by electrons is negligible.

In Fig. 2.6, κ is shown as a function of temperature for Pb. Circles (\circ) show $\kappa(T)$ data of a single crystal taken from [20] and triangles (\triangle) show $\kappa(T)$ of the polycrystalline sample used in our calibration. For both samples, κ shows an approximate T^3 dependence below 1 K ($\sim T^{2.7}$ for the polycrystal and $\sim T^{2.9}$ for the single crystal). This temperature dependence is theoretically expected for boundary scattering of phonons [13, 20]. The absolute value of κ depends directly on the mean-free path l_{ph} of the phonons. In the case of the single crystal, at low temperature, l_{ph} is of the size of the smallest side of the sample. In the case of the polycrystalline sample, l_{ph} is of the size of the grains and this lowers κ as may be seen from Fig. 2.6.

Another characteristic of superconductors is that, below T_c , they do not show thermoelectric effects, indicating that electrons do not transport entropy [13, 15]. In Fig. 2.7, a measurement of $S(T)$ of our polycrystalline Pb sample is shown. As expected, $S(T) = 0$ within the error bars. From this result we may estimate the resolution of $S(T)$ measurements with the “mini fridge” system used for the Pb measurement: it is better than $0.5 \mu\text{V}/\text{K}$ above 0.1 K.

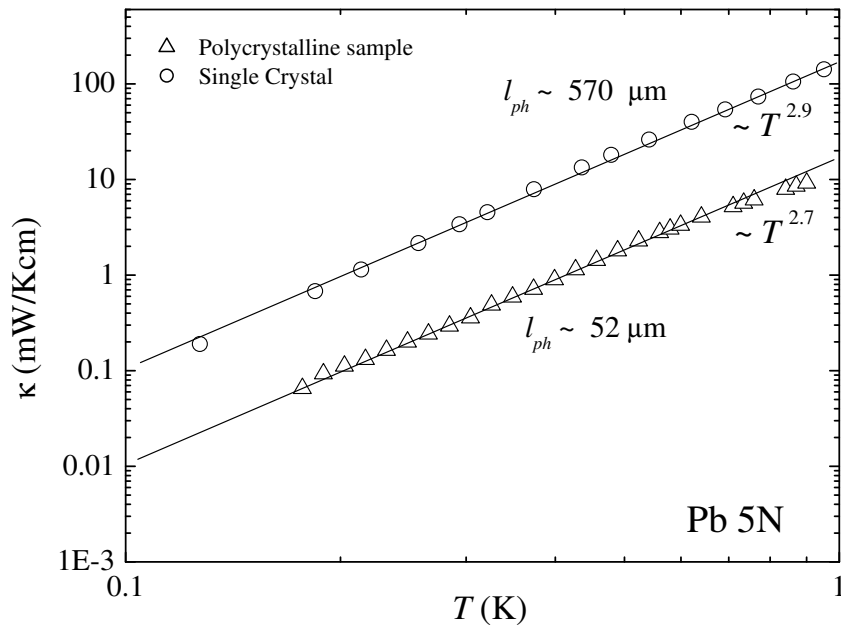


Figure 2.6: Thermal conductivity κ as a function of temperature T of Pb measured within the “mini fridge” system. Single crystal data are taken from Ref. 20.

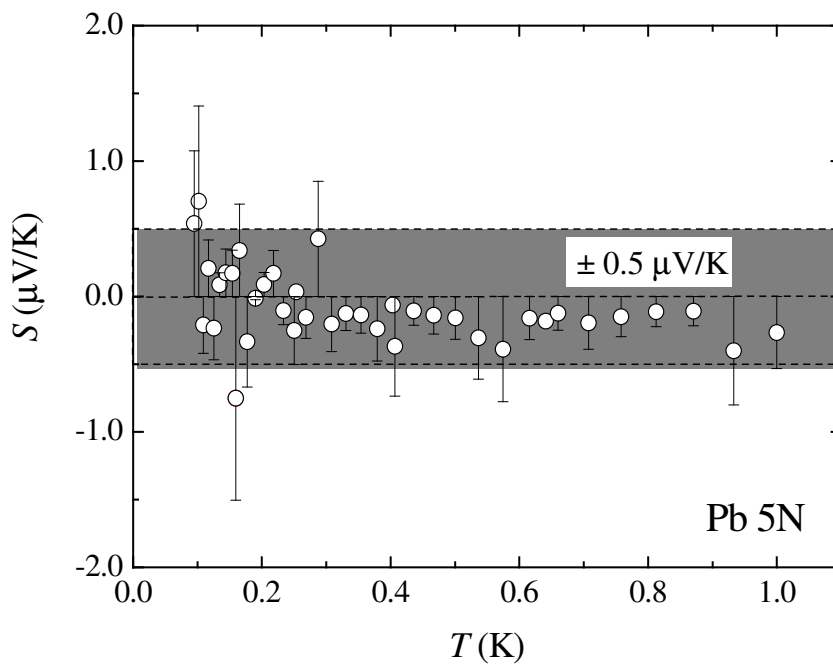


Figure 2.7: Thermopower S as a function of temperature T of a polycrystalline Pb sample measured with the “mini fridge” system.

Chapter 3

Theoretical concepts

This chapter is dedicated to introduce some theoretical concepts which will then be used during the discussion of the results.

3.1 Thermal Transport

The theoretical concepts and relations discussed in this section are mainly taken from the books “Electrons and Phonons” by Ziman [21], “Thermoelectric Power of Metals” by Blatt [6] and “Thermal Conduction in Solids” by Berman [5].

Expressions for the transport coefficients in the case of electronic transport are derived by solving the Boltzmann transport equation subject to appropriate boundary conditions. Under steady-state conditions in a bulk sample the distribution function must satisfy the equation

$$\dot{\vec{k}} \cdot \nabla_{\vec{k}} f + \vec{v}_{\vec{k}} \cdot \nabla_{\vec{r}} f = \left(\frac{\partial f}{\partial t} \right)_c \quad (3.1)$$

where $f = f(\vec{k}, \vec{r})$ is a function of the wave vector \vec{k} and of the position \vec{r} , which measures the number of carriers with momentum $\hbar\vec{k}$ in the neighborhood of \vec{r} . The terms on the left-hand side of equation 3.1 are the drift terms, which describe the change in the local distribution due to a temporal change of \vec{k} and \vec{r} (acceleration and velocity). The term on the right-hand side is the collision term, denoted by the subscript c , and gives the number of electrons scattered into the six-dimensional volume element $d\vec{k}d\vec{r}$ per time. The calculation of the collision

term is a difficult problem, and the result depends on the type of interactions which give rise to scattering, e.g., interaction with defects, lattice vibrations, mutual exchange interaction. Using the relaxation-time approximation to estimate the collision term and considering that at equilibrium the distribution of carriers among the available energy levels is given by the Fermi-Dirac distribution, the transport coefficients electrical conductivity σ , thermopower S and thermal conductivity κ can be written as a function of a single function. The transport coefficients are given by solutions of the Boltzmann equation as:

$$\sigma = e^2 \int_{-\infty}^{+\infty} d\varepsilon \left(-\frac{\partial f_0}{\partial \varepsilon} \right) \Sigma(\varepsilon), \quad (3.2)$$

$$T\sigma S = e \int_{-\infty}^{+\infty} d\varepsilon \left(-\frac{\partial f_0}{\partial \varepsilon} \right) \Sigma(\varepsilon)(\varepsilon - \mu), \quad (3.3)$$

$$T\kappa_0 = \int_{-\infty}^{+\infty} d\varepsilon \left(-\frac{\partial f_0}{\partial \varepsilon} \right) \Sigma(\varepsilon)(\varepsilon - \mu)^2, \quad (3.4)$$

where μ is the chemical potential, e is the electron charge, ε is the energy, and f_0 is the Fermi-Dirac distribution for the system in equilibrium:

$$\left(-\frac{\partial f_0}{\partial \varepsilon} \right) = \frac{1}{k_B T} \frac{e^{\left(\frac{\varepsilon - \mu}{k_B T}\right)}}{\left(e^{\left(\frac{\varepsilon - \mu}{k_B T}\right)} + 1 \right)^2}. \quad (3.5)$$

The transport distribution function $\Sigma(\varepsilon)$ is, in the case of parabolic bands, given by:

$$\Sigma(\varepsilon) = N(\varepsilon)v(\varepsilon)^2\tau(\varepsilon) \quad (3.6)$$

where $N(\varepsilon)$ is the density of states, $v(\varepsilon)$ is the group velocity of the carriers and $\tau(\varepsilon)$ is the carrier's lifetime.

The theory is just the same for phonons except that the Bose-Einstein statistics should be taken into account.

3.1.1 Thermopower

Thermoelectric phenomena are sensitive indicators of the electronic properties of metals, particularly of the interactions between electrons and phonons, impurities

and other defects. The interest in thermoelectric phenomena is based on the fact that they can shed light on fundamental features of electronic energy levels and on the interaction of conduction electrons with their environment.

Electronic contribution in metals

In the degenerate limit, expansion of the integral 3.3 leads to the Mott expression

$$S_d = -\frac{\pi^2 k_B^2 T}{3e} \left(\frac{\partial \ln \sigma(\epsilon)}{\partial \epsilon} \right)_{E_F}. \quad (3.7)$$

Here, e is the electron charge, T the temperature, k_B the Boltzmann constant, and E_F the Fermi energy. The function $\sigma(\epsilon)$ yields the dc electrical conductivity of the system. The Fermi energy E_F is given by the expression

$$E_F = \frac{\pi^2 \hbar^2}{2m^*} \left(\frac{3n}{\pi} \right)^{2/3} \quad (3.8)$$

where m^* is the effective mass, n is the charge carrier concentration and \hbar is the Planck constant divided by 2π .

S_d is the diffusion thermopower which is the contribution to the thermopower associated with a system of charge carriers that interact with a random distribution of scattering centers. It should be noted that the sign of S_d in equation 3.7 is not only determined by that of the charge carriers but also by the sign of the logarithmic derivative of $\sigma(\epsilon)$.

At very low temperature where the relaxation time is limited by impurity scattering, the diffusion thermopower in the free-electron approximation is:

$$S_d = \frac{\pi^2 k_B^2 T}{3eE_F}. \quad (3.9)$$

3.1.2 Thermal conductivity

There are several mechanisms by which heat can be transmitted through a solid and many processes which limit the effectiveness of each mechanism. In an electrical insulator heat is conducted by means of the thermal vibrations of the atoms (phonons). In simple metals, on the other hand, the thermal conductivity is usually dominated by electrons.

Electronic contribution and Wiedemann-Franz law

The high thermal conductivity of metals is closely connected to their high electrical conductivity. In the Drude theory of electrical conductivity, the electrical conductivity can be expressed as

$$\sigma = \frac{ne^2l_e}{2m_e v_e} \quad (3.10)$$

where n is the charge carrier concentration, e and m_e are the electric charge and the electron mass, v_e is the mean velocity and l_e is the mean-free path. Assuming that, in a temperature gradient, electrons travel just the same average distance l_e before transferring their excess thermal energy to the atoms by collisions, then the heat conductivity is given by

$$\kappa_e = \frac{1}{3}nc_e v_e l_e \quad (3.11)$$

where c_e is the heat capacity per electron (nc_e is the electronic heat capacity per unit volume, C_e). The Wiedemann-Franz law is obtained by comparing κ_e with σ as given in the equations 3.10 and 3.11. Taking into account that v_e is independent of temperature, while c_e is proportional to T , one obtains:

$$\frac{\kappa_e}{\sigma} = \frac{\pi^2}{3} \left(\frac{k_B}{e} \right)^2 T. \quad (3.12)$$

This is the Wiedemann-Franz law $\kappa_e/(\sigma T) = L_0$, where L_0 is the Lorentz number with the value of $2.4 \times 10^{-8} \text{ W}\Omega\text{cm}/\text{K}^2$. The Wiedemann-Franz law is valid for the strictly elastic processes that operate when T goes to zero.

Phonon contribution

Lattice vibrations, i.e., phonons, also play a role in thermal transport. Their mean-free path l_{ph} is a measure of the rate at which energy is exchanged between different phonon modes. l_{ph} is determined by a combination of scattering mechanisms ($\frac{1}{l_{ph}} = \sum_i \frac{1}{l_{ph-i}}$), assuming that the different scattering mechanism act independently. We can again use the expression

$$\kappa = \frac{1}{3}C_{ph}v_{ph}l_{ph} \quad (3.13)$$

to represent the heat conductivity, where v_{ph} is the mean phonon velocity, approximately equal to the sound velocity in the crystal, and C_{ph} is the heat capacity contributed by the lattice.

The phonons are scattered by many origins, e.g., by phonons themselves, electrons, imperfections of the crystal, or at the surface of the crystal. Each mechanism leads to a different temperature dependence of κ . The dominant scattering mechanism depends on the temperature and the concentration of scattering centers.

The conventional formulae for κ_{ph} and v_{ph} given by the Debye model are

$$\kappa_{ph} = \frac{k_B}{2\pi^2 v_{ph}} \left(\frac{k_B}{\hbar} \right)^3 T^3 \int_0^{\theta_D/T} \frac{z^4 e^z}{(e^z - 1)^2} \tau_{ph}(z, T) dz, \quad (3.14)$$

$$v_{ph} = \frac{k_B \theta_D}{\hbar} (6\pi^2 N)^{-1/3}, \quad (3.15)$$

where θ_D is the Debye temperature, N the number of atoms per unit cell, and $\tau_{ph}(z, T)$ is the phonon-relaxation time. The latter is related to the phonon mean-free path l_{ph} via the phonon velocity v_{ph} ($\tau_{ph} = l_{ph}/v_{ph}$) and $z = \hbar v_{ph} q / k_B T$ where q is the phonon wave number. The total heat current comes from the sum of the contributions of each mode. The problem of solving the equation 3.14 is to calculate $\tau_{ph}(z, T)$. The relaxation time is related to the heat rate that is transferred locally from one mode to another of the phonon system. Unfortunately, there are scattering processes which make the integral in Eq. 3.14 diverge at small values of q . One way of solving the problem is by considering that the phonon distribution at any given temperature tends to be concentrated about a particular frequency. The number of quanta in the range of frequencies $d\nu$ is proportional to

$$\frac{\nu^2 d\nu}{e^{\left(\frac{\hbar\nu}{k_B T}\right)} - 1}, \quad (3.16)$$

which has a maximum at $\hbar\nu_{dom} \approx 3.8k_B T$ or $\hbar v_{ph} q_{dom} \approx 3.8k_B T$ where ν_{dom} is the dominant phonon frequency and q_{dom} is the dominant phonon wave number.

1. Boundary Scattering At high temperatures l_{ph} is limited by direct interactions among the phonons themselves. As the temperature decreases, interactions

among the phonons become rapidly less effective in restricting l_{ph} . At low temperatures l_{ph} may reach several millimeters and is comparable with the smallest dimension of the sample. Then, the scattering of the phonons with the sample boundary has to be considered. The phonon mean-free path due to boundary scattering, also called Casimir mean-free path, can be expressed as

$$l_{ph-Casimir} = \sqrt{4A/\pi}, \quad (3.17)$$

where A is the cross section of the sample.

2. Phonon-electron scattering Most measurements have shown that the lattice component of the thermal conductivity in metals and alloys at low temperatures is proportional to T^2 . This T^2 behavior has been shown theoretically to arise when the lattice waves are scattered predominantly by the conduction electrons.

A theory developed by Ziman [22] shows that the phonon mean-free path for phonon charge-carrier scattering can be expressed as

$$l_{ph-e}^{-1} = \frac{m^* E_{def}^2 k_B}{2\pi \rho_m \hbar^4 v_{ph}^2} z T, \quad (3.18)$$

where m^* is the effective mass of the charge carriers, E_{def} is the deformation potential, ρ_m is the mass density of the compound and z comes from the dominant phonon approximation $z = \frac{\hbar v_{ph} q}{k_B T}$. The deformation potential measures the strength of the phonon-electron interaction.

However, the phonon-electron interaction is negligible if the product of the charge-carrier mean-free path l_e and the wave number of the dominating phonons q_{dom} is less than 1 (Pippard ineffectiveness condition) [23]. At low phonon frequencies, the electronic mean-free path is shorter than the phonon wavelength, and the electrons are invisible for the phonons.

To estimate the electronic mean-free path l_e , the electronic conductivity in the case of electron-phonon interaction is used

$$\sigma = \frac{e^2 l_e}{3\pi \hbar} (3\pi^2 n)^{2/3}, \quad (3.19)$$

where e is the charge of the carriers, l_e is the electronic mean-free path due to the electron phonon scattering, and n is the charge-carrier concentration.

Recently, Sergeev and Mitin [24] have discussed the validity of the condition $l_e q > 1$ for systems with extra disorder due to atoms which oscillate independently from the lattice (rattling) and they have found that in this case even for $l_e q < 1$ the phonon charge-carrier scattering can be dominant.

Using this last model, in the case that $l_e q > 1$, the mean-free path can be written as:

$$\frac{1}{l_{ph-e}} = 2\beta_l q \frac{v_{ph}}{v_F} \left(\frac{ql_e \arctan(ql_e)}{ql_e - \arctan(ql_e)} - \left(1 - \frac{l_e}{L}\right) \frac{3}{ql_e} \right) P(z), \quad (3.20)$$

where $P(z)$ is a cutoff function which allows only phonons with $q < 2k_F$ to contribute, v_F is the Fermi velocity and L is the electron mean-free path with respect to the scattering from the quasistatic potential.

In the case $l_e q < 1$ the phonon mean-free path is given by

$$\frac{1}{l_{ph-e}} = \frac{6\beta_l v_{ph}}{v_F L} + \frac{8}{5v_{ph}} \beta_l \tau_e \omega_q^2, \quad (3.21)$$

with

$$\beta_l = \left(\frac{2}{3} E_F \right)^2 \frac{m^{*2} v_F}{2\pi^2 \rho_m v_{ph}^2 \hbar^3}. \quad (3.22)$$

Using the dominant-phonon approximation and replacing $(\frac{2}{3} E_F)$ by E_{def} [21], β_l is expressed as

$$\beta_l = \frac{E_{def}^2 m^{*2} v_F}{2\pi^2 \rho_m v_{ph}^2 \hbar^3}. \quad (3.23)$$

In the limit $l_e q_{dom} > 1$ and $l_e/L = 0$, Eq. 3.20 combined with Eq. 3.23 correctly reproduces the Ziman equation (Eq. 3.18). Calculating the phonon thermal conductivity with equation 3.20 results in $\kappa_{ph} \sim T^\alpha$ with $1 \leq \alpha \leq 2$.

In the limit $l_e q_{dom} < 1$, the mean-free path is expressed as

$$\frac{1}{l_{ph-e}} = \frac{3E_{def}^2 m^{*2} v_{ph}}{\pi^2 \rho_m \hbar^3 L} + \frac{16 E_{def}^2 m^* P_F z^2 k_B^2 \tau_e}{5 \rho_m v_{ph} \hbar^5} T^2. \quad (3.24)$$

Calculating the phonon thermal conductivity with equation 3.24 results in $\kappa_{ph} \sim T^\alpha$ with $\alpha \leq 1$.

Magnetic contribution

In a magnetically ordered crystal the propagating excitations of the spin system, known as magnons, can transport heat in the same manner as the phonons. In 1955, Sato [25] pointed out that, at liquid-helium temperatures, the magnon system can have a specific heat equal to or greater than that of the phonons. The velocities of the two excitations are comparable and, at sufficiently low temperatures, their mean-free paths are equal, since both are limited only by the boundary of the sample. Therefore, at low temperatures, a large fraction of the total thermal conductivity of the system may be due to the magnons. In analogy to the electron and phonon cases the magnon thermal conductivity κ_m is given by

$$\kappa_m = \frac{1}{3} l_m v_m C_m, \quad (3.25)$$

where C_m is the magnetic heat capacity, v_m is the propagation velocity of the magnons and l_m is the mean-free path of the magnons. Sato showed that the thermal conductivity due to magnons scattered by the sample boundary would vary as T^2 . The magnons can also be scattered by phonons. The interaction is strongest at the point where the dispersion curves cross, since at this point energy and wave vector can be conserved in a one-phonon-one-magnon interaction. At the point of the intersection a gap opens in the dispersion curves, and near the gap the excitations are neither magnons nor phonons, but coupled magnetoelastic modes. The size of the gap is determined by the magnitude of the magnetoelastic coupling constant. The magnon-phonon interaction can also affect the phonon conductivity. Because of the gap, a band of phonons is effectively removed from the heat-carrier spectrum.

Magnon conductivity could be recognized by a departure of the thermal conductivity from the T^3 behavior expected for the boundary-limited phonon conductivity. Another useful technique is the measurement of the conductivity in an external magnetic field. For a ferromagnet, the applied magnetic field raises the magnon energies which decreases their population and thus lowers the magnon component of the conductivity. In an antiferromagnet, one magnon branch is lowered, causing an increase in the magnon contribution.

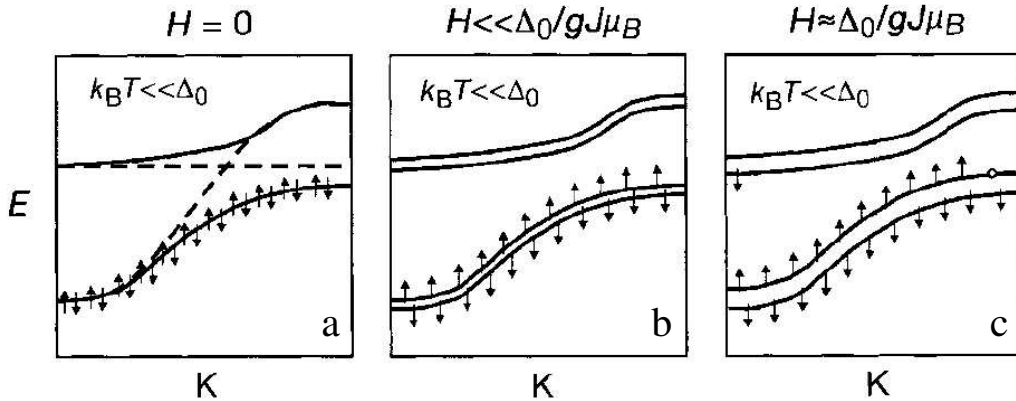


Figure 3.1: Schematic band structure and magnetic-field dependence in a Kondo insulator at low temperatures [28].

3.2 Kondo insulators

Kondo insulators are materials which show the behavior typical of Kondo lattices at high temperatures, but which evolve into a semiconducting state as the temperature is lowered. Characteristic is the high-temperature Curie-Weiss magnetic susceptibility which evolves into low-temperature paramagnetism on the same temperature scale describing the exponential rise in the electrical resistivity and electronic specific heat at low temperatures. This scale also gives the temperature development of the Hall constant [26, 27].

A simple model which captures most of these properties is that of a flat f -band hybridizing with a broad conduction band, with exactly two electrons per unit cell. At $T = 0$ these two electrons fill the lower hybridized band (see Fig. 3.1(a)). Furthermore, for applied magnetic fields small compared to the hybridization gap (see Fig. 3.1(b)), the magnetic response χ vanishes because the number of up- and down-spin electrons remains equal. As T grows from 0 K, however, the filling of the lower and upper bands deviates from unity and zero, respectively, and a thermally activated Pauli-like term dominates $\chi(T)$ (see Fig. 3.1(c)). Analogously, the transport properties at low T are those of a semiconductor while, at T of order of the gap and above, the resistivity should resemble that of a metal [27].

While this simple model explains most of the physical properties of cubic

systems such as $\text{Ce}_3\text{Bi}_4\text{Pt}_3$, it does not account for all the macroscopic properties of some other, in particular non-cubic, Kondo insulators [29]. This may be due to the fact that the conditions for gap formation (one f -band crossing exactly one conduction band, two relevant electrons per f -site) are more likely fulfilled in cubic materials.

A number of models has been proposed to account for the unusual properties of Kondo insulators [30–33]. A renormalized gap can be derived by a mean-field treatment of the Anderson-lattice Hamiltonian [31]. Another picture is the formation of a local Kondo singlet where the excitations are s -wave-type excitations, which was proposed to describe the strong k dependence of the magnetic excitations in the classical Kondo insulator SmB_6 [32]. In addition, there is a controversy on the problem whether or not the mechanism of the gap formation in YbB_{12} is similar to that in the Ce compounds [32].

Theoretical descriptions of the closure of the energy gap and the accompanying insulator-metal transition in Kondo insulators by means of a magnetic field [34, 35], of pressure [36], and of impurities [37, 38] have been given.

3.3 Fermi-Liquid State

The Fermi-liquid model is the correct description of the low-temperature measurable parameters of a metal provided that the electron interaction, as T goes to zero, becomes temperature independent and is short ranged in both space and time. Assuming a one-to-one correspondence of the excitations (quasiparticles) of an interacting-electron system and of a free-electron gas, Landau [39–42] derived that the low- T properties of the Fermi liquid obey the same laws as the Fermi gas, with a renormalized effective mass m^* , and a few additional parameters taking into account the residual interactions among the quasiparticles.

The thermodynamic and transport properties of a normal Fermi liquid are shown to be directly related to the effective mass m^* . The following properties are predicted by Landau-Fermi liquid theory when the temperature goes to zero.

The density of states at the Fermi energy is given by:

$$N(E_F) = \frac{m^* k_F}{\pi^2 \hbar^2}, \quad (3.26)$$

where k_F is the Fermi wave vector.

The temperature independent susceptibility χ has the form

$$\chi = \frac{\mu_0 \mu_B m^* k_F}{\pi^2 \hbar^2} \frac{1}{1 + F_0^a}, \quad (3.27)$$

where F_0^a is the antisymmetric Landau parameter. In comparison with the case of a non-interacting Fermi gas, χ is enhanced by a factor of $m^*/m_0(1 + F_0^a)$.

The electronic specific heat follows the relation

$$\frac{C_e}{T} = \gamma = \frac{m^* k_F k_B^2}{3\hbar^2}. \quad (3.28)$$

Therefore, specific-heat measurements should provide direct information on the effective mass m^* .

The electrical resistivity varies as

$$\rho = \rho_0 + AT^2, \quad (3.29)$$

where ρ_0 is the residual resistivity and the coefficient A reflects the cross section of the electron-electron scattering ($A \sim \gamma^2 \sim N(E_F)^2$).

3.4 Heavy-fermion metal

The Kondo effect describes the exchange interaction between a magnetic impurity (with a spin \vec{S}) and a conduction electron (with spin \vec{s}), given by the Hamiltonian

$$H = -J\vec{S} \cdot \vec{s}. \quad (3.30)$$

For a negative coupling J , the impurity spin is completely compensated by conduction electrons at low temperature, leading to the formation of a Kondo singlet. The binding energy of a Kondo singlet is determined by

$$k_B T_K \sim \frac{1}{N(E_F)} e^{-\frac{1}{JN(E_F)}}, \quad (3.31)$$

where T_K is the Kondo temperature.

Heavy-fermion compounds can be considered as a Kondo lattice composed of a periodic array of magnetic impurities. Characteristic features of a Kondo

lattice at low temperature are: The electronic specific heat is typically some 100 times larger than that found in most metals, the magnetic susceptibility can be two or more orders of magnitude larger than the temperature-independent Pauli susceptibility observed in conventional conducting materials, and, for $T \ll T_K$, $\rho = \rho_0 + AT^2$ with a large coefficient A [43]. The compensation of the magnetic moments of the f electrons by the conduction electrons via the Kondo effect leads to a non-magnetic ground state.

On the other hand, the f electrons can interact with each other via the conduction electrons, an indirect interaction referred to as Ruderman-Kittel-Kasuya-Yosida (RKKY) interaction. This RKKY interaction tends to form a magnetic state. The energy associated with the RKKY interaction is

$$k_B T_{RKKY} \sim J^2 N(E_F) \quad (3.32)$$

where T_{RKKY} is the characteristic temperature of the RKKY interaction.

In heavy-fermion materials, the evolution of ground states as a function of pressure or chemical environment is frequently discussed in terms of an intuitive model first proposed by Doniach [44]. This model considers a one-dimensional chain of Kondo impurity atoms that experience the effect of competing long-range RKKY and short-range Kondo interactions, which both depend on a coupling constant proportional to the magnetic exchange $|J|$. Because of their different functional dependencies on $|J|$, quadratic (RKKY) and exponential (Kondo), the RKKY interaction dominates for small values of $|J|$. As a consequence, the spin system orders magnetically. The Néel temperature T_N increases initially with the exchange. For modest values of $|J|$, the magnetic singlet state favored by the Kondo effect competes with long-range order, producing a maximum in T_N versus $|J|$ and, at sufficiently large $|J|$, the magnetic state is driven towards a zero-temperature transition.

The prototype heavy-fermion materials include actinide and rare-earth alloys, mostly containing U, Yb, and Ce, respectively, like CeAl₃, CeCu₆, UBe₁₃, UPt₃, etc. [45].

3.5 Non-Fermi-liquid behavior

In recent years, non-Fermi-liquid (NFL) behavior has been widely observed in heavy-fermion systems, high- T_c superconductors, d -transition-metal compounds and one-dimensional systems (see, e.g., recent reviews [46–48]). NFL behavior is observed as a non-quadratic temperature dependence of the electrical resistivity ($\rho \sim T^n$, $n < 2$), a strongly temperature-dependent electronic specific-heat coefficient γ ($\gamma \sim \log(T/T_0)$ or $\gamma \sim \gamma_0 - aT^{1/2}$) and a divergent magnetic susceptibility ($\chi \sim -\log(T/T_0)$ or $\chi \sim bT^\beta$). The divergence of the effective mass ($\sim \gamma$) indicates that Landau-Fermi-liquid theory breaks down in these situations. To understand these unusual physical properties, various theoretical models have been proposed: (1) scenario of a quantum critical point; (2) multi-channel Kondo model; (3) Kondo-disorder model; (4) the Griffiths-phase model and (5) the Luttinger-liquid model. In this section, we briefly overview the first two models which are considered to be relevant for the systems investigated in this thesis.

3.5.1 Quantum critical point (QCP) theories

In heavy-fermion compounds, NFL behavior usually occurs around a magnetic quantum critical point, at which the magnetic transition temperature is continuously tuned to zero by an external parameter δ (pressure, magnetic field, or doping). Similar to classical phase transitions at a finite temperature, quantum phase transitions are also characterized by a divergent correlation length ξ and correlation time τ , however, resulting from quantum fluctuations instead of thermal ones. ξ and τ are linked by the dynamical scaling exponent z as $\tau \sim \xi^z$ while approaching to the quantum critical point. For $T = 0$ phase transitions the finite lifetime τ of the fluctuations has to be taken into account, in contrast to finite- T transitions. This leads to an increase of the effective dimensions from d to $d + z$. Thus, a d -dimensional quantum system can be viewed as a $d + z$ -dimensional classical system, where z takes a value of 2 for antiferromagnetic and 3 for ferromagnetic fluctuations.

By utilizing the renormalization-group theory, Hertz [49] and Millis [50] investigated quantum critical phenomena in itinerant-fermion systems. Figure 3.2

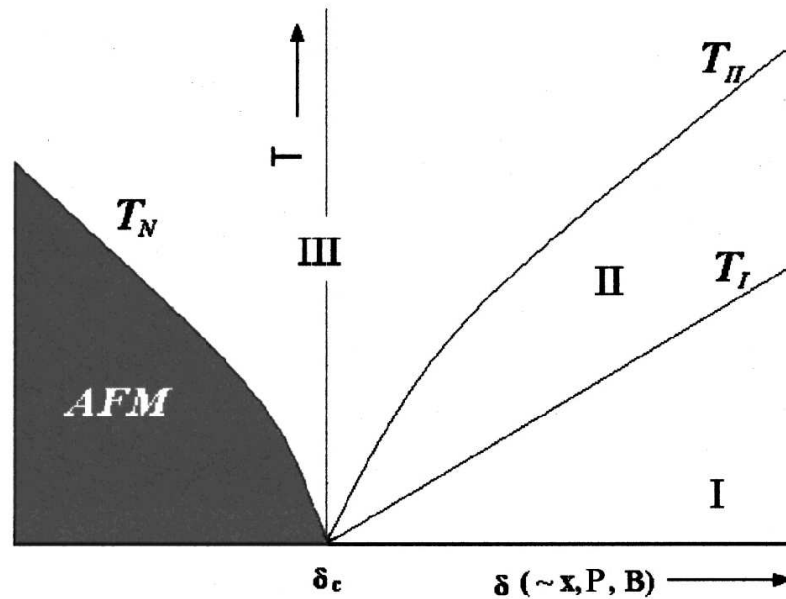


Figure 3.2: A qualitative phase diagram for a quantum critical point in the case of three-dimensional antiferromagnetic interactions [46].

illustrates a phase diagram for a three-dimensional antiferromagnetic system [50]. Regions of different behavior are separated by the crossover lines T_I and T_{II} . In the disordered phase of region I , the fluctuations on the scale ξ have an energy much larger than $k_B T$ and, therefore, are of quantum nature. Fermi-liquid behavior is expected to exist in this region. Region II is a quantum-classical crossover region, in which the fluctuation modes at the scale of ξ have energies less than $k_B T$ but ξ is still determined by $\xi^2 \sim |\delta - \delta_c|$. In region III , ξ is controlled by temperature rather than by $|\delta - \delta_c|$. Experimentally, no clear difference can be discerned between region II and region III .

Similar results were also derived within the phenomenological self-consistent renormalization model (SCR) by Moriya et al. [51], which takes into account the coupling among different modes of spin fluctuations in a self-consistent fashion. In comparison with the model studied by Millis and Hertz, a more systematic treatment of the mode-mode coupling between spin fluctuations at zero wave vector was considered in the SCR theory. Initially, the SCR theory was developed for d -electron systems. However, the behavior of many heavy-fermion compounds

is also tentatively explained within this theory.

In addition to the above theories, Lonzarich also presented a phenomenological theory of spin fluctuations at a QCP [52]. In all these models, the spontaneous spin fluctuations slow down, grow in magnitude and range, and become strongly temperature dependent as the system approaches the magnetic QCP, leading to the divergence of the dynamic susceptibility. This indicates that the concept of well-defined quasiparticles might break down at the magnetic QCP and therefore non-Fermi-liquid behavior occurs.

More recently, Rosch has studied the interplay of disorder and spin fluctuations at the quantum critical point and found that $\rho = \rho_0 + AT^n$ [53]. The exponent n is limited to the range of $1 \leq n \leq 1.5$ depending on the amount of disorder. For perfectly clean systems, one has $n = 2$. A small quantity of disorder may change the exponent n from $n = 2$ to $n = 1$ at the lowest temperature, followed by a ‘bump’-like rise and fall of n to higher temperatures. However, n tends to 1.5 as the temperature goes to zero in the dirty limit.

In Table 3.1, the main predictions of the above spin-fluctuation theories are summarized.

The theories discussed above were developed for itinerant fermion systems. Recently, it was found that $\text{CeCu}_{6-x}\text{Au}_x$ [54, 55] and $\text{YbRh}_2(\text{Si}_{1-x}\text{Ge}_x)_2$ [56, 57] display unusual properties at the quantum critical point, e.g., E/T and H/T scaling which cannot be explained within the above itinerant scenarios. To understand these new phenomena, Si et al. [58] and Coleman et al. [55, 59] have proposed another type of quantum critical scenario, the locally critical quantum phase transition. In this theory, vestiges of local moments remain as local critical moments which coexist with the long-wavelength critical fluctuations of the order parameter at the QCP. The dynamic susceptibility $\chi(q, \omega, T)$ displays an anomalous frequency and temperature dependence everywhere in the Brillouin zone:

$$\chi(q, \omega, T) = \frac{1}{f(q) + A\omega^\alpha M(\omega/T)} \quad (3.33)$$

where $f(q)$ is a non-zero smooth functional and $M(\omega/T)$ is a scaling function. The static uniform ($q = 0$) spin susceptibility has a modified Curie-Weiss form

| Theories | Physical quantities | AFM $z = 2$ $d = 3$ | AFM $z = 2$ $d = 2$ | FM $z = 3$ $d = 3$ | FM $z = 3$ $d = 2$ |
|----------|---------------------|------------------------|------------------------|-----------------------|-----------------------|
| (a) | C/T | $\gamma_0 - aT^{1/2}$ | $\log(T_0/T)$ | $\log(T_0/T)$ | $T^{-1/3}$ |
| | $\Delta\chi$ | $T^{3/2}$ | $\chi_0 - dT$ | - | - |
| | $\Delta\rho$ | $T^{3/2}$ | T | T | - |
| (b) | C/T | $\gamma_0 - aT^{1/2}$ | $-\log(T/T_0)$ | $-\log(T/T_0)$ | $T^{-1/3}$ |
| | χ_Q | $T^{-3/2}$ | $-(\log T)/T$ | $T^{-4/3}$ | $-1/T \log T$ |
| | $\Delta\rho$ | $T^{3/2}$ | T | $T^{5/3}$ | $T^{4/3}$ |
| (c) | C/T | $\gamma_0 + T^{1/2}$ | - | $-\log(T/T_0)$ | $T^{-1/3}$ |
| | $\Delta\chi$ | $T^{-3/2}$ | - | $T^{-4/3}$ | T^{-1} |
| | ρ | $T^{3/2}$ | - | $T^{5/3}$ | $T^{4/3}$ |

Table 3.1: Temperature dependence of electronic specific heat C/T , susceptibility (χ), and electrical resistivity (ρ) at a QCP derived from the spin-fluctuation theories by (a) Millis/Hertz, (b) Moriya et al., (c) Lonzarich [46].

$$\chi(T) = \frac{1}{\theta + BT^\alpha}. \quad (3.34)$$

Reflecting on experiments, one has $\chi^{-1} - \chi_0^{-1} \sim T^\alpha$ ($\alpha < 1$), which has been observed in some heavy-fermion systems as $\text{CeCu}_{5.9}\text{Au}_{0.1}$ [54, 55] and YbRh_2Si_2 [56, 57]. It was shown that the two-dimensional spin fluctuations favor such type of quantum critical point [58].

3.5.2 The single-impurity multichannel Kondo model

The multichannel Kondo model for a single impurity which was first introduced by Nozières and Blandin [60] can be written as:

$$H = \sum_{k,\sigma,m} \epsilon_k n_{k,\sigma,m} + J\vec{S} \cdot \sum_{\sigma}^m \vec{s}_{\sigma} \quad (3.35)$$

where \vec{S} and \vec{s} are the spin operators of the magnetic impurity and of the conduction electrons, respectively. The α labels are the orbital channels or the degrees of freedom of the conduction electrons. The spins of the conduction electrons near the magnetic impurity are bound together to partially or wholly compensate the impurity spin, giving rise to the following three scenarios:

(1) $m = 2S$: the impurity spin is just compensated by the conduction electron spins to form a singlet state. This gives rise to the normal Fermi-liquid behavior.

(2) $m < 2S$: The impurity spin is not fully compensated by the conduction electrons.

(3) $m > 2S$: In this case, the conduction electron spins overcompensate the impurity spin and the magnetic ion can no longer form the usual non-magnetic singlet state. But the new magnetic state can still undergo further Kondo scattering. The resulting ground state bears no resemblance to the non-interacting gas of electrons and is a local non-Fermi liquid.

The single-impurity multichannel Kondo model can be solved exactly and NFL behavior was found to exist only in the case of $m > 2S$. In the two-channel model ($m = 2$, $S = 1/2$), a single spin one half magnetic impurity interacts antiferromagnetically with two conduction electron seas (hence the two channels). These two seas do not interact with each other; they do not even experience a Pauli exclusion principle on each other. Only the magnetic impurity sees that there are two channels. Experimentally this is hard to realize, but there are claims that tunneling experiments through certain two-level systems can be modeled in a very similar way [8, 61].

The specific-heat coefficient and the magnetic susceptibility diverge at very low temperature, following

$$\frac{C}{T} = -\frac{1}{T_K} \ln \frac{T}{b_1 T_K}, \quad (3.36)$$

$$\chi \sim -\frac{1}{T_K} \ln \frac{T}{b_2 T_K}, \quad (3.37)$$

where b_1 and b_2 are constant. The electrical resistivity is

$$\rho = \rho_0 - \tilde{A} \left(\frac{T}{T_K} \right)^{1/2}. \quad (3.38)$$

It should be noted that, while the logarithmic divergence of C/T and χ appears for $T < 0.5 T_K$, $\Delta\rho = -\tilde{A}T^{1/2}$ is observable only for $T < 0.05 T_K$. In the intermediate temperature range, $\Delta\rho = -\tilde{A}T$.

Chapter 4

$\text{U}_2\text{Ru}_2\text{Sn}$

4.1 Introduction

There is a number of f -electron compounds that show narrow-gap semiconducting behavior at low temperatures, with an activation-type behavior of the electrical resistivity as function of temperature. These materials have in the literature been referred to either as Kondo insulators [27] or as heavy-fermion semiconductors [62]. In Kondo insulators, the localized f -derived magnetic moments are progressively quenched with decreasing temperature, leading to a paramagnetic ground state. Most of the Kondo insulators do not behave as ideal intrinsic semiconductors because the hybridization gap is frequently only a pseudogap and/or there are intrinsic states or impurity states in the band gap [62]. The signature of the gap formation in Kondo insulators is usually found in transport (resistivity, Hall effect, thermopower, thermal conductivity), magnetic-susceptibility and specific-heat measurements [26].

Kondo insulators can be distinguished from conventional semiconductors by the small gap of the order of 10-500 meV [27, 62], the magnetic moments accompanying excitations across the low-temperature gap [27] and the observation that the gap disappears above a characteristic temperature T^* [26]. The gap energy evaluated from electron-tunneling and optical-conductivity studies is larger than T^* [63–65]. The tunneling spectra give clear evidence for a crossover from a well-developed gap state at low temperature, to a partially gaped state at $T \sim 0.1T_K$ and to a Kondo-metallic state at $T \sim 0.2T_K$, where T_K is the Kondo temperature.

The existence of two characteristic energies distinguishes these compounds from the conventional semiconductors, where the gap closes due to thermal activation of electrons from the rigid band edges [63].

It has been shown that these materials undergo a metal-insulator transition under the effect of temperature [66], external pressure [67–69], doping [66, 67, 70, 71] and strong magnetic field [28, 72–76]. However, measurements of electrical resistance under pressure on $Ce_3Bi_4Pt_3$ show the gap being further opened upon increasing the pressure [77].

Kondo insulators are Ce, Yb, or U-based narrow-gap semiconductors, e.g., $CeNiSn$, $Ce_3Bi_4Pt_3$, YbB_{12} , $U_3Sb_4Pt_3$. The magnitude of the hybridization gap ranges for example from 3500 K in $TmTe$, to 1200 K in $U_3Ni_3Sb_4$, to 42 K in $Ce_3Bi_4Pt_3$ and to as low as 10 K in $CeNiSn$ [62].

The cubic systems $Ce_3Bi_4Pt_3$, SmB_6 , YbB_{12} and the orthorhombic ones $CeNiSn$ and $CeRhSb$ have been most thoroughly investigated [26, 62, 78–80]. Earlier samples of $CeNiSn$ and $CeRhSb$ with the orthorhombic $TiNiSi$ -type structure showed semiconducting behavior in the resistivity. However, the semiconducting behavior of $CeNiSn$ has turned into metal-like behavior as the sample quality was improved [80]. This is not the case for the cubic compounds YbB_{12} , $Ce_3Bi_4Pt_3$ and $U_3Sb_4Pt_3$ where the resistivity, for good single crystals, increases by several orders of magnitude as the temperature decreases [67, 77, 81, 82]. The significant difference in the low-energy excitations between the orthorhombic systems and the cubic ones was first pointed out by NMR measurements of the spin-lattice relaxation rate $1/T_1$. For both $CeNiSn$ and $CeRhSb$, $1/T_1$ is proportional to T^3 [83], as opposed to the exponential behavior in YbB_{12} [78] and $Ce_3Bi_4Pt_3$ [84]. A T^3 -dependence in $1/T_1$ has been reproduced theoretically using a gap with a V-shape structure. This means that the quasiparticle density of states is linearly proportional to the energy near the Fermi level at low temperatures [85]. An exponential behavior of $1/T_1$, on the other hand, is consistent with the formation of a gap where the density of states is zero within the energy gap at low temperatures [78, 85].

The uranium-based Kondo insulators are, in general, cubic systems with gaps in the range from 500 K for $U_3Sb_4Pt_3$ [67], to 1400 K for $UNiSn$ [86–89], to 1740 K for $U_3Pt_3Sb_4$ [90], to 2320 K for $U_3Ni_3Sb_4$ [90], to 2668 K for $U_3Pd_3Sb_4$ [90],

to 3945 K for UPtSn [87], and to as high as 5000 K for URhSb [87]. Among uranium-based Kondo insulators, the compound U_2Ru_2Sn investigated here is the first tetragonal Kondo insulator, with an energy gap of only around 160 K [91, 92]. The physical properties of U_2Ru_2Sn will be discussed in detail in the next section.

The investigation of Kondo insulators by means of thermal-transport measurements is, on one hand, motivated by the desire to improve the understanding of the physical properties, e.g., to clarify the origin of the energy-gap formation and, on the other hand, to determine whether they could be used as thermoelectric materials for refrigeration applications.

Thermoelectric refrigeration is currently attracting renewed interest because of the increasing need for a portable refrigerator without the use of refrigerants [4]. Conventional narrow-gap semiconductors have been intensively studied over the last decades for such propose and Bi_2Te_3 and its alloys are found to be the most efficient materials at room temperature (highest figure of merit). The performance efficiency of thermoelectric materials is determined by the dimensionless figure of merit $ZT = TS^2\sigma/\kappa$, where S is the thermopower, σ is the electrical conductivity and κ is the thermal conductivity. For a good thermoelectric material, one needs a low thermal conductivity but a high electrical electrical conductivity and a high thermopower. Recently, materials with high values of $|S|$ were found among the Kondo insulators. Kondo insulators exhibit large thermopower values at temperatures below T^* , due to the opening of the gap in the density of states [93]. The relationship between the large thermopower and the opening of the gap was confirmed by measurements of Kondo insulators under doping [70, 71, 94, 95] or in high magnetic fields [72]; both are known to close the gap. For example, YbB_{12} which has an energy gap of the order of 100 K shows $|S_{max}| \sim 140 \mu V/K$ at around 100 K, and the only transition-metal based Kondo insulator FeSi exhibits $|S_{max}| \sim 500 \mu V/K$ at $T = 50$ K. The fact that many Kondo insulators have characteristic temperatures below room temperature and thus display large maxima in $S(T)$ below room temperature makes them promising candidates for low-temperature cooling applications [10, 96].

The characteristic feature of the thermal conductivity $\kappa(T)$ of Kondo insulators is a pronounced increase of $\kappa(T)$ upon lowering the temperature below T^* . It

is believed to be related to the gap opening: the large enhancement of the phonon dominated thermal conductivity is due to the enhancement of the phonon lifetime τ_{ph} as a result of the reduction of the number of the charge carriers, which act as scattering centers for the phonons at high temperatures [11, 70, 79, 97]. As for the thermopower, the relationship between the enhancement of the thermal conductivity and the opening of the gap was confirmed by measurements of Kondo insulators under doping [70, 94, 98] and in high magnetic fields [72].

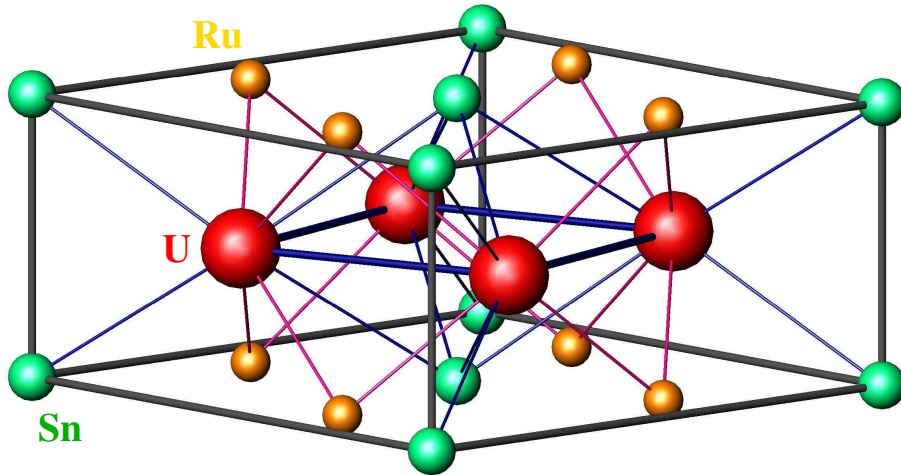
In this chapter thermal-transport measurements of $\text{U}_2\text{Ru}_2\text{Sn}$ are presented at low temperatures and in different magnetic fields. The continuation of the measurements to higher temperatures will be presented in another PhD thesis [99].

4.2 Physical properties

The first evidence for semiconducting behavior of $\text{U}_2\text{Ru}_2\text{Sn}$ was provided by the temperature dependence of the electrical resistivity. Below 30 K, the resistivity of polycrystalline samples was reported to increase with decreasing temperature in a thermally activated manner [100]. Magnetic susceptibility, specific-heat, and NMR measurements are all consistent with the existence of a gap of around 160 K [91, 92]. Recent inelastic neutron-scattering measurements using high-energy incident neutrons, however, were taken as evidence for the formation of a spin gap of around 800 K [101]. Big discrepancies in energy-gap values extracted from different experiments have also been observed for other Kondo insulators. E.g., for $\text{Ce}_3\text{Bi}_4\text{Pt}_3$ the energy gap ranges from 50 K as extracted from electrical resistivity and thermopower measurements [66, 102] to 100 K as extracted from neutron-scattering measurements [103] and for CeNiSn the energy gap ranges from 10 K as extracted from resistivity measurements [80, 103] to 25 K as extracted from neutron-scattering measurements [104].

$\text{U}_2\text{Ru}_2\text{Sn}$ crystallizes in the tetragonal $P4/mbm$ structure ($a = 7.500(1)$ Å, $c = 3.563(1)$ Å) (cf. Fig. 4.1), which is an ordered version of the U_3Si_2 -type structure [105].

The magnetic susceptibility $\chi(T)$ measured on a single-crystalline sample along two crystallographic directions shows anisotropy, with the c axis identi-

Figure 4.1: Crystal structure of U_2Ru_2Sn

fied as the magnetic easy axis [cf. Fig. 4.2(a)]. $\chi(T)$ shows a broad maximum at around 160 K and decreases strongly at lower temperatures, which indicates the opening of an energy gap at approximately this temperature [91].

Figure 4.2(b) shows the specific heat $C(T)$ of a single crystal of U_2Ru_2Sn and of a polycrystal of the non- f reference compound Th_2Ru_2Sn . The difference between the U_2Ru_2Sn and the Th_2Ru_2Sn data was attributed to a magnetic contribution to $C(T)$ because, in this range of temperature, the sample dependence and electronic contributions to $C(T)$ are not important. The magnetic contribution to the specific heat was fitted by a simple Schottky-type anomaly, with a spacing between the two levels of around 150-160 K. From 300 mK to 3 K, $C(T)$ of the U_2Ru_2Sn single crystal is well described by $C(T) = 26.3 \text{ mJ/molK}^2 \times T + 0.73 \text{ mJ/molK}^4 \times T^3$ (data not shown) [106]. Using the phonon term of the specific heat, the Debye temperature θ_D is estimated as $\theta_D = 240 \text{ K}$.

Also, the electrical resistivity $\rho(T)$ of U_2Ru_2Sn , measured along two crystallographic directions (cf. Fig. 4.3 (a)), is anisotropic. $\rho(T)$ shows a (local) maximum at around 130 K and drops strongly below that temperature. This drop was associated with the onset of coherence among the regularly spaced U derived magnetic moments [107]. Below the temperature of the minimum at around 30 K, $\rho(T)$ shows an upturn and tends to saturate at temperatures below 10 K.

In Fig. 4.3(b) the temperature dependence of the Hall coefficient $R_H(T)$ is

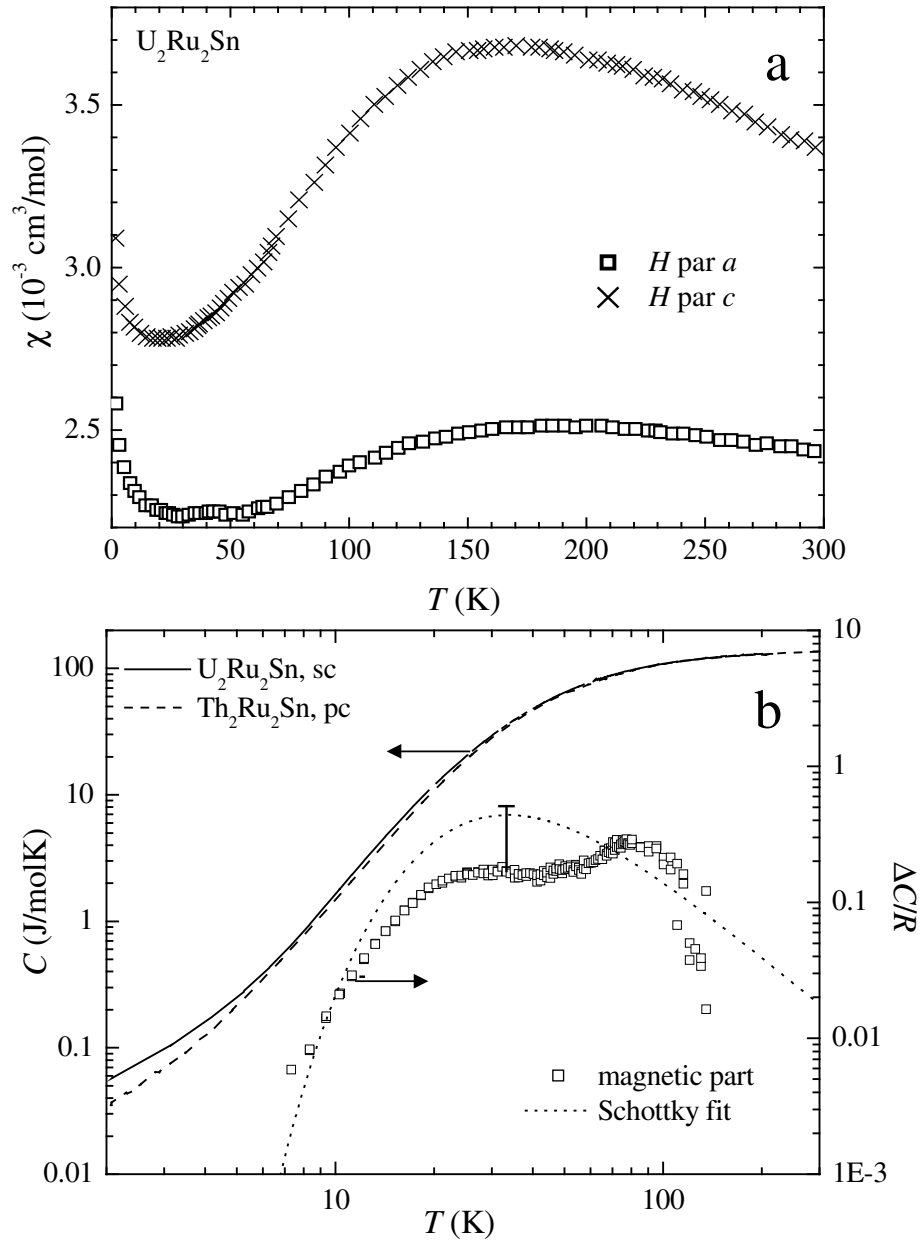


Figure 4.2: (a) Temperature dependence of the magnetic susceptibility, $\chi(T)$, of a single crystal with the magnetic field H along either the a or the c axis, in an applied magnetic field of 1 T. Modified from [91]. (b) Temperature dependence of the specific heat, $C(T)$. Left scale: $C(T)$ of a single crystal of U_2Ru_2Sn and of a polycrystal of Th_2Ru_2Sn . Right scale: Difference of the U_2Ru_2Sn and Th_2Ru_2Sn data, ΔC , in units of the gas constant R vs temperature T . The dotted curve shows the best Schottky fit. Modified from [91].

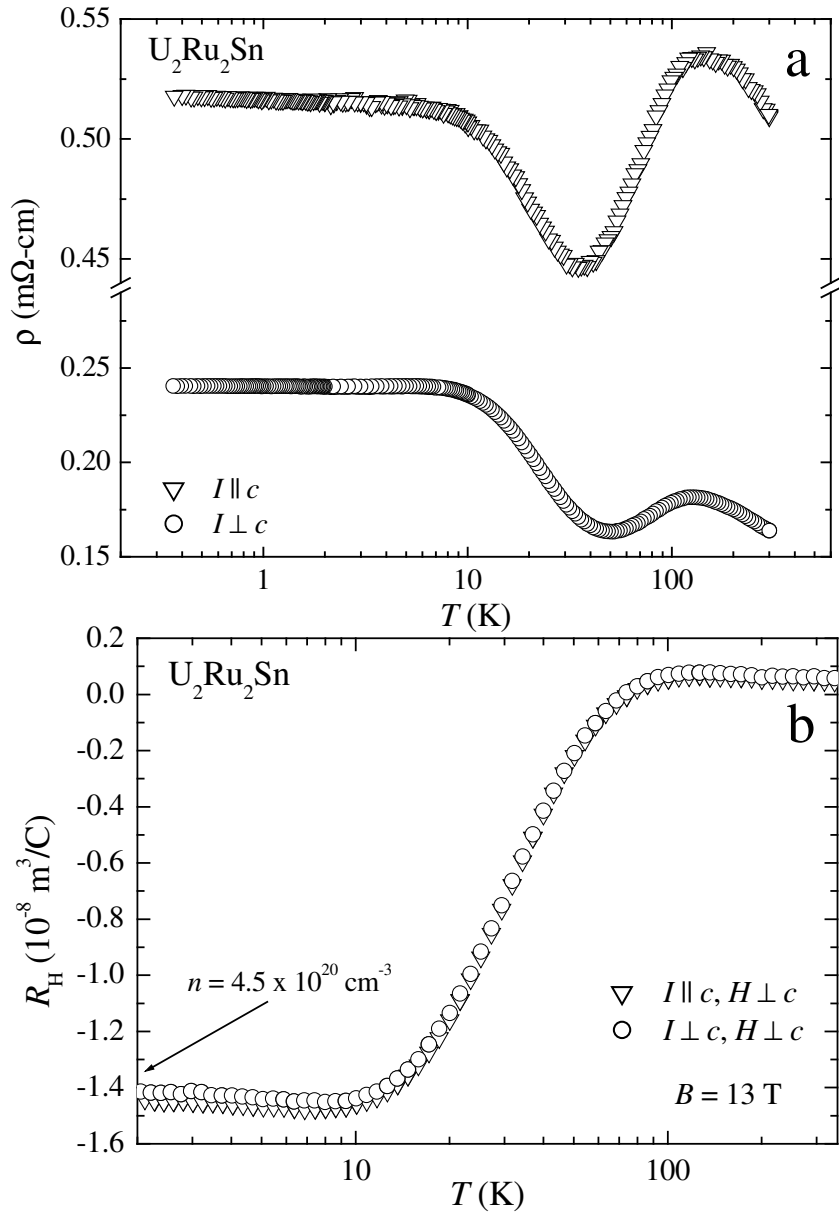


Figure 4.3: (a) Electrical resistivity as a function of temperature, $\rho(T)$, with the current, I , along and perpendicular to c . (b) Temperature dependence of the Hall coefficient, $R_H(T)$, with I either along or perpendicular to the c axis and with H perpendicular to the c axis. Data unpublished [106].

shown, with the electrical current I either along or perpendicular to the c axis and with the magnetic field H perpendicular to the c axis. $R_H(T)$ is isotropic with large absolute values at low temperatures. Thus, together with $\rho(T)$, an anisotropic Hall mobility ($\mu_H = R_H/\rho$), with higher mobility for $I \perp c$, follows. The charge-carrier concentration n , determined assuming a simple one-band model ($R_H = 1/ne$), was found to be $n = 4.5 \times 10^{20} \text{cm}^{-3}$ at 2 K [106].

4.3 Results and discussion

The measurements presented here were performed on phase-pure bars of approximately $2 \text{ mm} \times 1 \text{ mm} \times 0.3 \text{ mm}$ cut from a single crystal grown in a four-mirror furnace. These samples were provided by Professor John Mydosh. Thermopower and thermal conductivity were measured with the heat current \dot{Q} along and perpendicular to the c axis.

4.3.1 Thermopower

Figure 4.4 shows the temperature dependence of the thermopower $S(T)$ along and perpendicular to c in zero field and in 6 T. For both directions, $S(T)$ shows a behavior linear in T . For $\dot{Q} \parallel c$, $S(T)$ is positive while for $\dot{Q} \perp c$ it is negative. This linear behavior is attributed to the diffusion thermopower, since other contributions to $S(T)$ such as the phonon drag are expected to be negligible in the temperature range investigated here. The phonon-drag mechanism is important in the temperature range $(0.1-0.2) \times \theta_D$ which is, in our case, in the temperature range between 20 and 40 K. A linear behavior of $S(T)$ has also been observed in CeNiSn below 1 K [72], and in FeSi and YbB₁₂ at low temperatures [70, 71] and it was predicted theoretically by T. Saso [96]. Whether this behavior is intrinsic to Kondo insulators or due to nonstoichiometry/impurities remains to be clarified [10]. Surprising at first sight are the different signs of S for both crystallographic directions since Hall-effect measurements [106] yield electron-like carriers for both directions. However, the sign of S is, according to the Mott relation (Eq. 3.7), determined by the product of the sign of the charge carriers and the sign of the logarithmic derivative of the electrical conductivity $\sigma(\varepsilon)$ with respect to energy ε

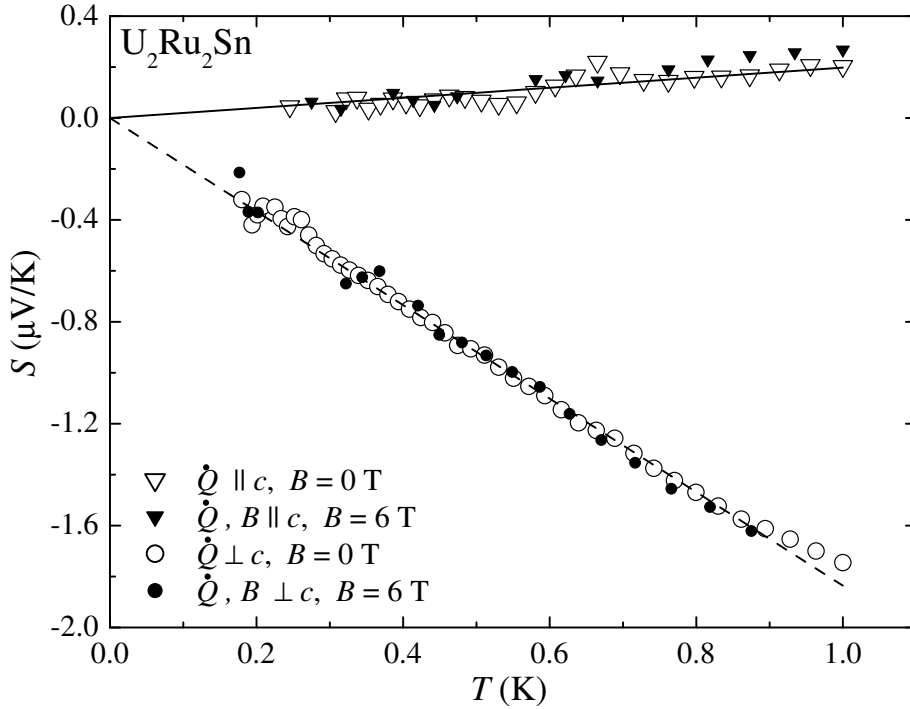


Figure 4.4: Thermopower as a function of temperature, $S(T)$, of $\text{U}_2\text{Ru}_2\text{Sn}$ with the magnetic field B along and perpendicular to the c axis, in fields of 0 and 6 T. The solid and dashed lines represent best linear fits to the data.

at the Fermi level [6]. Since from Hall-effect measurements the sign of the charge carriers is negative for both directions, the opposite sign of S must be due to different signs of the derivative of $\sigma(\varepsilon)$ at the Fermi level. This indicates that there is an anisotropy in the density of states in the Fermi level. Also in CeNiSn and CeRhSb , R_H and S do not have the same sign. R_H for CeNiSn becomes negative at temperatures below 5 K while S stays positive. For CeRhSb , S becomes negative below 5 K while R_H remains positive [82].

Combining the thermopower results with the charge-carrier concentration n ($n = 4.5 \times 10^{20} \text{ cm}^{-3}$ at 2 K, independent of direction) estimated from the Hall-effect measurements [106] in a one-band model, one may estimate the effective mass m^* of the charge carriers. For $\dot{Q} \parallel c$, m^* is $2m_0$ while for $\dot{Q} \perp c$ we obtain $m^* = 16m_0$, where m_0 is the free-electron mass. The same trend of a larger residual density of states for the direction perpendicular to c is suggested from recent Knight-shift experiments [108]. The origin of this remarkable anisotropy

remains to be understood.

$S(T)$ does, in fields up to 6 T, not present any magnetic-field dependence in the temperature range investigated (cf. Fig. 4.4). This is plausible since the temperature equivalent of 6 T is approximately 6 K, which is much smaller than the energy-gap temperature of 160 K. In several other Kondo insulators the field-induced insulator to metal transition occurs at a critical field which is of the order of the gap-opening temperature. The gap decreases progressively under applied magnetic field until, at the critical field, the gap vanishes. This is believed to be due to the up- and down-spin bands being shifted by the Zeeman effect [34, 75, 89].

4.3.2 Thermal conductivity

Figure 4.5 shows the temperature dependence of the thermal conductivity $\kappa(T)$ of $\text{U}_2\text{Ru}_2\text{Sn}$ along and perpendicular to c in magnetic fields B applied parallel to the heat current \dot{Q} . As for $S(T)$, $\kappa(T)$ does not present any change under an applied magnetic field of 6 T.

Comparing our data with previous results of $\kappa(T)$ on polycrystalline samples [109], the agreement in the overlapping temperature range is within experimental error. The electronic contribution to the thermal conductivity κ_e^{WF} may be estimated from the electrical resistivity (cf. Fig. 4.3(a)) measured on the same samples between 350 mK and 10 K using the Wiedemann-Franz law (Eq. 3.12). For temperatures below 350 mK, the resistivity was extrapolated from the measured values. As may be seen in Fig. 4.5, κ_e^{WF} is distinctly smaller than the measured total $\kappa(T)$ (cf. solid line for $\dot{Q} \parallel c$ and dashed line $\dot{Q} \perp c$). The phonon contribution due to boundary scattering $\kappa_{ph}^{Casimir}$ is estimated using the kinetic gas equation (Eq. 3.13), with the low-temperature lattice specific heat $C_{ph} = 0.73 \text{ mJ/molK}^4 \times T^3$, the sound velocity $v_{ph} = 2189 \text{ m/s}$ (Eq. 3.15) taking $\theta_D = 240 \text{ K}$ calculated from C_{ph} at temperatures below 3 K [106], and by taking the smallest dimensions of both samples ($\approx 0.3 \text{ mm}$) for the phonon mean-free path (cf. dotted line). $\kappa_{ph}^{Casimir}$ is much larger than the total measured $\kappa(T)$. Thus, the phonons appear to be subject to an additional scattering mechanism. We may estimate the total phonon contribution as $\kappa_{ph}(T) = \kappa(T) - \kappa_e^{WF}(T)$. Below 400

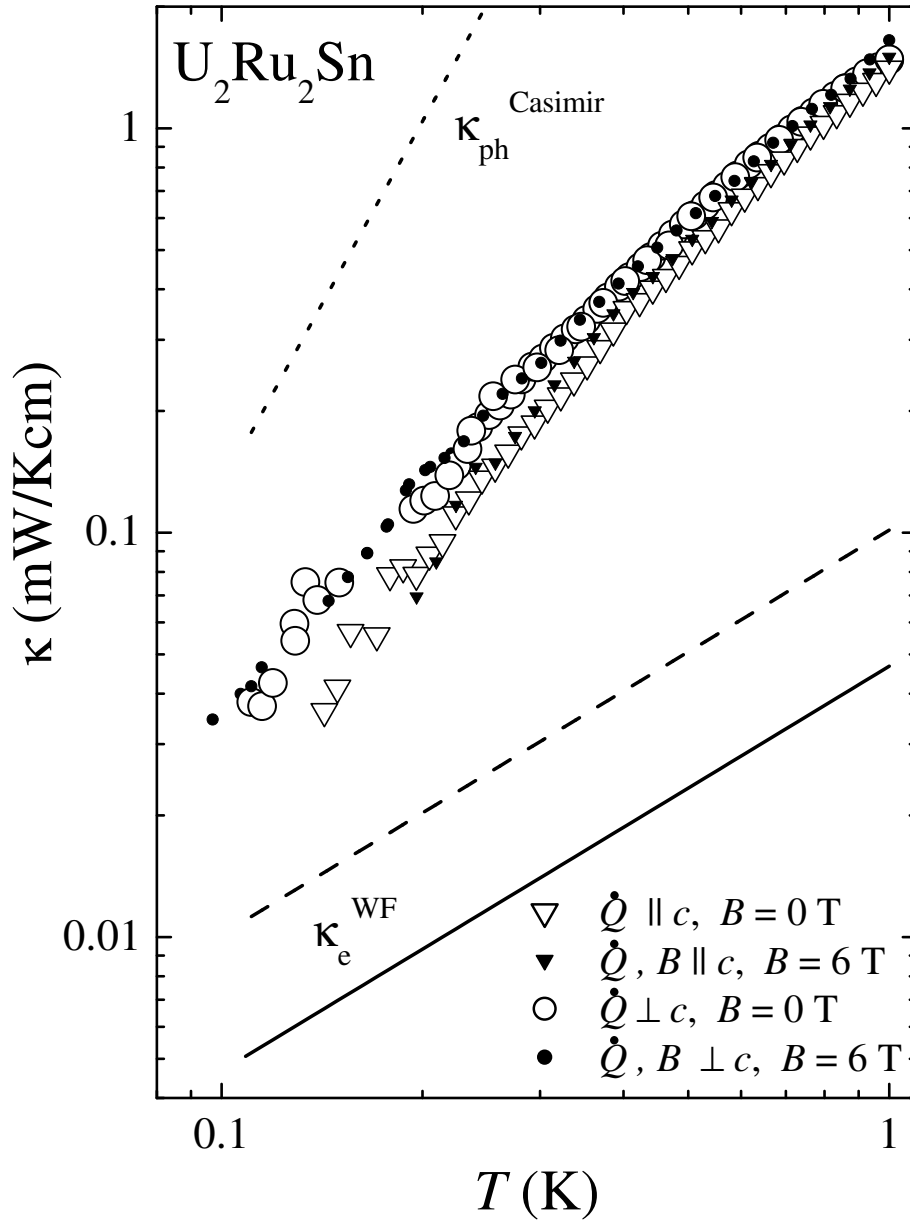


Figure 4.5: Temperature dependence of the thermal conductivity, $\kappa(T)$, of U_2Ru_2Sn with the magnetic field B along and perpendicular to the c axis, in fields of 0 and 6 T. The solid and dashed lines represent the electronic contribution calculated using the Wiedemann-Franz law, κ_e^{WF} , for $\dot{Q} \parallel c$ and $\dot{Q} \perp c$, respectively. The dotted line is the phonon contribution due to boundary scattering, $\kappa_{ph}^{Casimir}$.

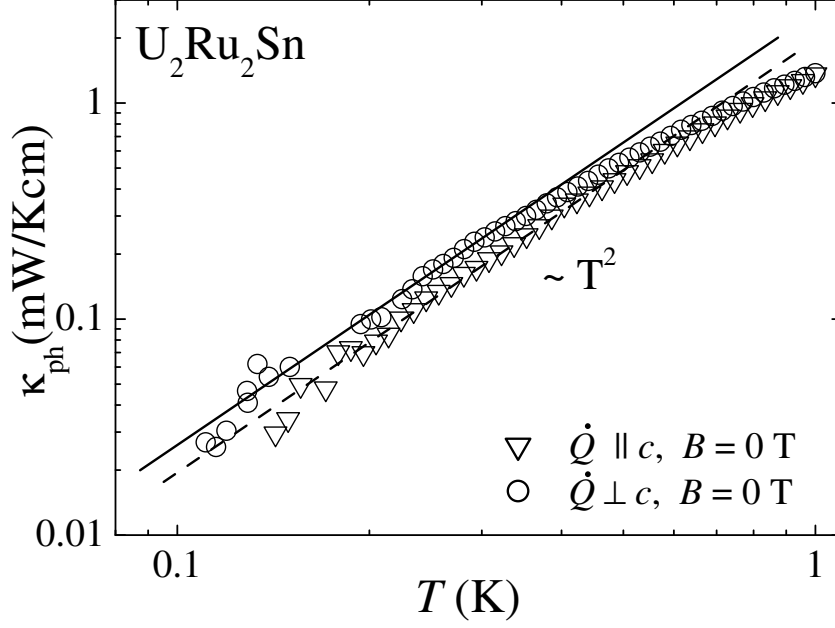


Figure 4.6: Temperature dependence of the phonon thermal conductivity, $\kappa_{ph}(T)$ of U_2Ru_2Sn along and perpendicular to the c axis. The dashed and solid lines show the temperature range where a T^2 dependence holds for $\dot{Q} \parallel c$ and $\dot{Q} \perp c$, respectively.

mK, $\kappa_{ph}(T)$ is well approximated by a T^2 law for both crystallographic directions (cf. Fig. 4.6). This temperature dependence can be attributed to scattering of phonons from charge carriers [5]. The slight tendency to a higher power law at temperatures below 200 mK may indicate a crossover to the boundary-scattering mechanism at lower temperatures. The approximate $T^{1.8}$ power law at $T > 400$ mK may indicate that additional scattering mechanisms become important here. The reduced Lorenz number L/L_0 , where $L = \rho\kappa/T$, decreases with decreasing temperature for both crystallographic directions from about 30 for $\dot{Q} \parallel c$ and 14 for $\dot{Q} \perp c$ at 1 K to about 9 for $\dot{Q} \parallel c$ and 5 for $\dot{Q} \perp c$ at 0.2 K, in agreement with $\kappa(T)$ being phonon dominated in the entire temperature range investigated here.

The process of scattering of phonons from charge carriers is usually negligible if the product of the charge-carrier mean-free path l_e and the wave number of the dominating phonons q_{dom} is less than 1 (Pippard ineffectiveness condition) [23]. Combining resistivity results with the charge-carrier concentration n at 2 K from Hall-effect measurements, we find $l_e q_{dom} = 1.9$ for $\dot{Q} \parallel c$ and $l_e q_{dom} = 4.1$ for $\dot{Q} \perp c$

c , confirming that phonon-charge-carrier scattering may indeed be the dominant process here. Using the Ziman model for phonon-electron scattering [22], and the effective masses calculated using the one-band model for the thermopower, it is possible to estimate the deformation potential E_{def} , a measure of the strength of the phonon-electron interaction. For $\text{U}_2\text{Ru}_2\text{Sn}$, E_{def} is 1.44 eV for $\dot{Q} \parallel c$ and 0.16 eV for $\dot{Q} \perp c$. These values of E_{def} are comparable with values of a normal semiconductors with similar n [110, 111].

4.4 Outlook

- In order to clarify whether the observed thermal-transport behavior is intrinsic to $\text{U}_2\text{Ru}_2\text{Sn}$ or related to unavoidable residual impurities, measurements on samples of different qualities and/or on doped samples should be performed.
- Thermal-conductivity and thermopower measurements above 1 K should be performed for a set of single crystals and in different magnetic fields to study the behavior of the energy-gap formation in this compound.

Chapter 5

$\text{Yb}_4(\text{As}_{0.7}\text{P}_{0.3})_3$

5.1 Introduction

One- and two-dimensional quantum spin systems have received considerable attention during the past decade both from a theoretical and an experimental point of view. A considerable amount of research has been carried out since the discovery of high- T_c superconductivity in layered cuprates. This is because of the proposal of a quantum spin liquid as a possible origin of the exotic properties of high- T_c superconductors [112]. The parent cuprate insulators are now considered the best example of planar spin 1/2 antiferromagnets with isotropic and predominantly nearest-neighbor coupling. They show simple long-range antiferromagnetic order at low temperatures in agreement with the prediction for the $S = 1/2$ antiferromagnetic Heisenberg model on a two-dimensional square lattice [113, 114]. Due to the investigations of the two-dimensional superconducting cuprates and the search for related transition-metal oxides a fascinating field of copper oxide compounds, vanadates, manganites, and nickelates opened [115–120].

The theory of magnetism in one dimension, on the other hand, has a history reaching back to the origin of quantum mechanics. This is due to the fact that many problems of a spin chain can be solved either analytically or numerically [121]. There is a considerable theoretical interest in one-dimensional Heisenberg spin-1/2 systems because they exhibit a number of properties that are entirely dominated by quantum-mechanical behavior and have no analogue

in three-dimensional systems. The properties of the $S = 1/2$ Heisenberg antiferromagnetic model in one dimension are well known. The model is defined by the Hamiltonian $H = J \sum_{\langle i,j \rangle} \vec{S}_i \cdot \vec{S}_j$ where i labels lattice sites where spin-1/2 operators \vec{S}_i are located, $\langle i, j \rangle$ denotes nearest-neighbors sites, and $J (>0)$ is the antiferromagnetic exchange coupling that provides the energy scale to the problem [122]. A famous solution found by Bethe showed that quantum fluctuations prevent true long-range antiferromagnetic order, giving instead a slow decay of the spin correlations at a rate that varies essentially inversely with the separation between the spins. Uniform one-dimensional spin systems have no spin gap [123].

The dimension of the spins and the spin value determine the nature of ground states and elementary excitations of quantum spin systems. In contrast to a classical three-dimensional system, low-dimensional spin systems with exotic exchange topology and/or geometrical frustration show a variety of possible ground states: Superconductivity, spin-density waves, charge order, or spin-Peierls are just a selection of the possible ground states [114–116, 124–126]. Understanding these effects is the most intriguing challenge at present. These compounds show effects of strong electronic correlations and magnetism in low-dimension. Thus spin dynamics are expected to be closely related to charge, orbital, and lattice degrees of freedom [115, 116].

Usually the magnetic excitations of these spin systems are experimentally studied by spectroscopic techniques or thermodynamic quantities that provide information on the magnetic ground state and the excitation spectra. In principle, dispersive magnetic excitations should also contribute to transport properties, e.g., to the thermal conductivity. The experimental investigation of the magnon heat transport can give interesting information on the magnetic excitations, e.g., on the dissipation and scattering of magnons [126, 127].

It has been shown that the Heisenberg $S = 1/2$ chain represents an integrable system characterized by a macroscopic number of conservation laws. One important conserved quantity is the energy current, implying an ideal (infinite) thermal conductivity along the chains at nonzero temperatures, if perturbations from impurities, phonons, or interchain coupling, which always leads to nonintegrable models, are negligible [128]. It is an open question, to what extent a real material may be regarded as an ideal integrable system [129]. Probably the

most obvious evidence for the predicted anomalous (infinite) heat transport is the observation of an unusually high quasi-one-dimensional magnon thermal conductivity in the series $(\text{Sr,Ca,La})_{14}\text{Cu}_{24}\text{O}_{41}$ [7, 117, 130]. However, this anomalous behavior has not yet been explained. Some theoretical calculations have suggested that the magnetic energy transport tends to be ballistic (dissipationless) in low-dimensional spin systems, leading to an infinite value of the magnon thermal conductivity [119, 131–133].

A large number of studies of thermal heat conductivity in low-dimensional spin systems has been performed and magnetic contributions to the thermal conductivity are discussed in low-dimensional spin systems such as the spin-Peierls compound CuGeO_3 [134, 135], the model Heisenberg spin-1/2 chain cuprates Sr_2CuO_3 [136], SrCuO_3 and SrCuO_2 [127], the four-leg spin-ladder system $\text{La}_2\text{Cu}_2\text{O}_5$ [137], in quasi two-dimensional spin systems [138] as well as in two-dimensional cuprates [139, 140]. However, in many compounds the interpretation of the data is controversial, since a clear discrimination of the different contributions to the thermal conductivity is difficult or even impossible [127, 141].

In this chapter, thermal-conductivity measurements of the one-dimensional $S = 1/2$ antiferromagnet $\text{Yb}_4(\text{As}_{0.7}\text{P}_{0.3})_3$ at low temperatures and in different magnetic fields are presented. The thermal conductivity of $\text{Yb}_4(\text{As}_{0.7}\text{P}_{0.3})_3$ will be compared with the thermal conductivity of the pure compound, Yb_4As_3 , in order to show that the low-temperature thermal conductivity is essentially unaffected by the dramatic reduction of the charge-carrier concentration that occurs upon doping Yb_4As_3 with P, putting the earlier interpretation of magnon dominated heat transport in Yb_4As_3 [142] on a firmer ground.

5.2 Physical properties

5.2.1 Physical properties at $B = 0$

Yb_4As_3 behaves as an ordinary metal at room temperature, where it has the anti- Th_3P_4 -type cubic crystal structure (space group $I\bar{4}3d$). The arrangement of the Yb sites can be viewed as being aligned on four families of interpenetrating chains oriented parallel to the space diagonal of a cube. Chemical-valence counting

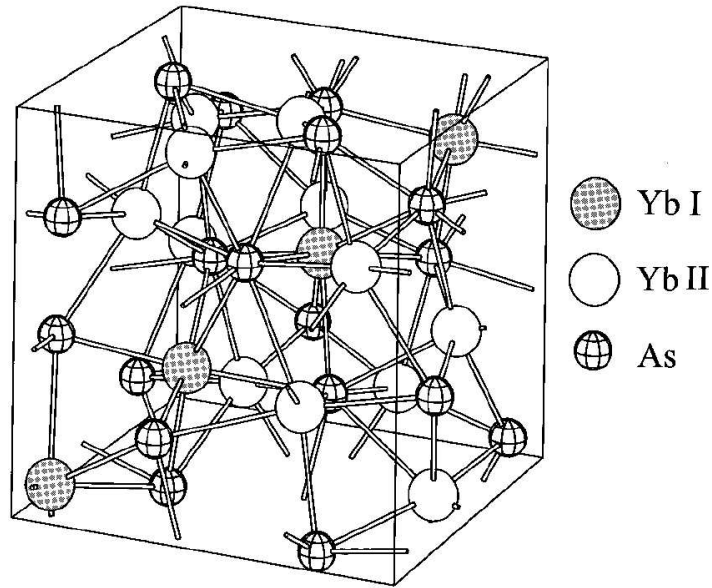


Figure 5.1: Crystal structure of Yb_4As_3 in the trigonal phase at $T < 295$ K. Yb_I are Yb^{3+} ions and Yb_{II} are Yb^{2+} ions [144].

assuming that the As-ions are trivalent shows that three quarter of the Yb-ions have valency 2+, and one quarter valency 3+. In the high-temperature phase, which is stable above 295 K, all Yb sites are equivalent, and the holes in the f shells are moving between the Yb ions due to hybridization with the As-4*p* holes. The compound is in a metallic intermediate-valent state with an average valence of Yb of 2.25+. At 295 K, Yb_4As_3 undergoes a first-order structural phase transition: Yb_4As_3 shrinks along one of the four equivalent chain directions, resulting in a trigonal structure with $\alpha = 90.8^\circ$ (space group $R3c$) (cf. Fig. 5.1) [143]. Along with the transition to the trigonal phase, various quantities (e.g., resistivity, Hall coefficient) present discontinuities.

In the trigonal phase, the electronic state of Yb_4As_3 is quite unusual. The magnetic susceptibility $\chi(T)$ of the compound shows Curie-Weiss behavior at high temperatures but a tendency of saturation is seen below 20 K. Below 7 K $\chi(T)$ increases again steeply and the value extrapolated to zero is rather large (cf. Fig. 5.2). However, the compound exhibits no long-range magnetic ordering down to at least 0.045 K [145]. Between 0.5 and 8 K, the specific heat is dominated by a

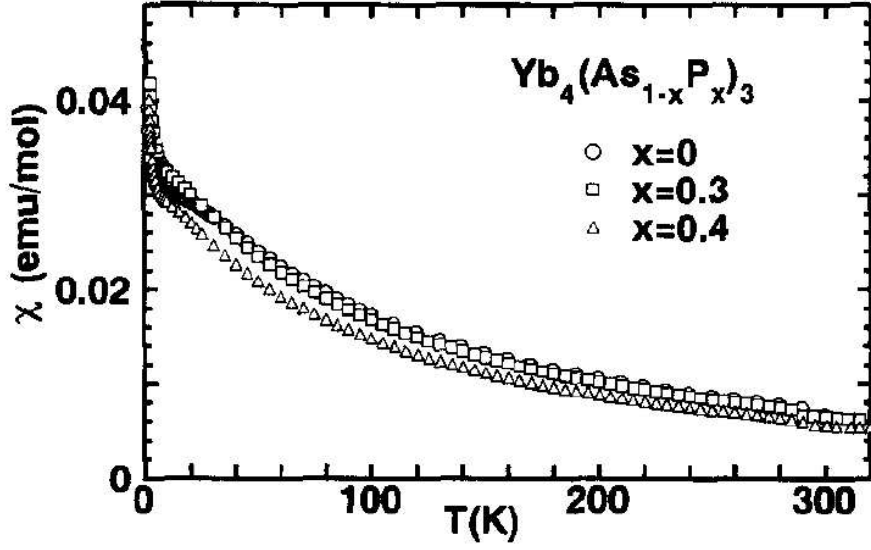


Figure 5.2: Temperature dependence of the magnetic susceptibility, $\chi(T)$, of $\text{Yb}_4(\text{As}_{1-x}\text{P}_x)_3$ [148].

linear-in-temperature term, $C = \gamma T$, with $\gamma \sim 200 \text{ mJ/molK}^2$ (see Fig. 5.3). Due to this large value Yb_4As_3 was originally classified as a heavy-fermion compound [146, 147]. Also, for $4 \text{ K} < T < 100 \text{ K}$, the electrical resistivity of Yb_4As_3 exhibits a temperature dependence that can be described well by $\rho(T) = \rho_0 + AT^2$, with a strongly enhanced A -coefficient ($A = 0.75 \mu\Omega \text{ cm/K}^2$). Above 100 K, a $-\ln T$ dependence in the electrical resistivity in the trigonal phase is observed (cf. Fig. 5.4). The γ value versus susceptibility at about 10 K, where it shows a shoulder, as well as the A value versus γ^2 at low temperatures lie on the same lines as those of typical heavy-fermion materials [146].

The temperature dependence of the Hall coefficient R_H is shown in Fig. 5.5. The charge-carrier concentration n , estimated from the Hall coefficient at 4.2 K by assuming a one-band model is $7 \times 10^{18} \text{ cm}^{-3}$ corresponding to about one charge carrier per 10^3 Yb ions. These carriers consist mainly of As p -holes with a low effective mass [146]. Such a low charge-carrier concentration may be judged insufficient to screen the $4f$ moments. Thus, no heavy quasiparticles can be formed at E_F , implying that the standard Kondo picture for the origin of the low-energy excitations of “heavy-fermion” metals can not be applied.

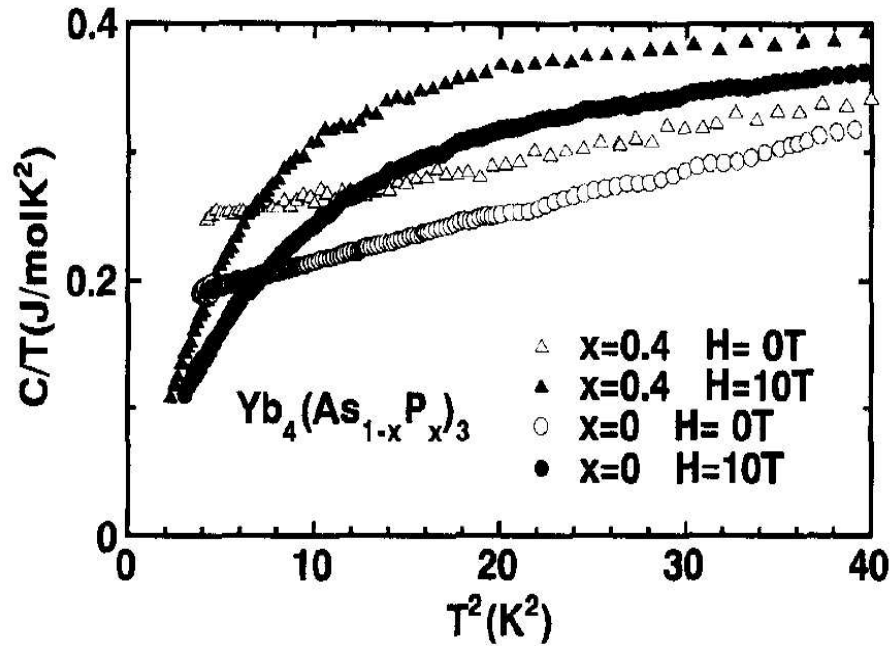


Figure 5.3: Specific heat C plotted as C/T as a function of T^2 of $\text{Yb}_4(\text{As}_{1-x}\text{P}_x)_3$ [148].

Magnetic-susceptibility [146], Mössbauer [145], and perturbed angular-correlation [149] measurements suggest that the structural phase transition is accompanied by charge ordering from a valence fluctuating state in the cubic phase to a charge-ordered state in the trigonal phase. Figure 5.1 illustrates the expected charge ordering in Yb_4As_3 . With the trigonal distortion, the distance between Yb atoms becomes shorter in the chain along one $\langle 111 \rangle$ axis and longer in the other three chains. It has been suggested [146] that the charge order in Yb_4As_3 is such that the Yb ions in the short chain (Yb_I) become trivalent, whereas those in the long chain (Yb_{II}) become divalent. Polarized-neutron measurements reveal that the charge ordering in Yb_4As_3 is nearly perfect. However, there is still a small amount of magnetic moments at the Yb_{II} sites which behave as those of magnetically isolated Yb ions. The polarized-neutron experiments also revealed that the increase of the susceptibility below 7 K is not due to an impurity effect but is a bulk property [150, 151].

Inelastic neutron-scattering experiments revealed low-energy magnetic excita-

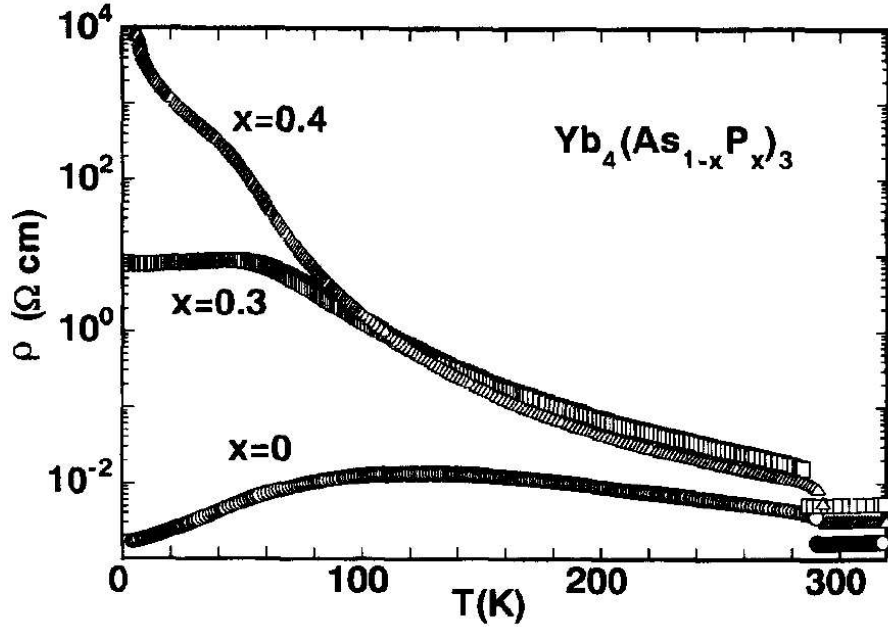


Figure 5.4: Temperature dependence of the resistivity, $\rho(T)$, of $\text{Yb}_4(\text{As}_{1-x}\text{P}_x)_3$. Logarithmic scale in Y-axis [148].

tions which were attributed to antiferromagnetic coupling within the Yb^{+3} chains [144]. Furthermore, these experiments [144] have demonstrated that the magnetic excitations are well described by means of a one-dimensional isotropic Heisenberg chain, i.e., by a des Cloiseaux-Pearson spectrum [152], $\epsilon(q) = \frac{1}{2}\pi J_{eff} |\sin q|$, $-\pi \leq q \leq \pi$ and $J_{eff}/k_B \approx 25$ K. It was found that this model explains the value of C/T at low temperatures, as well as the enhanced susceptibility of Yb_4As_3 . The steep upturn of the susceptibility below 7 K and the T^2 dependence of the resistivity cannot be explained with the simple Heisenberg model. These results suggest that the heavy-fermion-like behavior in Yb_4As_3 is closely related to the formation of Yb^{+3} chains caused by the charge ordering rather than being due to the Kondo effect [144]. As mentioned above, the small charge-carrier concentration is also incompatible with the standard Kondo picture [142].

To confirm this proposal the charge-carrier concentration was changed by doping Yb_4As_3 with P and Sb. With increasing concentration x of P, the electrical resistivity of $\text{Yb}_4(\text{As}_{1-x}\text{P}_x)_3$ grows drastically. At 40 % P doping, the behavior of the resistivity is very similar to that typical for semiconductors with impurities

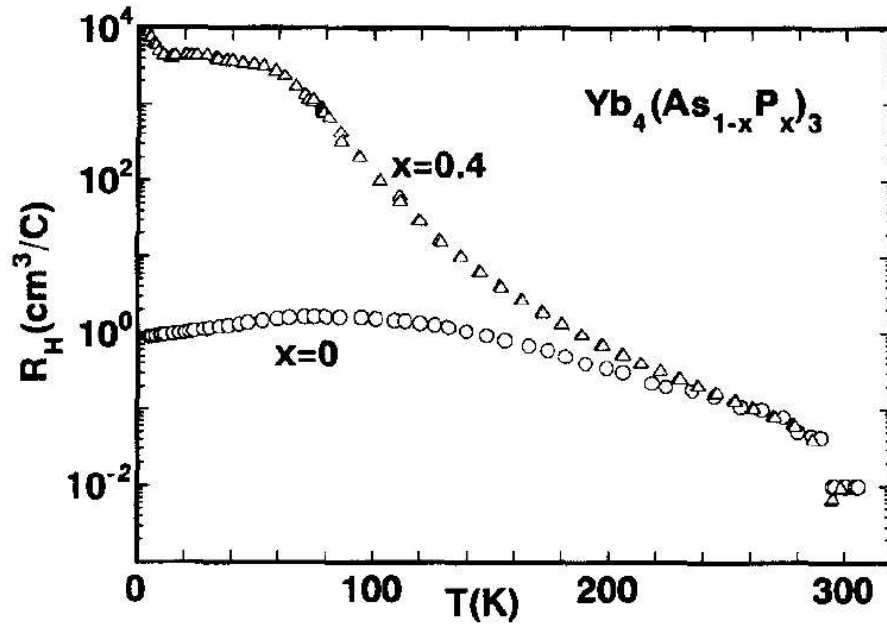


Figure 5.5: Temperature dependence of the Hall coefficient, $R_H(T)$, of $\text{Yb}_4(\text{As}_{1-x}\text{P}_x)_3$ [148].

(cf. Fig. 5.4). In Fig. 5.5 the temperature dependence of the Hall coefficient R_H of the 40 % P-doped system is shown. As $\rho(T)$, also $R_H(T)$ is semiconductor-like for the 40 % P-doped system. It should be noted that R_H is always positive even in P-doped samples suggesting dominant hole conduction in the valence band. In Fig. 5.2 the magnetic susceptibilities of pure Yb_4As_3 and of two P-doped samples are shown. Contrary to the transport properties the characteristic features of all three samples are almost the same. The results of the specific-heat measurements are shown in Fig. 5.3 as C/T versus T^2 . Most surprisingly, even in the very low charge-carrier-concentration system (40 % P) a large γ -value was observed [148]. Thus, a reduction of the charge-carrier concentration by four orders of magnitude upon going from Yb_4As_3 to $\text{Yb}_4(\text{As}_{0.6}\text{P}_{0.4})_3$ has almost no influence on the heavy-fermion-like features (large γ values). With increasing Sb content x , the absolute value of the resistivity of $\text{Yb}_4(\text{As}_{1-x}\text{Sb}_x)_3$ decreases due to the increase of the number of charge carriers; the system becomes more metallic. The decrease of the charge-ordering temperature reflects the increase of the screening effect. At 29 % Sb the charge ordering seems to disappear. The γ value of the specific

heat is, however, still large even in the 29 % Sb sample [153]. Thus the γ value is essentially independent of the charge-carrier concentration, showing that the enhancement of γ is not of Kondo type.

Cyclotron-resonance experiments in $\text{Yb}_4(\text{As}_{0.6}\text{P}_{0.4})_3$ and $\text{Yb}_4(\text{As}_{0.71}\text{Sb}_{0.29})_3$ were performed to investigate the effective mass of the carriers at the Fermi level. In the former material the results indicate cyclotron masses of (0.6 - 0.87) m_0 , where m_0 is the free-electron mass. This again excludes the possibility that $\text{Yb}_4(\text{As}_{0.6}\text{P}_{0.4})_3$ is a heavy-fermion material. In the latter compound the measurements indicate a lower limit for the cyclotron mass of 5.3 m_0 [154].

With the substitution of Sb/P for As, transport properties vary drastically from more metallic (for Sb substitution) through semimetallic (for Yb_4As_3) to semiconducting (for P substitution), whereas the behavior of $C(T)$ and $\chi(T)$ (including its low- T upturn) is insensitive to the substitution. Thus, there is an apparent decoupling between magnetic and transport properties. This decoupling has also been observed in NMR and NQR studies of $\text{Yb}_4(\text{As}_{1-x}\text{P}_x)_3$ [155]. Detailed inelastic-neutron-scattering studies on the semiconducting compound $\text{Yb}_4(\text{As}_{0.6}\text{P}_{0.4})_3$ show that there are similar low-energy magnetic excitations as in the case of Yb_4As_3 . This indicates that the charge-ordering phenomenon is common to both compounds [156].

5.2.2 Physical properties under magnetic field

When a magnetic field is applied to Yb_4As_3 , a gap in the magnetic excitation spectrum appears to open. This refers to measurements of the specific heat [157] where it has been found that a field of 4 T leads to a dramatic decrease of the linear term in the specific heat below 0.5 K, indicating that an additional energy scale exists. This field-induced gap can theoretically be accounted for by a weak inter-chain coupling [158].

Several proposals have been made in order to explain this unusual behavior [159]. The first model is based on the observation that a staggered Dzyaloshinsky-Moriya interaction, which generates an effective staggered g tensor, is allowed in this $4f$ compound [160–162]. It is known that a staggered g tensor leads to a gap formation in an external field [163, 164]. The second model, based on a

mean-field analysis of the anisotropic spin chain, proposes that a gap opens in the presence of a uniform transversal magnetic field [159].

Upon increasing the magnetic field, $C(T)/T$ becomes progressively reduced below its zero-field value, while at higher temperatures a broad hump forms which is continuously shifting towards higher T . These specific-heat maxima have their correspondence in even more pronounced peaks in the thermal-expansion coefficient. Since there are four equivalent cubic space diagonals above the structural transition, the samples exhibit a polydomain structure in the charge-ordered state. Monodomain crystals are obtained only if an uniaxial pressure is applied parallel to one of the four cubic space diagonals prior to cooling below 295 K. In thermal expansion it is possible to apply uniaxial pressure along the measurement direction. A detailed study of the field-induced peaks in the thermal-expansion coefficient revealed that a finite-field component perpendicular to the short axis (Yb_I ions) is required to produce the anomaly [165].

Using the classical sine-Gordon solutions (solitons) to fit the thermal-expansion coefficient, it is possible to explain those results assuming solitary excitations for magnetic fields containing a nonzero component perpendicular to the spin chains [166].

Inelastic neutron-scattering experiments in the charge-ordered state of Yb_4As_3 show that the magnetic-field dependence of the magnetic response from the one-dimensional spin chains can be well explain by the quantum sine-Gordon theory for the staggered field effect due to the existence of the Dzyalosinsky-Moriya interaction [167].

Recently, specific-heat measurements at low temperatures and in magnetic fields could also be well explained using the predictions of the quantum sine-Gordon model [168].

5.2.3 Thermal conductivity of Yb_4As_3

In Fig. 5.6, the temperature dependence of the thermal conductivity $\kappa(T)$ of Yb_4As_3 is plotted for different magnetic fields B [142]. The zero-field data of Yb_4As_3 may be well approximated by $aT + bT^2$, with $a = 0.65$ mW/cmK² and $b = 0.33$ mW/cmK³. The electronic contribution to the thermal conductivity,

estimated from the electrical resistivity using the Wiedemann-Franz law, is more than one order of magnitude smaller than the measured total $\kappa(T)$ (cf. dotted line in Fig. 5.6), and the phonon contribution due to boundary scattering from the smallest sample dimensions ($\sim 800 \mu\text{m}$) is much larger than $\kappa(T)$ (cf. dashed line in Fig. 5.6). The $aT+bT^2$ dependence was attributed to the dominating role of 1D magnons in the thermal conductivity of Yb_4As_3 , which act as heat carriers (aT term) and as scatterers for the phonons (bT^2 term). Above 1 K, κ decreases with increasing magnetic field. The thermal conductivity data $\kappa(B, T)$ normalized to the zero-field data $\kappa(T)$ were fitted using the classical sine-Gordon solutions (solitons) [169]. The magnetic-field dependence of the thermal conductivity $\kappa(B)$ is attributed to the scattering of the three-dimensional phonons from the magnetic solitons. These solitons act as scattering centers for the phonons but they are not able to carry heat [142, 166].

5.3 Results and analysis

The measurements presented here were performed on single crystals of approximately $1 \text{ mm} \times 0.7 \text{ mm} \times 0.4 \text{ mm}$. The samples, provided by Professor Akira Ochiai, were prepared using a technique explained elsewhere [146]. Thermal-conductivity measurements were performed on a multi-domain $\text{Yb}_4(\text{As}_{0.7}\text{P}_{0.3})_3$ crystal in magnetic fields up to 8 T.

Thermal conductivity as a function of temperature T for $\text{Yb}_4(\text{As}_{0.7}\text{P}_{0.3})_3$ is shown in Fig. 5.7 in different magnetic fields. As for the pure sample, the zero-field data of $\text{Yb}_4(\text{As}_{0.7}\text{P}_{0.3})_3$ can, between 0.4 and 3 K, be well approximated by $aT + bT^2$, with $a = 0.39 \text{ mW/cmK}^2$ and $b = 0.76 \text{ mW/cmK}^3$.

The electronic contribution, as estimated from the electrical-resistivity data [142] using the Wiedemann-Franz law (Eq. 3.12), is four orders of magnitude smaller for the doped compound ($\kappa^{WF}(7\text{K}) = 1.7 \times 10^{-5} \text{ mW/Kcm}$) than for the pure compound ($\kappa^{WF}(7\text{K}) = 1.7 \times 10^{-1} \text{ mW/Kcm}$), ruling out that the experimentally observed linear term is due to an electronic thermal conductivity and also showing that electrons cannot be important scatterers for the phonons.

The phonon contribution may be estimated from the gas kinetic equation (Eq. 3.13) taking $C_{ph} = 3 \text{ mJ/molK}^4 \times T^3$ for the phonon specific heat and

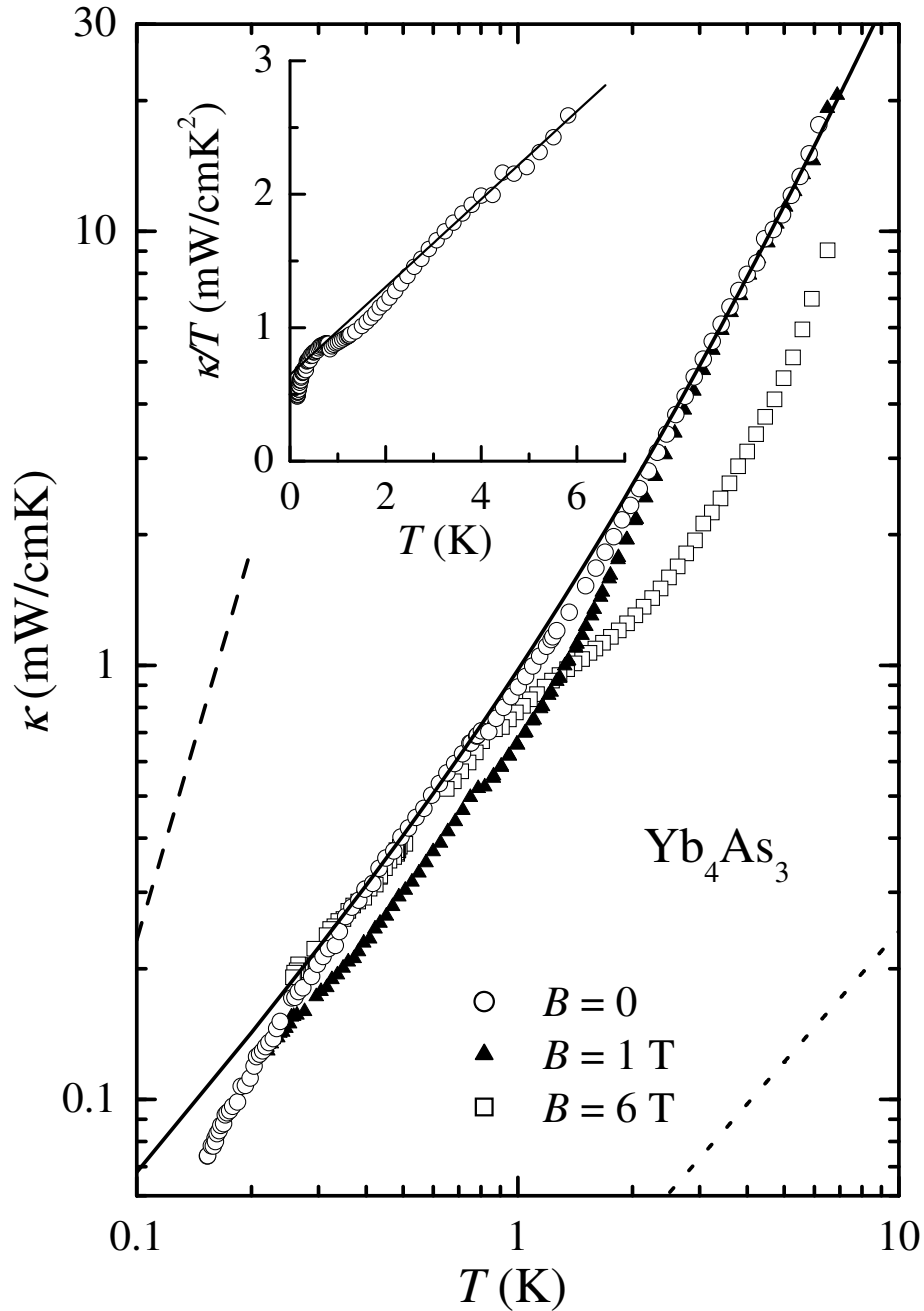


Figure 5.6: Temperature dependence of the thermal conductivity, $\kappa(T)$, of Yb_4As_3 in different applied magnetic fields B . The solid line represents the best $aT + bT^2$ fit to the data. The dotted line represents the electronic contribution calculated using Wiedemann-Franz law, κ_e^{WF} . The dashed line is the phonon contribution due to boundary scattering, $\kappa_{ph}^{Casimir}$. The inset shows that $\kappa = aT + bT^2$ holds between 0.4 K and 6 K [142].

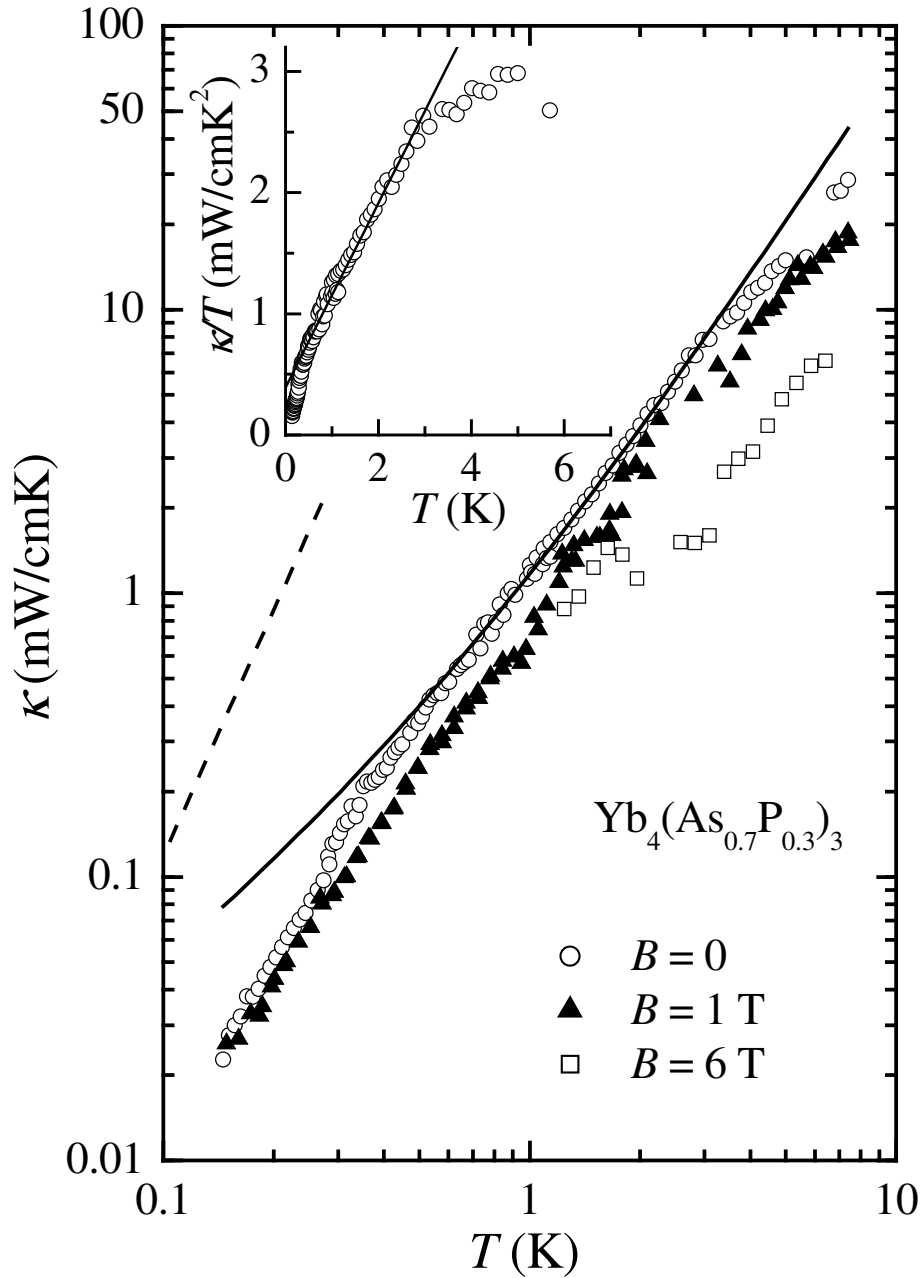


Figure 5.7: Temperature dependence of the thermal conductivity, $\kappa(T)$, of $\text{Yb}_4(\text{As}_{0.7}\text{P}_{0.3})_3$ in different applied magnetic fields. The solid line represents the best $aT + bT^2$ fit to the data. The dashed line is the phonon contribution due to boundary scattering, $\kappa_{ph}^{\text{Casimir}}$. The inset shows that $\kappa = aT + bT^2$ holds between 0.4 K and 3K.

$v_{ph} = 2975$ m/s for the sound velocity [142]. If boundary scattering from the smallest sample dimensions (~ 400 μm) determines the mean-free path l , the dashed line in Fig. 5.7 results. The phonon contribution due to this boundary scattering is much larger than the measured $\kappa(T)$. Thus, the phonons appear to be subject to an additional scattering mechanism.

The magnons play an important role in the thermal conductivity of Yb_4As_3 . Since the magnetic properties of Yb_4As_3 and $\text{Yb}_4(\text{As}_{0.7}\text{P}_{0.3})_3$ are similar it is possible to consider magnons as scatterers for the phonons leading to the bT^2 term. In addition, the magnons act as heat carriers (aT term). Applying the gas kinetic equation to magnon thermal conductivity (Eq. 3.25), taking $C_m = 200$ mJ/molK² for the magnon specific heat and $v_m = 2020$ m/s, the magnon mean-free path l_m can be estimated as $l_m \sim 310$ \AA , which corresponds to 80 times the Yb^{3+} - Yb^{3+} distance (130 times for the pure compound). This mean-free path is most probably due to scattering from static point defects on the Yb^{3+} chains. Below 0.4 K, the thermal conductivity drops below the $aT + bT^2$ line due to spin-glass freezing [142, 168].

The magnetic-field dependence of the thermal conductivity below 1 K is plausible within this interpretation. For both compounds, at $B = 1$ T, the magnon thermal conductivity is reduced, but the reduction of the phonon-magnon scattering rate reinforces the phonon conductivity and, thus, overcompensates this effect at higher magnetic fields such that, at $B = 6$ T, the zero-field thermal conductivity is almost recovered. The opening of a gap in the magnon-excitation spectrum is a possible explanation of this behavior. Above 1 K, $\kappa(B)$ decreases with increasing magnetic field as it was observed in the pure compound. As in Yb_4As_3 , the scattering of the three-dimensional phonons by the magnetic solitons could explain this behavior [142].

In conclusion, the electronic contribution to the thermal conductivity is reduced by four orders of magnitude when doping Yb_4As_3 with 30 % of P due to the reduction of the number of charge carriers. The fact that the aT term is virtually unchanged rules out an electronic origin of this term. Instead, we attribute the thermal conductivity at low temperatures and in zero magnetic field of Yb_4As_3 and $\text{Yb}_4(\text{As}_{0.7}\text{P}_{0.3})_3$ to heat carried by magnons.

5.4 Outlook

- Thermal conductivity measurements of $\text{Yb}_4(\text{As}_{0.7}\text{P}_{0.3})_3$ in a single-domain sample at low temperatures and in applied magnetic fields with the heat current parallel and perpendicular to the spin chains will be important. Because of the negligible electronic contribution to the thermal conductivity, they will allow to unambiguously separate the magnetic thermal conductivity from the phonon contribution.

Chapter 6

$\text{YbRh}_2(\text{Si}_{1-x}\text{Ge}_x)_2$ with $x = 0, 0.05$

6.1 Introduction

Since the discovery of non-Fermi-liquid behavior in $\text{U}_{0.2}\text{Y}_{0.8}\text{Pd}_3$ [170], non-Fermi-liquid research has become a very active field. Today, non-Fermi liquid behavior and quantum critical phenomena in strongly correlated electron systems are among the most intensively studied subjects in condensed matter physics [171]. Non-Fermi-liquid behavior – a characteristic deviation from conventional Landau-Fermi-liquid behavior – is observed in a number of f -electron systems when they are tuned through a quantum critical point (continuous phase transition at $T = 0$) by varying a control parameter such as doping, pressure, or magnetic field [46, 172–177]. The character of the magnetic fluctuations near a quantum critical point has been investigated not only to elucidate the behavior of magnetic order in metals but also with relation to unconventional superconductivity that sometimes appears upon suppressing the magnetic order by applying pressure [178–180]. Quantum critical magnetic fluctuations have been proposed as a promising pairing mechanism for this unconventional superconductivity, the character of which has not been fully understood.

In recent years there is a growing interest in investigating heavy-fermion metals which are located at or close to a magnetic quantum critical point [46, 59]. Systematic experiments in these systems promise to shed considerable light on the general physics of this unconventional metallic ground state. In fact, there is an increasing number of examples of Ce- and U-based systems which

have been found to exhibit non-Fermi-liquid behavior either by doping such as $\text{CeCu}_{6-x}\text{R}_x$ ($\text{R} = \text{Au}, \text{Ag}$) [54, 181, 182], $\text{UCu}_{5-x}\text{Pd}_x$ [183], $\text{U}_{1-x}\text{Th}_x\text{Be}_{13}$ [184–187], $\text{Ce}_{1+x}\text{Ni}_{2+y}\text{Ge}_{2+z}$ [188, 189], $\text{Ce}(\text{Ni}_{1-x}\text{Pd}_x)_2\text{Ge}_2$ [190–192], $\text{CeNi}_2(\text{Ge}_{1-y}\text{Si}_y)_2$ [191], and $\text{CeCu}_2(\text{Si}_{1-x}\text{Ge}_x)_2$ [193, 194] or by applying external pressure such as CeIn_3 [179, 195] and CePd_2Si_2 [196]. Among this class of systems, YbRh_2Si_2 has attracted considerable excitement as being the first ordered Yb-based heavy-fermion compound which is located extremely close to a quantum critical point and exhibits pronounced non-Fermi-liquid behavior [56, 57].

In a normal metal at sufficiently low temperatures, the electrical and thermal conductivities are determined by the scattering of electrons by lattice defects. The electrical conductivity approaches a constant, while the heat conductivity $\kappa(T) \sim T$ is related to the electrical conductivity via the Wiedemann-Franz law. In a Fermi liquid, it is expected that this law still holds at low enough temperature, when the quasiparticles cannot exchange energy during collisions (elastic scattering) [5]. Theoretically, electrons are predicted to obey the Wiedemann-Franz law at $T \rightarrow 0$ in a very wide range of environments: in both three dimensions and two dimensions (but not strictly in one dimension), for any strength of disorder and interactions, scattering, and magnetic field. Experimentally, the Wiedemann-Franz law does appear to be universal at $T \rightarrow 0$: until very recently [9, 197–199], no materials have been reported to violate it. The Wiedemann-Franz law holds in simple metals like copper, but also in systems with strong electron correlations such as the heavy-fermion compounds CeAl_3 [200], the antiferromagnet CeB_6 [201, 202], the normal phase of UBe_{13} [201] and CeRu_2Si_2 [203], as well as in the Kondo compounds CeNi_2Al_5 [204] and CeCu_6 [205]. For a review see [206]. The Wiedemann-Franz law may even hold in the presence of non-Fermi-liquid behavior: For CeNi_2Ge_2 , which is close to an antiferromagnetic quantum critical point, at very low temperatures ($T < 0.1$ K) the Wiedemann-Franz law is observed. With increasing temperature, a deviation from the Wiedemann-Franz law due to an inelastic spin-fluctuation contribution is observed [207].

Thermal-conductivity studies in high- T_c superconductors have shown anomalous behavior of the electronic thermal conductivity in the field-induced normal state [197–199]. The deviations from the Wiedemann-Franz law recently observed in the normal state of a copper-oxide superconductor have been interpreted as

evidence for the breakdown of Fermi-liquid theory [9].

For disordered conductors [208, 209] as well as for mesoscopic degenerate conductors with strong electron-electron scattering [210], theoretical evaluations of the electron-electron interaction correction to the electronic thermal conductivity show that the Wiedemann-Franz law is violated.

For heavy-fermion compounds, the fractionalized Fermi-liquid theory provides a possible explanation of the weak-moment magnetism and its relation to the non-Fermi-liquid behavior. This theory predicts that a decoupling between the conduction electrons and the spin liquid leads to a violation of Wiedemann-Franz law [211, 212]. This topic is currently much discussed [9, 209, 212].

Recently, a model for the behavior of the thermopower in heavy-fermion compounds close to an antiferromagnetic quantum critical point was proposed [213]. The model predicts an anomalous logarithmic temperature dependence of the thermopower, which has already been observed in $\text{CeCu}_{6-x}\text{Au}_x$ [214].

In this thesis thermopower S and thermal-conductivity κ measurements on single crystals of $\text{YbRh}_2(\text{Si}_{1-x}\text{Ge}_x)_2$ ($x = 0, 0.05$) between 200 mK and 7 K are presented.

6.2 Physical properties

YbRh_2Si_2 crystallizes in the tetragonal ThCr_2Si_2 structure in the space group $I4/mmm$ with lattice parameters $a = 4.007 \text{ \AA}$ and $c = 9.858 \text{ \AA}$ (cf. Fig. 6.1). YbRh_2Si_2 contains Yb^{+3} ions whose single-ion Kondo temperature $T_K \sim 20 - 30$ K can be inferred from various experimental probes [56].

The Sommerfeld coefficient of the electronic specific heat $\gamma = C_e/T$ is shown in Fig. 6.2 as a function of temperature T . The electronic specific heat has been obtained by subtracting the phonon contribution from the raw data, determined by measurements of LuRh_2Si_2 [56, 215]. Below 10 K, C_e/T increases logarithmically upon cooling. C_e/T was found to be described as $C_e/T \sim \ln(T_0/T)$, with $T_0 = 24$ K in a wide temperature range $0.3 \text{ K} < T < 10 \text{ K}$ (cf. dashed line). Below 0.3 K, C_e/T diverges stronger than logarithmically. A comparison with the reference compound LuRh_2Si_2 [215] shows that C/T of YbRh_2Si_2 is electron dominated below 10 K (cf. solid line).

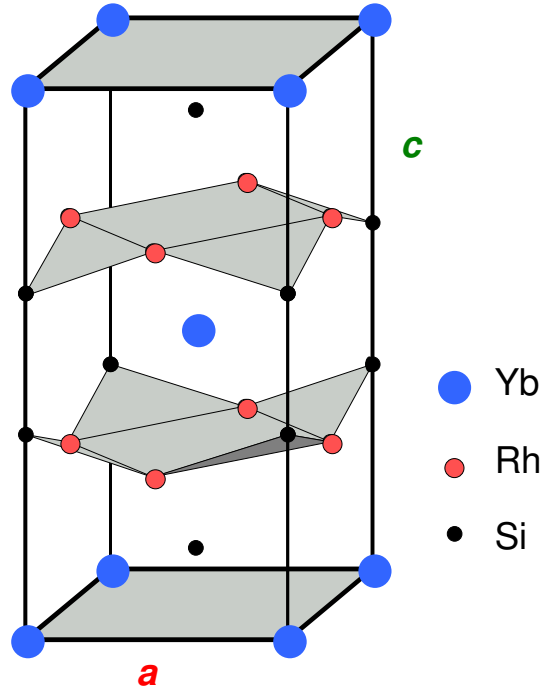
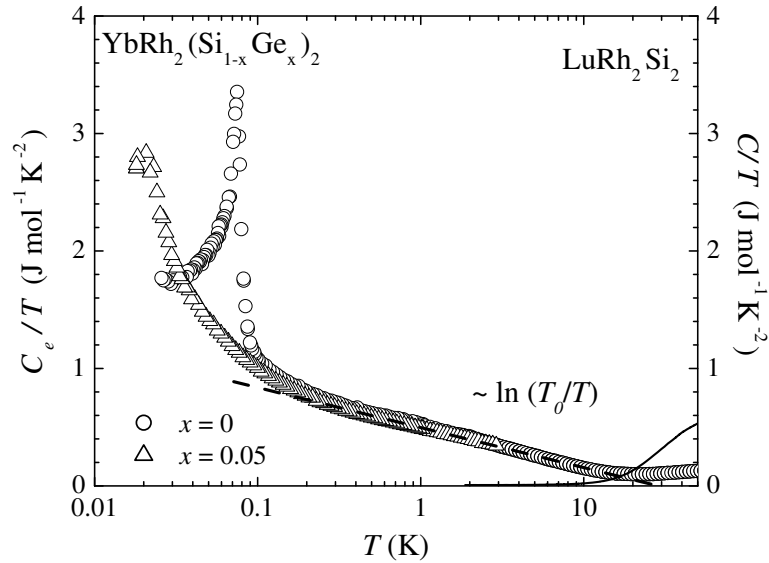
Figure 6.1: Crystal structure of YbRh_2Si_2 .

Figure 6.2: Temperature dependence of the Sommerfeld coefficient of the electronic specific heat, $C_e(T)/T$, of $\text{YbRh}_2(\text{Si}_{1-x}\text{Ge}_x)_2$ ($x = 0, 0.05$) [216]. The dashed line represents $C_e(T)/T \sim \ln(T_0/T)$. Temperature dependence of the specific heat divided by temperature, $C(T)/T$, for the reference compound LuRh_2Si_2 (right axis, solid line) [215].

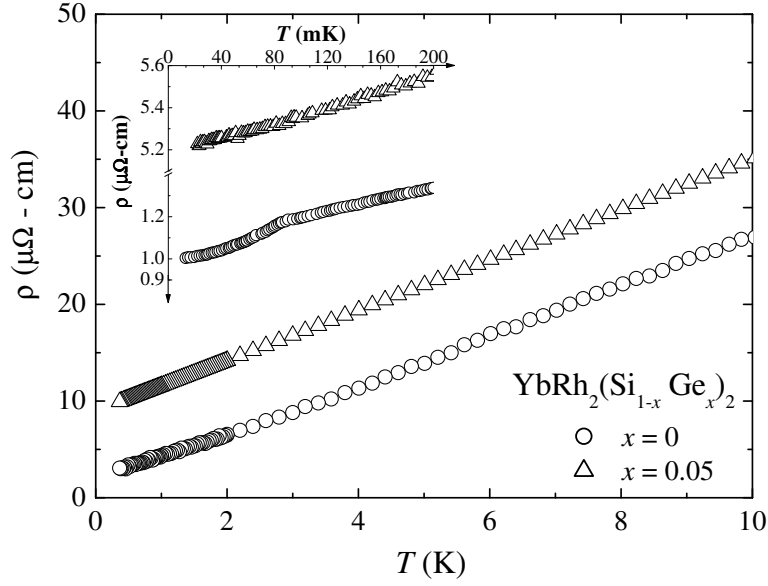


Figure 6.3: Temperature dependence of the low-temperature electrical resistivity $\rho(T)$ of $\text{YbRh}_2(\text{Si}_{1-x}\text{Ge}_x)_2$ ($x = 0, 0.05$) of the samples used in this investigation. The inset shows the electrical resistivity as a function of temperature between 20 mK and 200 mK, taken from [217].

The temperature dependence of the electrical resistivity $\rho(T)$ is shown at low temperatures in Fig. 6.3. The resistivity was measured in the temperature range between 350 mK and 10 K on the same samples used to measure thermal conductivity and thermopower. Below 10 K, $\rho(T)$ presents an almost linear temperature dependence over more than two decades in temperature. In measurements performed at lower temperatures, the electrical resistivity has shown a kink at $T \approx 70$ mK, related to an antiferromagnetic phase transition (see inset Fig. 6.3) [217]. Below the transition, Landau-Fermi-liquid behavior is recovered and $\rho(T)$ can be described by $\rho(T) = \rho_0 + AT^2$. At around 100 K, $\rho(T)$ shows a Kondo-like maximum and above 100 K, $\rho(T)$ is almost constant [56].

At high temperatures ($T \geq 200$ K) the magnetic susceptibility of YbRh_2Si_2 measured along both crystallographic directions (a and c) follows a Curie-Weiss law with an effective magnetic moment very close to the value of free Yb^{+3} ($\mu_{eff} = 4.5\mu_B$); but due to the strong magnetic anisotropy there is a marked difference in the respective extrapolated values for the Weiss temperatures, $\Theta_P^a \approx -9$ K and $\Theta_P^c \approx -180$ K [56]. At $T = 2$ K, the magnetic susceptibility measured

along the basal plane is about 20 times larger than the one measured with the applied magnetic field parallel to the c axis. The highly anisotropic magnetic response suggests that Yb^{3+} -moments are forming an easy-plane perpendicular to the crystallographic c direction. At low temperatures AC-susceptibility measurements on YbRh_2Si_2 have detected an antiferromagnetic transition at $T \approx 70$ mK. The anomaly at 70 mK has been confirmed in recent muon-spin relaxation (μSR) measurements [218]. The static magnetism occurs over the entire sample, with a tiny ordered Yb^{3+} moment, $\leq 2 \times 10^{-3} \mu_B$ [218]. In addition, the existence of spin fluctuations in this low-moment state of YbRh_2Si_2 has been reported from low-temperature ^{29}Si NMR and μSR experiments [218, 219].

The linear temperature dependence of the electrical resistivity and the logarithmic divergence of the Sommerfeld coefficient of the electronic specific heat clearly demonstrate non-Fermi-liquid behavior [56, 57, 216]. Electrical resistivity [57] as well as AC-susceptibility [56], μSR [218], thermal-expansion [220], and specific-heat [57] results revealed a very weak antiferromagnetic phase transition at $T_N \approx 70$ mK. Below the antiferromagnetic phase transition YbRh_2Si_2 enters a Landau-Fermi-liquid state with very heavy quasiparticles as evidenced by electrical-resistivity measurements [57].

The magnetic-field dependence of the electrical resistivity, AC susceptibility, and specific heat strongly suggest that there exists a magnetic field-induced quantum critical point [57, 216]. The anomalies in the zero-field AC susceptibility, specific heat and resistivity around 70 mK can be suppressed in a magnetic field of $B_c \approx 0.06$ T applied perpendicular to the c axis and $B_c \approx 0.66$ T applied parallel to the c axis [57]. For magnetic fields larger than B_c , Landau-Fermi-liquid behavior is recovered at the lowest temperature.

On the other hand, T_N increases with pressure [221]. Extrapolating $T_N(p) \rightarrow 0$ one obtains a critical pressure $p_c = -0.3$ GPa. Thus, a small expansion of the unit-cell volume would tune $T_N \rightarrow 0$. This can be achieved by the substitution of Si by the isoelectronic, but larger, Ge. Using the bulk modulus of $\text{YbRh}_2(\text{Si}_{1-x}\text{Ge}_x)_2$, the quantum critical point is expected to be reached at $x_c = 0.05$ [221].

Specific-heat measurements of samples with the nominal composition $\text{YbRh}_2(\text{Si}_{0.95}\text{Ge}_{0.05})_2$ show that the Néel temperature has been substantially sup-

pressed compared to pure YbRh_2Si_2 , but is still finite ($T_N \approx 20$ mK, [216]). The electrical resistivity depends linearly on temperature over more than three decades, i.e., from 20 mK to above 20 K (cf. Fig. 6.3). The Sommerfeld coefficient diverges logarithmically between 10 K and 0.3 K and the AC-susceptibility follows a dependence $\chi^{-1} \sim T^\alpha$ with $\alpha \sim 0.75$ in the temperature range $0.2 \text{ K} \leq T \leq 1.5 \text{ K}$. Below 0.3 K, the Sommerfeld coefficient shows a pronounced upturn, while the uniform susceptibility can be well described by a Curie-Weiss law, as also found for YbRh_2Si_2 in the temperature range $T_N < T < 0.5 \text{ K}$, with equally large paramagnetic moments, $\mu_{eff} \approx 1.4 \mu_B$, and similar Weiss temperatures, $\theta \approx -0.3 \text{ K}$. The weak antiferromagnetic order of $\text{YbRh}_2(\text{Si}_{0.95}\text{Ge}_{0.05})_2$ below 20 mK is suppressed by a small magnetic field of $B_c \approx 0.027 \text{ T}$ applied in the easy plane, as shown by specific-heat [216] and magnetostriction measurements [220].

6.3 Results and discussion

The measurements presented here were performed on single-crystalline platelets of approximately $2.3 \text{ mm} \times 1.4 \text{ mm} \times 0.16 \text{ mm}$ grown in In flux, using a molten-metal-solvent technique in closed Ta crucibles. From a careful microprobe analysis on samples of the nominal composition $\text{YbRh}_2(\text{Si}_{0.95}\text{Ge}_{0.05})_2$, the effective Ge concentration was found to be $x_{eff} \approx 0.02 \pm 0.01$. The large difference between the nominal and effective Ge content is due to the fact that Ge dissolves better than Si in the In flux [57]. To be consistent with the literature, the Ge-doped single crystal studied in this chapter is labeled by its nominal Ge concentration $x = 0.05$. The samples were provided by Octavio Trovarelli (MPI CPfS, Dresden). Thermopower and thermal conductivity were measured with the heat current \dot{Q} perpendicular to the c axis.

6.3.1 Thermopower

Figure 6.4 shows the temperature dependence of the thermopower $S(T)$ of $\text{YbRh}_2(\text{Si}_{1-x}\text{Ge}_x)_2$ ($x = 0, 0.05$). $S(T)$ is negative in the whole temperature range. The negative sign of the thermopower may be attributed to the Abrikosov-Suhl resonance (ASR) being situated below the Fermi energy E_F , in contrast to

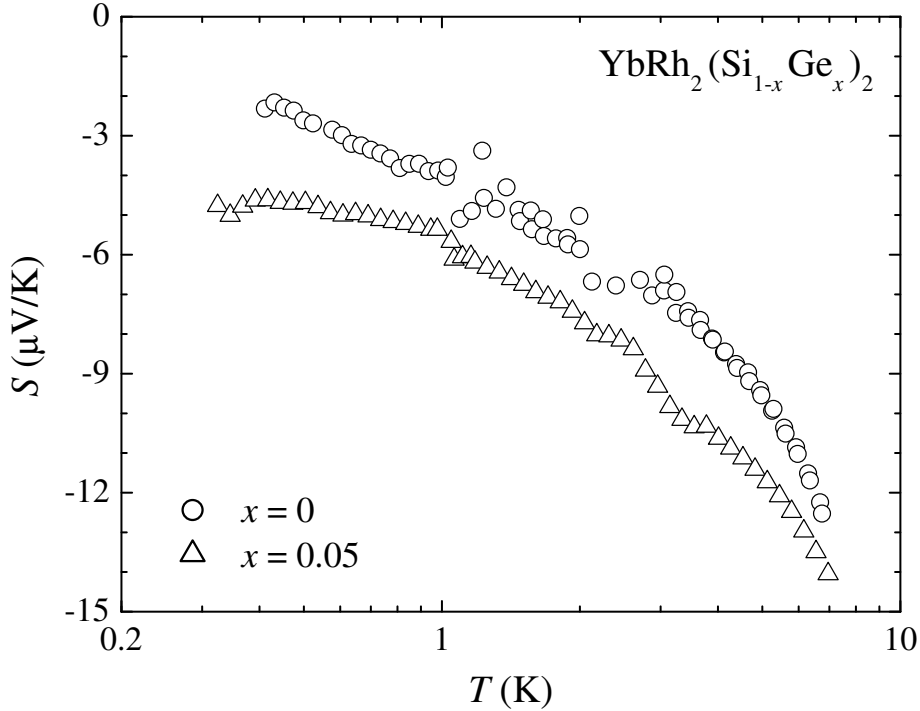


Figure 6.4: Temperature dependence of the thermopower, $S(T)$, of $\text{YbRh}_2(\text{Si}_{1-x}\text{Ge}_x)_2$ ($x = 0, 0.05$).

Ce-compounds where the ASR lies above E_F and S is positive. As expected for magnetic compounds, $S(T)$ does not show a simple linear behavior [222].

In Fig. 6.5, the thermopower and specific heat of $\text{YbRh}_2(\text{Si}_{1-x}\text{Ge}_x)_2$ ($x = 0, 0.05$) are plotted as S/T and C_e/T versus temperature T . For a certain range of temperature, the S/T data follow the predictions made by Paul et al [213]: $S/T \sim \ln(T_0^*/T)$. For $x = 0$, T_0^* is estimated to be 20 K while, for $x = 0.05$, $T_0^* = 15$ K. A logarithmic behavior was also observed in the measurements of the volume thermal-expansion coefficient for $\text{YbRh}_2(\text{Si}_{0.95}\text{Ge}_{0.05})_2$ [223] in the same range of temperature as the S/T data, with a similar value of T_0^* .

6.3.2 Thermal Conductivity

Figure 6.6 shows the temperature dependence of the thermal conductivity $\kappa(T)$ of $\text{YbRh}_2(\text{Si}_{1-x}\text{Ge}_x)_2$ ($x = 0, 0.05$). The thermal conductivity of heavy-fermion compounds is, at very low temperatures ($T < 4$ K), strongly dominated by

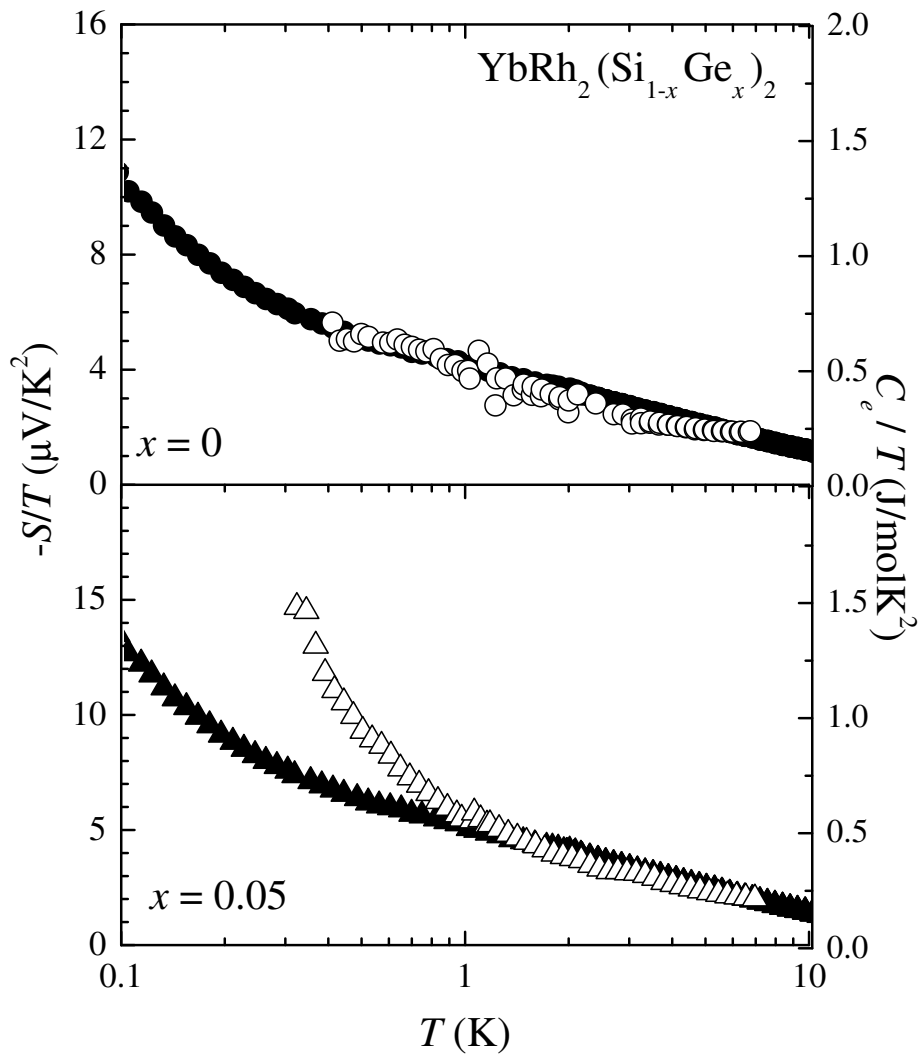


Figure 6.5: Thermopower (open symbols) and specific heat (full symbols) plotted as S/T and C_e/T as a function of the temperature T of $\text{YbRh}_2(\text{Si}_{1-x}\text{Ge}_x)_2$ ($x = 0, 0.05$).

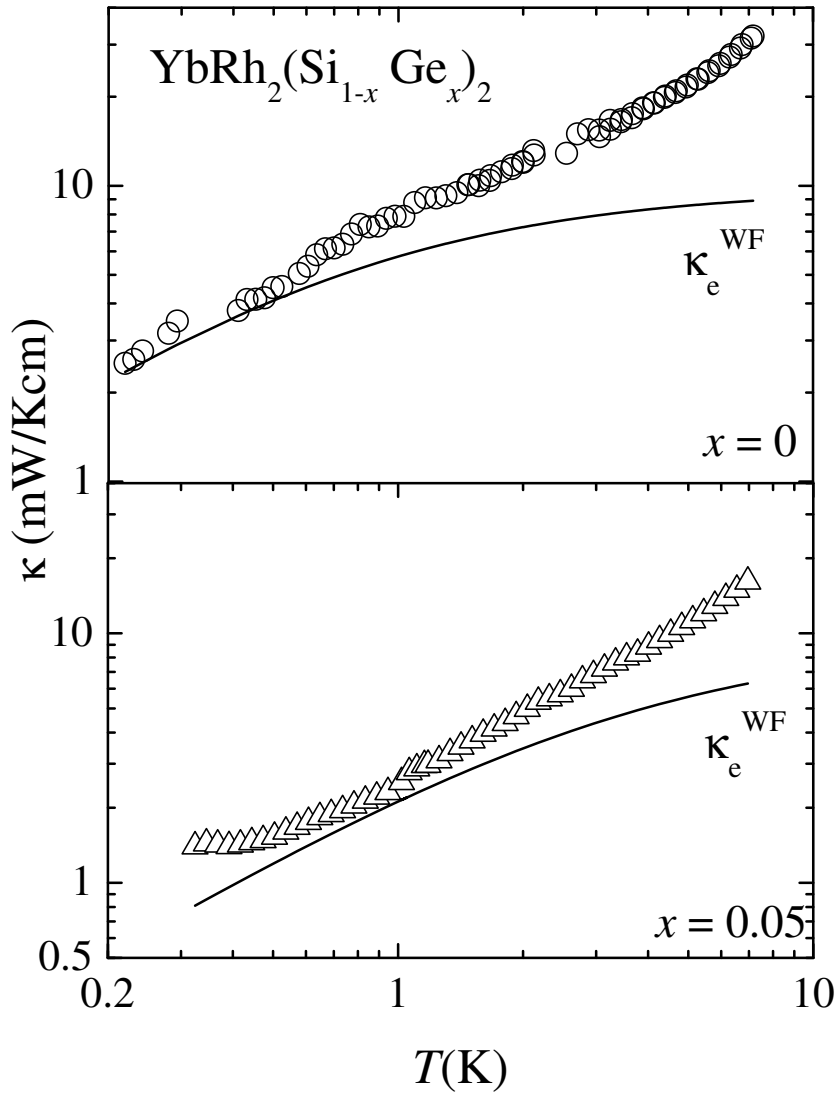


Figure 6.6: Temperature dependence of the thermal conductivity, $\kappa(T)$, of $\text{YbRh}_2(\text{Si}_{1-x}\text{Ge}_x)_2$ ($x = 0, 0.05$). The solid lines represent the electronic contribution estimated using the Wiedemann-Franz law.

the electronic contribution κ_e [206]. Indeed, from specific-heat measurements of YbRh_2Si_2 and LuRh_2Si_2 , it is expected that the phonon contribution κ_{ph} of $\text{YbRh}_2(\text{Si}_{1-x}\text{Ge}_x)_2$ is negligible below 7 K (cf. Fig. 6.2). The electronic contribution to the thermal conductivity κ_e^{WF} was estimated using the Wiedemann-Franz law (Eq. 3.12, cf. solid line in Fig. 6.6), calculated from the electrical resistivity measured on the same samples (with the same contacts) between 350 mK and 10 K. For temperatures below 350 mK, the resistivity was extrapolated from the measured values. As may be seen in Fig. 6.6, κ_e^{WF} does not behave as it is expected for a metal. In a wide range of temperatures, the Wiedemann-Franz law does not appear to be obeyed. For YbRh_2Si_2 at the lowest measured temperature, $\kappa_e^{WF}(T)$ and the measured $\kappa(T)$ coincide. For $\text{YbRh}_2(\text{Si}_{0.95}\text{Ge}_{0.05})_2$, however, $\kappa_e^{WF}(T)$ and $\kappa(T)$ deviate from each other. Further measurements with other samples are highly desired to clarify whether this behavior is intrinsic.

In Fig 6.7, the thermal conductivity plotted as κ/T versus T^2 is presented. This is done in order to separate the contributions of phonons and electrons: In a simple metal, phonons are expected to have a thermal conductivity which varies as T^3 and the electronic thermal conductivity should follow a behavior linear in T , at sufficiently low temperature, leading to $\kappa(T) = \kappa_e(T) + \kappa_{ph}(T) = AT + BT^3$. In a κ/T versus T^2 plot the ordinate (A) accounts for the electronic contribution and the slope (B) of the straight line represents the phonon contribution. The slopes of the κ/T curves above 10 K² are nearly zero, indicating that the contribution of phonons is negligible in the investigated temperature range. Below 10 K², κ/T increases rapidly upon cooling. Thus, also here no phonon contribution can be resolved and the electronic part is strongly T dependent.

The phonon contribution due to boundary scattering from the borders of the sample $\kappa_{ph}^{Casimir}$ is estimated from the gas kinetic equation (Eq. 3.13) using the low-temperature lattice specific heat of the reference compound LuRh_2Si_2 ($C_{ph} = 0.13 \text{ mJ/molK}^4 \times T^3$, $\theta_D = 240 \text{ K}$) [215], and taking the smallest dimensions of both samples ($\sim 0.16 \text{ mm}$) for the mean-free path. $\kappa_{ph}^{Casimir}/T$ versus T^2 is presented in Fig. 6.7 (cf. dashed line). The slope of $\kappa_{ph}^{Casimir}/T$ is much larger than the slope of the κ/T data. This shows that additional scattering mechanisms must suppress the phonon thermal conductivity in $\text{YbRh}_2(\text{Si}_{1-x}\text{Ge}_x)_2$.

The thermal conductivity plotted as κ/T versus T is shown in Fig. 6.8 in order

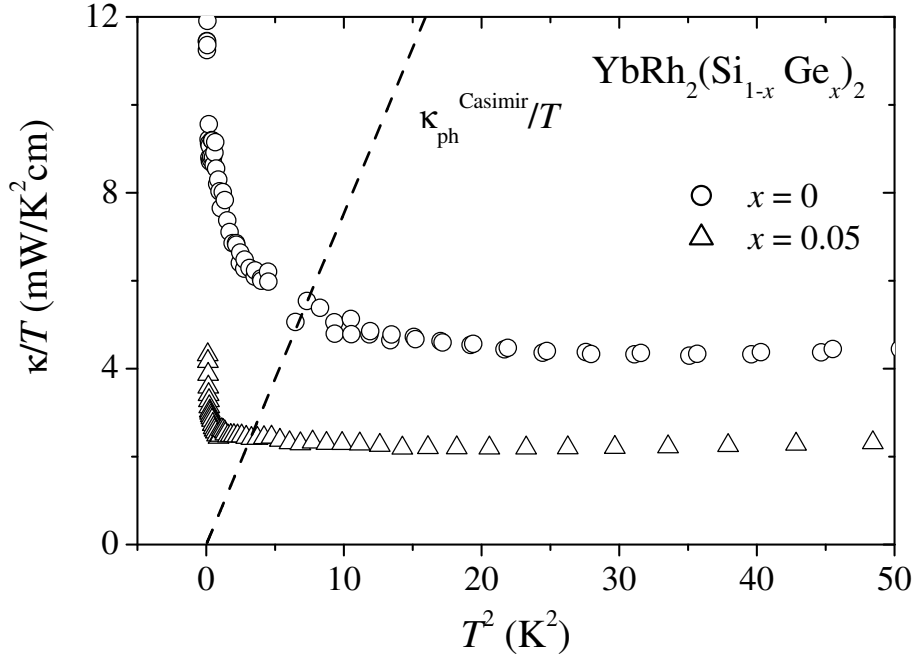


Figure 6.7: Temperature dependence of thermal conductivity, $\kappa(T)$, shown as κ/T versus T^2 of $\text{YbRh}_2(\text{Si}_{1-x}\text{Ge}_x)_2$ ($x = 0, 0.05$). The dashed line shows the phonon contribution due to boundary scattering divided by temperature $\kappa_{\text{ph}}^{\text{Casimir}}/T$ as a function of T^2

to study the temperature dependence of the coefficient of the electronic thermal conductivity. It is possible to discern temperature ranges where $\kappa/T \sim \ln(T_0/T)$.

Spin fluctuations may play an important role in the electrical resistivity and thermal resistivity W_e of compounds close to an antiferromagnetic quantum critical point [207] and in compounds with an antiferromagnetic transition [224]. The magnetic fluctuations may affect the electrical resistivity and the heat resistivity in different ways, leading to a deviation from the Wiedemann-Franz law between the antiferromagnetic transition and the characteristic temperature of the spin fluctuations [224]. In Fig. 6.9, the temperature dependences of the thermal resistivity $W_e(T)$ and of the electrical resistivity $\rho(T)$ of $\text{YbRh}_2(\text{Si}_{1-x}\text{Ge}_x)_2$ ($x = 0, 0.05$) are shown. $W_e(T)$ was estimated using the relation $W_e = 1/\kappa_e$, assuming that the measured thermal conductivity is electron dominated ($\kappa(T) = \kappa_e(T)$). In order to compare W_e with the electrical resistivity, W_e is multiplied by L_0T with $L_0 = 2.44 \times 10^{-8} \text{ W } \Omega \text{ K}^{-2}$, assuming that W_e obeys

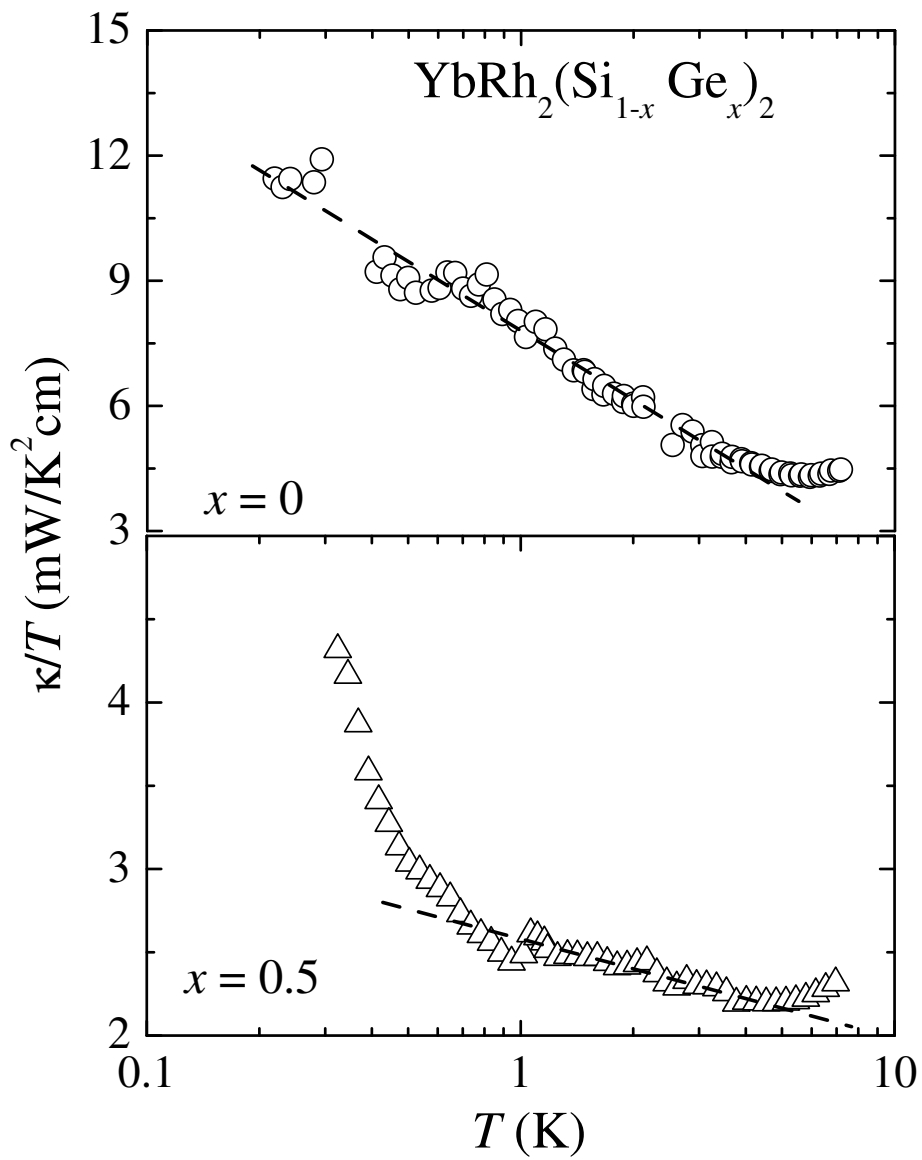


Figure 6.8: Temperature dependence of the thermal conductivity divided by temperature $\kappa(T)/T$, of $\text{YbRh}_2(\text{Si}_{1-x}\text{Ge}_x)_2$ ($x = 0, 0.05$). The dashed line represents $\kappa/T \sim \ln(T_0/T)$.

the Wiedemann-Franz law. There is a large difference between the two resistivities at high temperatures. At low temperatures, the two resistivities are similar for the pure sample, but, in the case of the Ge-doped sample, upon decreasing the temperature the two resistivities first approach each other but then, below 1 K, they separate again. To obtain conclusive information about the influence of spin fluctuations on the thermal and electrical resistivity it is necessary to measure in the temperature range between the antiferromagnetic transition at 70 mK and the characteristic temperature of the spin fluctuations which is around 24 K in YbRh_2Si_2 [56].

6.4 Outlook

- Thermal conductivity and thermopower of YbRh_2Si_2 should be measured below 70 mK, where Fermi-liquid behavior is recovered, and up to and above 24 K, the characteristic temperature of the spin fluctuations.
- Measurements of the thermal conductivity and the thermopower of YbRh_2Si_2 should be performed in applied magnetic field in order to study their behavior when tuning the system through its magnetic-field-induced quantum critical point.
- Measurements of the Nernst effect would be very interesting in connection with the giant Nernst effect observed in CeCoIn_5 [225]. This anomalous behavior could be associated with the non-Fermi-liquid features in various transport properties of CeCoIn_5 . However, the origin of the anomalous Nernst signal is still not understood.
- Additional measurements of the low-temperature thermal conductivity shall reveal whether and where the Wiedemann-Franz law is violated.

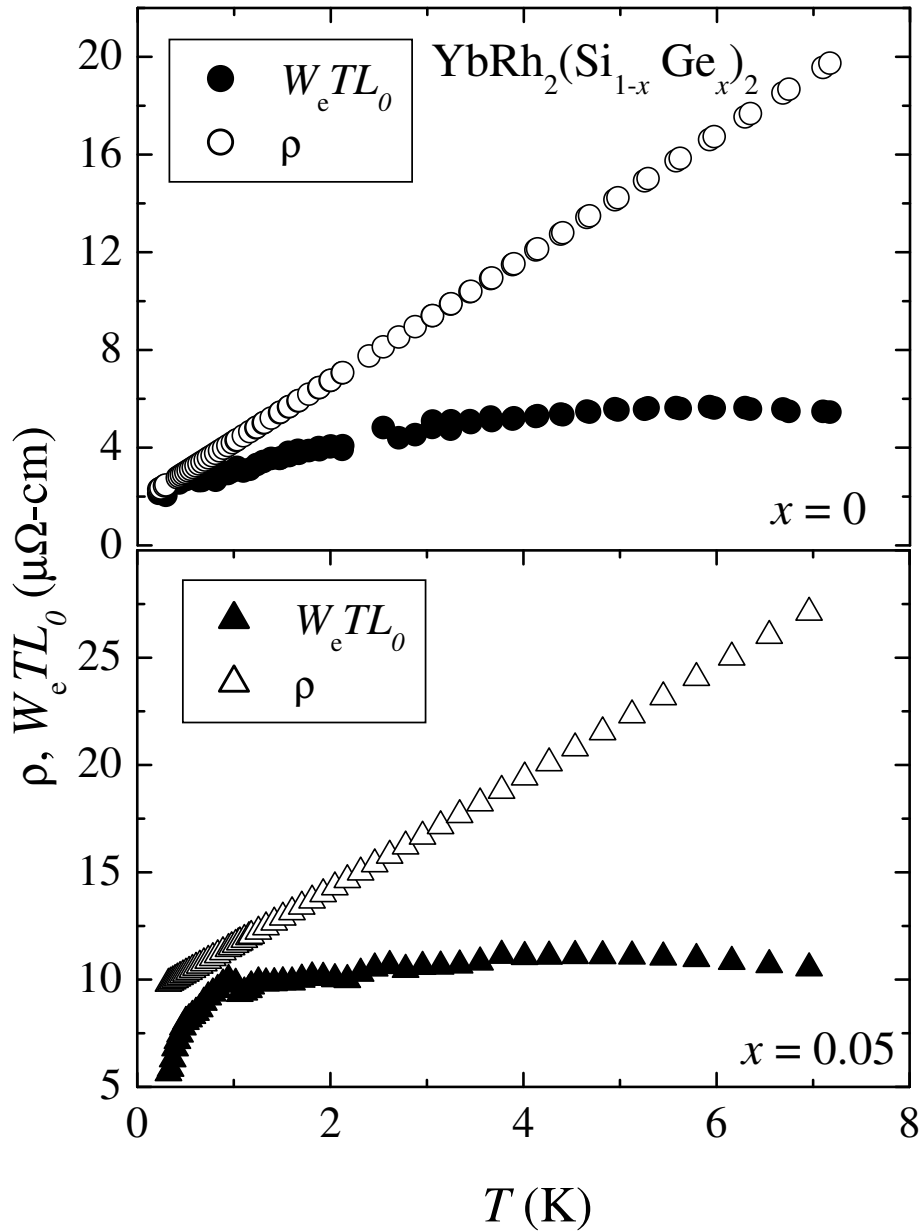


Figure 6.9: Thermal resistivity and electrical resistivity plotted as $W_e L_0 T$ and $\rho(T)$ as a function of the temperature T of $\text{YbRh}_2(\text{Si}_{1-x}\text{Ge}_x)_2$ ($x = 0, 0.05$).

Chapter 7

T^2 phonon thermal conductivity

7.1 ThAsSe

7.1.1 Introduction

Since the anomalous features of insulating glasses have been understood, the low-temperature behavior of metallic glasses has attracted considerable interest. The key step in the understanding of glasses was the introduction of the concept of two-level system (TLS). TLS's are the typical excitations of a glass. They are associated with a large “free atomic volume” at some positions where the atom or group of atoms can be found in two different configurations with a small energy difference between them. If only one atom is involved, then a double potential describes the two quasistable energy minima well, and the atom oscillates between these minima by tunneling [226]. These tunneling transitions are rare and a much more efficient mechanism is electron-assisted tunneling, in which the scattering of a conduction electron from the tunneling atom induces the transition [227].

One of the interesting aspects of a TLS is the appearance of an exotic Kondo effect: The Hamiltonian of a TLS interacting with a degenerate Fermi gas can be mapped to the Hamiltonian of a spin-1/2 antiferromagnetic Kondo problem [8, 228–231]. Furthermore, it is expected that the system would have a non-Fermi-liquid ground state below the Kondo temperature T_K as a realization of a two-channel Kondo effect. A logarithmic temperature dependence of the electrical conductivity is also expected in this systems above T_K , [229–233]. This nonmag-

netic analogue of the ordinary Kondo problem is called the TLS Kondo effect. However, there is only a limited number of well-defined TLS Kondo systems to be used for verification of the theoretical predictions [8].

Uranium-pnictochalcogenide crystals show the TLS Kondo effect, especially strong in UAsSe [234, 235] and UPS [236]. In UAsSe, the electrical resistivity presents Kondo-like behavior of nonmagnetic origin [237]. Neutron-scattering measurements of UAsSe show that about 6 % of the As-atom positions are occupied by Se-atoms and vice versa [234]. Moreover, electrical-resistivity measurements in $\text{UAs}_{1-x}\text{Se}_{1+x}$ ($0 \leq x \leq 0.06$) show that the Kondo-like resistivity decreases when x increases [234, 235]. Thus, the Kondo effect in this compound may originate from a disordered occupation of the As and Se sublattices. In the temperature dependence of the thermopower, a peak related with the Kondo temperature is observed in UAsSe. Changes in the thermoelectric power introduced by tiny variations of the Se excess are clear signs of the incoherent Kondo scattering from the TLS centers in UAsSe [238, 239]. As well as in UAsSe, UPS shows a low-temperature upturn in the electrical resistivity and a peak at the Kondo temperature in the thermopower, both related to the TLS Kondo effect [236, 239]

Two-level systems influence the low-temperature properties in disordered solids. The most remarkable result was the discovery of a set of universal low-temperature properties of the insulating and metallic glasses. These properties are normally not found in crystals and are often called “anomalous”. Examples are the excess specific heat and extra sources for phonon scattering. Below 1 K, the specific heat varying as $C \sim T$ and the thermal conductivity κ varying as $\kappa \sim T^\alpha$ with $\alpha = 1.9 \pm 0.1$ are characteristic of the TLS states [240–243].

In this section, thermal-conductivity κ measurements on single crystals of ThAsSe between 300 mK and 1 K in zero magnetic field and at 6 T are presented.

7.1.2 Physical properties

The diamagnetic compound ThAsSe crystallizes in a tetragonal structure (PbFCI-type, space group $P4/nmm$) with lattice parameter $a = 4.084 \text{ \AA}$ and $c = 8.578 \text{ \AA}$. The crystallographic unit cell with exposed polyhedrons, formed by the closest

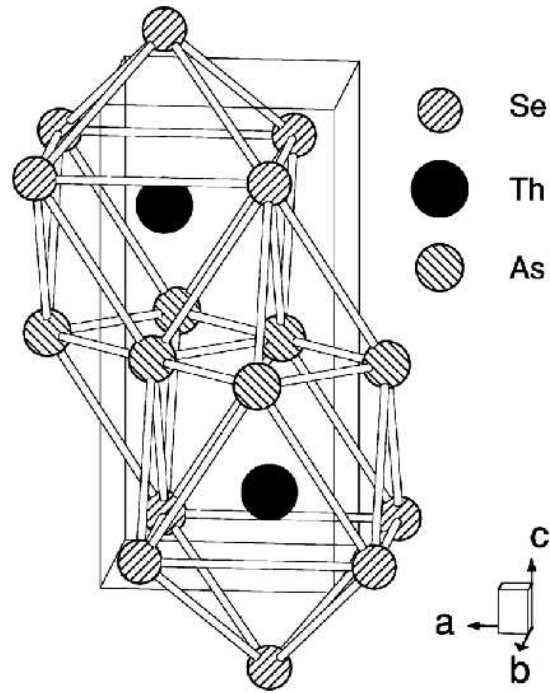


Figure 7.1: Crystal structure of ThAsSe [244].

anion neighborhood of thorium, is shown in the Fig. 7.1.

Figure 7.2 shows the normalized resistance $R/R(300K)$ as a function of temperature T for several single crystals of ThAsSe. The resistance increases with decreasing temperature. Although the low- T resistance is strongly sample dependent, for several specimens a distinct $-\ln T$ behavior was observed between 2 and 20 K (not shown). This behavior is unaffected by both magnetic field and pressure, showing that it is not related to the magnetic Kondo effect but that it could be related to the interaction between the TLS and the conduction electrons. At low temperatures, the resistance is found to saturate [244]. A detailed analysis of the electrical resistivity revealed an anomalous scattering mechanism, which is apparently derived from two-level systems: Below 4 K, the resistivity presents non-Fermi-liquid behavior that is again suppressed below 0.2 K. This complex behavior can be consistently interpreted in terms of the TLS Kondo model [245].

Magnetic-susceptibility measurements of ThAsSe yield a constant negative value in a wide range of temperature as expected for a diamagnetic material. Below 50 K, the susceptibility increases and saturates below 8 K; this can be

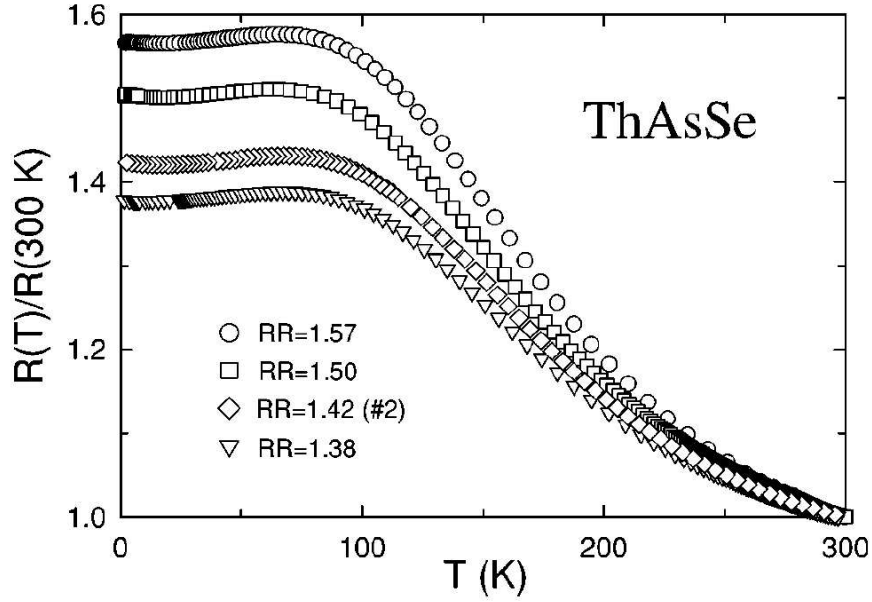


Figure 7.2: Temperature dependence of the normalized resistance, $R(T)/R(300K)$, of several samples of ThAsSe [244].

attributed to a very small amount of magnetic impurities carrying around $5.4 \times 10^{-4} \mu_B/\text{f.u.}$ [244].

Figure 7.3 shows the temperature dependence of the specific heat $C(T)$, at low temperatures. Between 1.7 and 5 K, the specific heat is well approximated by $C = \gamma T + \beta T^3$ with $\gamma = 0.3 \text{ mJ/molK}^2$ and $\beta = 3 \times 1944/\theta_D \text{ J/molK}^4$, where $\theta_D = 254 \text{ K}$. Below 1.7 K, an additional contribution to C is detected: A linear term of non-electronic origin dominates the low-temperature specific heat. It was ascribed to the dynamic disorder derived from the two-level system [244]. This behavior is strikingly similar to the one of the heat capacity of vitreous SiO_2 , a well known TLS material [240, 244].

A charge-carrier density of $n = 8.4 \times 10^{21} \text{ cm}^{-3}$ at 300 K was derived from Hall-effect measurements using the one-band model. $n(T)$ decreases upon cooling down until 100 K, where $n(T)$ approaches the constant value $n = 1.1 \times 10^{21} \text{ cm}^{-3}$ [244, 246].

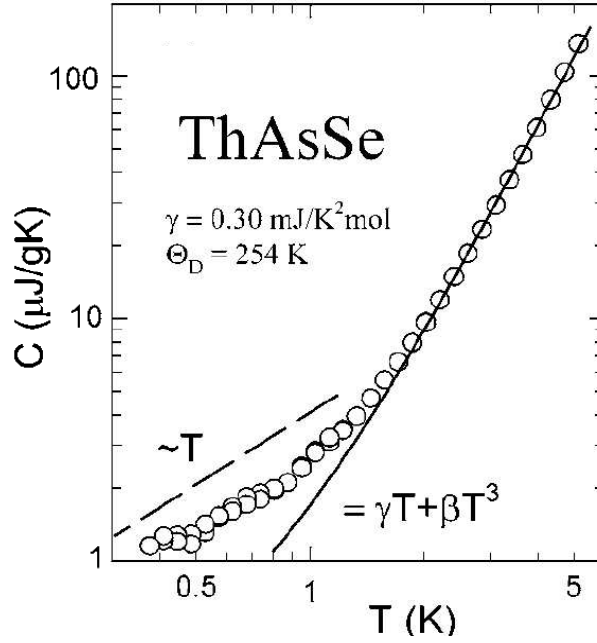


Figure 7.3: Temperature dependence of the specific heat, $C(T)$, of ThAsSe [244].

7.1.3 Results and discussion

The measurements presented here have been performed on a single crystal of approximately $2 \text{ mm} \times 1 \text{ mm} \times 0.1 \text{ mm}$ grown by a chemical-vapor transport method. The sample was provided by Dr. Zygmunt Henkie and Dr. Andrzej Wojakowski from the Institute of Low Temperature and Structure Research, Polish Academy of Sciences.

Figure 7.4 shows the temperature dependence of the thermal conductivity $\kappa(T)$ of ThAsSe in zero field and at 6 T. $\kappa(T)$ does not present any magnetic-field dependence in the temperature range investigated. The electronic contribution κ_e^{WF} was estimated from the electrical resistivity using the Wiedemann-Franz law (Eq. 3.12). The electrical resistivity was measured on the same sample using the same contacts and it was found to saturate below 100 K at $\rho \sim 495 \mu\Omega\text{cm}$ [247]. As κ_e^{WF} (cf. dotted line) is distinctly smaller than the measured total $\kappa(T)$, phonons are the dominating heat carriers. The phonon contribution due to boundary scattering $\kappa_{ph}^{Casimir}$ (cf. dashed line) is estimated from the gas kinetic equation (Eq. 3.13) using the low-temperature lattice specific heat ($C_{ph} = 0.73 \text{ mJ/molK}^4 \times T^3$, $\theta_D = 254 \text{ K}$) [244], and taking the smallest dimensions of the

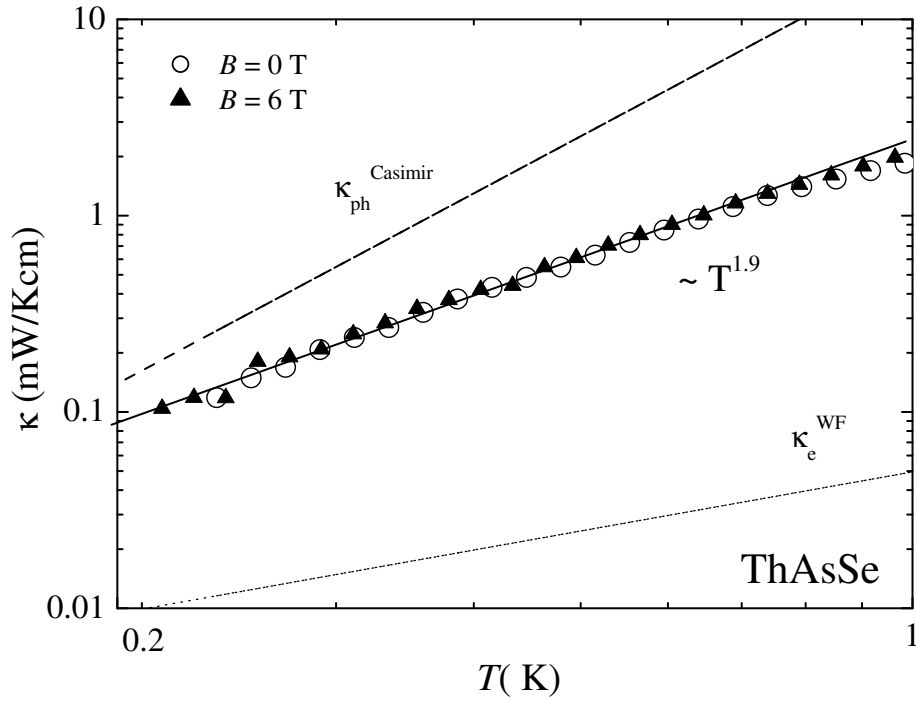


Figure 7.4: Temperature dependence of the thermal conductivity, $\kappa(T)$, of ThAsSe in zero magnetic field and at 6 T. The solid line is the best fit of the data ($\kappa \sim T^\alpha$). The dotted line represents the electronic contribution calculated using the Wiedemann-Franz law, κ_e^{WF} . The dashed line is the phonon contribution due to boundary scattering, $\kappa_{ph}^{Casimir}$.

sample (~ 0.1 mm) for the mean-free path. $\kappa_{ph}^{Casimir}$ is much larger than the total measured $\kappa(T)$. Thus, the phonons appear to be subject to an additional scattering mechanism. Below 0.7 K, $\kappa(T)$ of ThAsSe is well approximated by the relation $\kappa(T) = B(T/\alpha)^\delta$ with $\alpha = 1$ K, $\delta = 1.92$ and $B = 22.5 \times 10^{-4}$ W/(Kcm) (cf. solid line). A power law with $\delta = 1.9 \pm 0.1$ is universal for compounds which present scattering of phonons from tunneling states [240]. It is important to mention, though, that a similar behavior, $\kappa \sim T^2$, is expected for phonons scattered from electrons. Usually this process is negligible if the product of the charge-carrier mean-free path l_e and the wave number of the dominating phonons q_{dom} is less than 1 (Pippard ineffectiveness condition) [23]. Combining resistivity results with the charge-carrier concentration n from Hall measurements [244], for ThAsSe we have estimated $l_e q_{dom}$ to be 0.5. In systems containing atoms which move differently from the host lattice the phonon electron coupling can be enhanced even if $l_e q_{dom} < 1$. However, in this case the thermal conductivity should behave as $\kappa \sim T^\alpha$ with $\alpha \leq 1$ [24], in disagreement with the experimental observation. Thus, the low-temperature $\kappa(T)$ data presented here provide additional evidence for the presence of TLS in ThAsSe.

7.2 Ba₈Ga₁₆Ge₃₀

7.2.1 Introduction

Current investigations to explore new thermoelectric materials for Peltier cooling or power generation include rattling compounds, Kondo insulators, semiconductors, superlattices, etc [4, 248]. The performance efficiency of thermoelectric materials is determined by the dimensionless figure of merit $ZT = TS^2\sigma/\kappa$, where S is the thermopower, σ is the electrical conductivity, and κ is the thermal conductivity. For a good thermoelectric material, one needs a low thermal conductivity but a high electrical conductivity and a high thermopower. To obtain high S values, semiconductor- or semimetal-like compounds are preferred. Up to now, the maximum value of ZT is still limited to approximately 1 at ambient conditions. Recently, Slack has proposed the concept of a phonon glass and electron crystal (PGEC model) for obtaining new thermoelectric materials with high

ZT [249]. The basic idea of the PGEC model is that guest atoms “rattle” inside a host framework and produce low-frequency anharmonic phonon modes, which strongly scatter the heat carrying acoustic modes from the host atoms. The rattler scattering will significantly reduce the (phonon) thermal conductivity to a glass-like value without seriously reducing the electrical conductivity, which is mainly determined by the framework. In the last few years, the PGEC model has been argued to be realized in the clathrates [249].

In the clathrates, molecules or atoms of one substance are enclosed within the crystal structure of another substance. Chemically, one component (e.g. Si, Ge, Sn) forms “host” cages and the “guest” atoms/molecules (e.g. alkali metals, alkali-earth metals, rare-earth metals or gas molecules) are trapped within the cages. The guest atoms can rattle inside the oversized cavities. The cages are face sharing and the constituent atoms are sp^3 hybridized, forming covalent bonds with their nearest neighbors. The intermolecular forces between the host atoms and the guest atoms usually are weak compared to the covalent bonds. A large number of clathrate types and compositions exists. Of interest here are the type-I clathrates, with the formula $\text{II}_8\text{III}_{16}\text{IV}_{30}$ where the roman numbers indicate the group of the periodic table. These cubic solids are, from simple valence counting arguments, expected to be intrinsic semiconductors. However, most of them show metal-like resistivities and n -type properties. The only exception are $\text{Ba}_8\text{Ga}_{16}\text{Si}_{30}$, $\text{Ba}_8\text{Ga}_{16}\text{Ge}_{30}$, $\text{Ba}_8\text{Ga}_{16}\text{Sn}_{30}$ and $\text{Sr}_8\text{Ga}_{16}\text{Ge}_{30}$ which have temperature dependent transport properties typical for heavily-doped semiconductors [250]. p -type properties have only been observed in slightly Sb doped $\text{Ba}_8\text{Ga}_{16}\text{Ge}_{30}$ samples [251] and in $\text{Ba}_8\text{Ga}_{16}\text{Ge}_{30}$ samples with an excess of Ga. The sample studied in this section is such a p -type $\text{Ba}_8\text{Ga}_{16}\text{Ge}_{30}$ sample [252].

As expected from the PGEC model, studies of the thermal conductivity in many clathrates have indeed revealed glass-like temperature dependences: Ge clathrates doped with Sr and/or Eu [12, 253, 254], Na-doped Si clathrate [255], type-I Sn clathrates [256, 257]. The majority of all these measurements has been performed above liquid-helium temperature. Only $\text{Sr}_8\text{Ga}_{16}\text{Ge}_{30}$ has been measured at temperatures below 1 K [12].

Here, thermal-conductivity measurements on single crystalline $\text{Ba}_8\text{Ga}_{16}\text{Ge}_{30}$ between 200 mK and 7 K are presented.

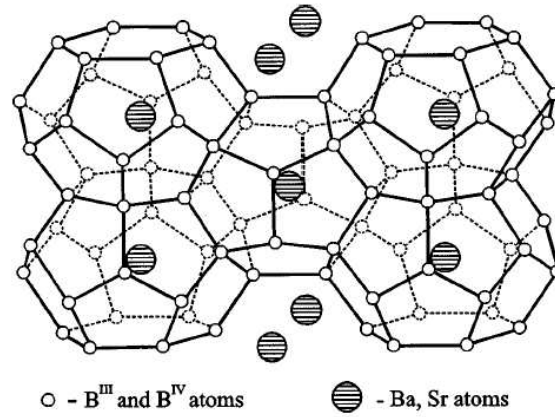


Figure 7.5: Crystal structure of $\text{Ba}_8\text{Ga}_{16}\text{Ge}_{30}$ [250].

7.2.2 Physical properties of $\text{Ba}_8\text{Ga}_{16}\text{Ge}_{30}$

The physical properties presented in this section were measured on samples from the same batch as the one used to measure thermal conductivity.

Figure 7.6 shows the electrical resistivity ρ as a function of temperature of $\text{Ba}_8\text{Ga}_{16}\text{Ge}_{30}$. ρ increases upon decreasing the temperature. At around 1.5 K a kink is observed [252].

Figure 7.7 shows the Hall coefficient R_H as a function of temperature of $\text{Ba}_8\text{Ga}_{16}\text{Ge}_{30}$. R_H is positive in the whole temperature range indicating that the majority carriers are holes. R_H increases upon decreasing the temperature. The charge-carrier concentration was calculated from the Hall coefficient using a one-band model. It was found to be $n \sim 0.069/\text{f.u.}$ at 2 K [252].

The temperature dependence of the specific heat C of $\text{Ba}_8\text{Ga}_{16}\text{Ge}_{30}$ is shown in Fig. 7.8. Above 5 K, the electronic contribution to the specific heat is negligible and the lattice contribution can be well described with a combined Debye and Einstein model. A linear fit of C/T versus T^2 between 1.5 K and 4 K gives a Debye temperature θ_D of approximately 311 K and $C_{ph} = 0.0077 \text{ J/molK}^4 \times T^3$ [258].

The thermopower S of $\text{Ba}_8\text{Ga}_{16}\text{Ge}_{30}$ is positive and increases with increasing temperature. Above 70 K, $S(T)$ follows a $T^{0.6}$ dependence. The deviation from the expected linear temperature dependence can be attributed to the increase of n with increasing temperature. Combining the thermopower results (not shown)

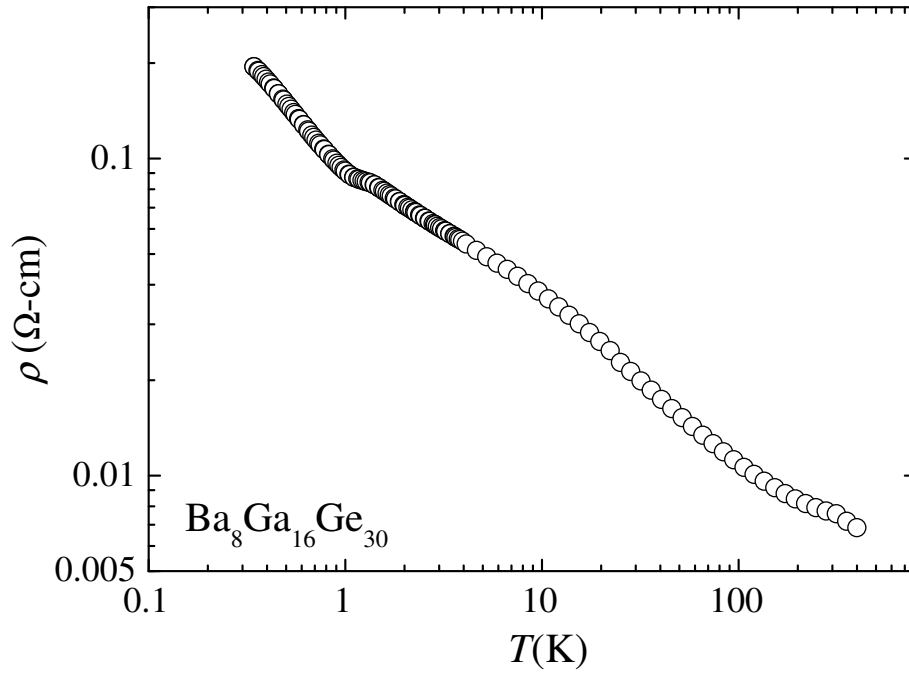


Figure 7.6: Temperature dependence of the electrical resistivity, $\rho(T)$, of $\text{Ba}_8\text{Ga}_{16}\text{Ge}_{30}$ [252].

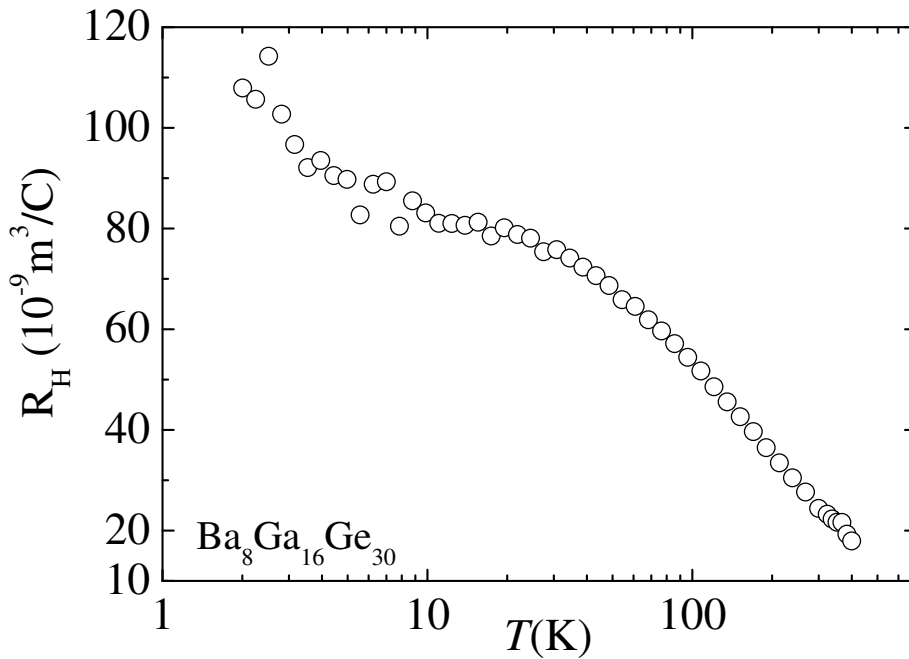


Figure 7.7: Temperature dependence of the Hall coefficient, $R_H(T)$, of $\text{Ba}_8\text{Ga}_{16}\text{Ge}_{30}$ [252].

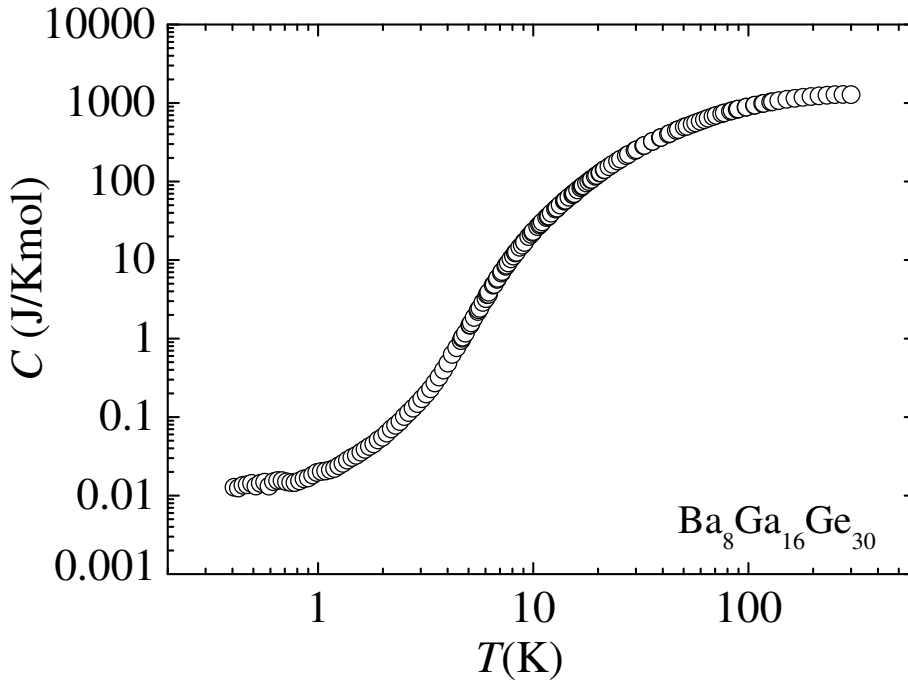


Figure 7.8: Temperature dependence of the specific heat, $C(T)$, of $\text{Ba}_8\text{Ga}_{16}\text{Ge}_{30}$ in a log-log plot [258].

with the charge-carrier concentration n at 300 K, one may estimate the effective mass m^* of the charge carriers to be $m^* = 3.6m_0$, where m_0 is the free-electron mass [252].

7.2.3 Results and discussion

The measurements presented here were performed on a single crystal of approximately $3.5 \text{ mm} \times 2.4 \text{ mm} \times 1.5 \text{ mm}$ grown from Ga flux, using a molten-metal-solvent technique [258]. The sample was provided by B. B. Iversen (University of Aarhus, Denmark).

The electronic contribution to the thermal conductivity κ_e^{WF} was estimated from the electrical resistivity [252, 258] measured on the same sample (with the same contacts) between 350 mK and 400 K using the Wiedemann-Franz law (Eq. 3.12). For temperatures below 350 mK, the resistivity was extrapolated from the measured values. κ_e^{WF} is three orders of magnitude smaller than the total measured thermal conductivity over the whole temperature range. Hence one can

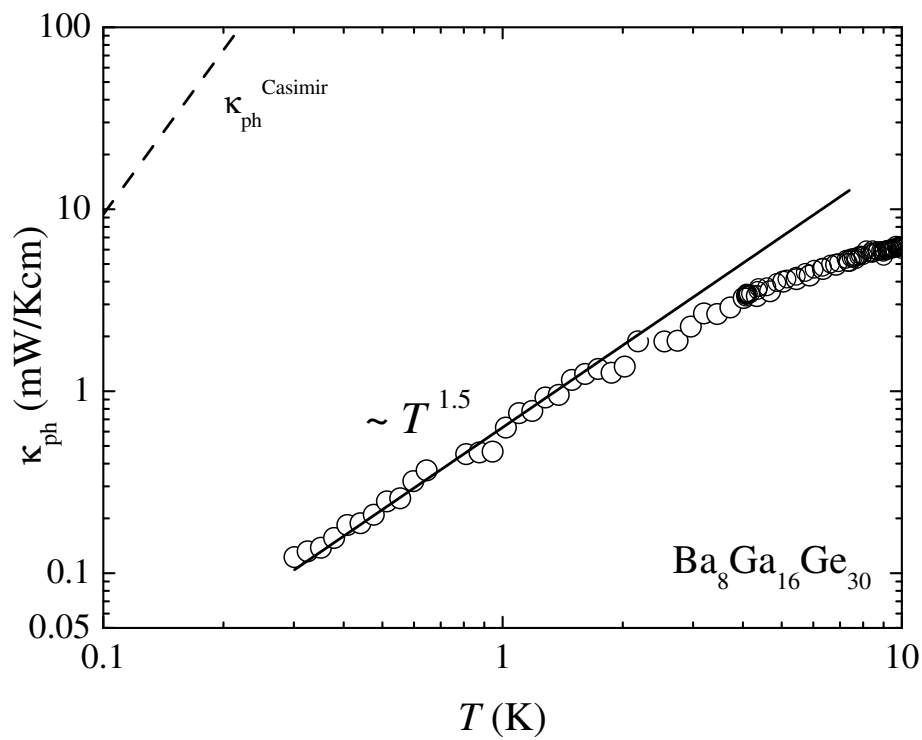


Figure 7.9: Temperature dependence of the phonon thermal conductivity, $\kappa_{ph}(T)$, of $Ba_8Ga_{16}Ge_{30}$. The solid is the best fit of the data ($\kappa \sim T^\alpha$). The dashed line is the phonon contribution due to boundary scattering, $\kappa_{ph}^{Casimir}$.

consider that $\kappa(T) = \kappa_{ph}$. Figure 7.9 shows the temperature dependence of the phonon thermal conductivity $\kappa_{ph}(T)$ of Ba₈Ga₁₆Ge₃₀. The phonon contribution due to boundary scattering $\kappa_{ph}^{Casimir}$ is estimated from the gas kinetic equation (Eq. 3.13) using the low-temperature lattice specific heat ($C_{ph} = 0.0077 \times T^3$ J/molK⁴, $\theta_D = 311$ K) [258], and taking the smallest dimensions of the sample (~ 1.5 mm) for the mean-free path (cf. dashed line). $\kappa_{ph}^{Casimir}$ is much larger than the total measured $\kappa(T)$. This indicates that there is an additional scattering mechanism that suppresses the phonon thermal conductivity. Below 1.5 K, $\kappa_{ph}(T)$ is well approximated by a $T^{1.5}$ law (cf. solid line). This temperature dependence can be attributed either to scattering of phonons from charge carriers or to the scattering of phonons from tunneling states. Neutron-diffraction experiments have shown that the density of tunneling states in Ba₈Ga₁₆Ge₃₀ is very low [259], excluding those as possible scatters of the phonons. It appears more probable that the temperature dependence of the phonon thermal conductivity is due to phonons scattered from electrons. Usually this process is negligible if the product of the charge carrier mean free path l_e and the wave number of the dominating phonons q_{dom} is less than 1 (Pippard ineffectiveness condition) [23]. Combining resistivity results with the charge-carrier concentration n from Hall-effect measurements and the effective mass m^* obtained from thermopower measurements [258], $l_e q_{dom}$ of Ba₈Ga₁₆Ge₃₀ has been estimated to be 1. However, according to a recent theoretical study for systems containing atoms which move differently from the host lattice, the phonon-electron coupling can be enhanced even if $l_e q_{dom} < 1$ [24]. This leads to an increased phonon-charge-carrier scattering rate as l_e decreases. Numerical calculations using equation 3.20 show that the phonon thermal conductivity varies as $\kappa_{ph} \sim T^\alpha$ with $1 < \alpha < 2$. Using the Ziman model for the electron-phonon scattering [22], and the effective mass calculated using the one-band model for the thermopower, it is possible to estimate the deformation potential E_{def} which is the strength of the phonon-electron interaction. For Ba₈Ga₁₆Ge₃₀, E_{def} is ~ 0.5 eV. This value of E_{def} is comparable with values of a normal semiconductor with similar n [260]. Thus, the possibility that the “glass-like” thermal conductivity of clathrates at the lowest temperature is due to phonon-electron scattering and not – as generally believed – due to scattering of phonons from rattling atoms must be considered very seriously, also

for other clathrates.

7.3 Outlook

- Further thermal-conductivity investigations of other clathrates at very low temperatures could help to clarify the scattering mechanism of the phonons in this class of materials.

Chapter 8

Summary

In this thesis thermal-conductivity κ and thermopower S measurements have been performed on: the Kondo insulator $\text{U}_2\text{Ru}_2\text{Sn}$, the quasi-one-dimensional spin system $\text{Yb}_4(\text{As}_{0.7}\text{P}_{0.3})_3$, the heavy-fermion compound $\text{YbRh}_2(\text{Si}_{1-x}\text{Ge}_x)_2$ ($x = 0, 0.05$), the diamagnet ThAsSe , and the clathrate $\text{Ba}_8\text{Ga}_{16}\text{Ge}_{30}$.

The temperature dependence of the thermopower, $S(T)$, of the tetragonal Kondo insulator $\text{U}_2\text{Ru}_2\text{Sn}$ presents a linear behavior in the whole temperature range, which is attributed to a diffusion thermopower. The thermopower is positive along the c axis and negative perpendicular to the c axis. Considering the Mott relation, this difference in sign could indicate that there is an anisotropy in the density of states at the Fermi level. Using a one-band model the effective mass m^* is estimated to be $2m_0$ and $16m_0$ along and perpendicular to the c axis, respectively, where m_0 is the free-electron mass. This indicates that $\text{U}_2\text{Ru}_2\text{Sn}$ has a highly anisotropic residual density of states within the pseudogap. From resistivity measurements and using the Wiedemann-Franz law, the electronic contribution to the thermal conductivity was found to be smaller than the measured thermal conductivity. Thus, the thermal conductivity κ of $\text{U}_2\text{Ru}_2\text{Sn}$ is phonon dominated. Below 400 mK, the phonon contribution to $\kappa(T)$ shows a T^2 behavior for both directions that can be attributed to phonons scattered from electrons. No magnetic-field dependence was observed for both the thermopower and the thermal conductivity of $\text{U}_2\text{Ru}_2\text{Sn}$ in the investigated temperature range. This is attributed to the fact that the energy equivalent of the applied magnetic field is much smaller than the energy gap.

The temperature dependence of the thermal conductivity, $\kappa(T)$, of the quasi-one-dimensional $S = 1/2$ Heisenberg antiferromagnet $\text{Yb}_4(\text{As}_{0.7}\text{P}_{0.3})_3$ was found to follow the relation $aT + bT^2$ between 0.4 and 3 K at zero magnetic field which was attributed to the dominating role of magnons. The magnons act as heat carriers at the lowest temperatures and as scatterers for the phonons at higher temperatures. Below 0.4 K, the thermal conductivity drops below the $aT + bT^2$ law due to spin-glass freezing in agreement with specific-heat measurements. The electronic contribution to the thermal conductivity is reduced by four orders of magnitude when doping Yb_4As_3 with 30 % of P due to the reduction of the number of charge carriers. The fact that the aT term is virtually unchanged by the doping rules out an electronic origin of this term. We attribute the thermal conductivity at low temperatures and in zero magnetic field of Yb_4As_3 and $\text{Yb}_4(\text{As}_{0.7}\text{P}_{0.3})_3$ to heat carried by magnons. The thermal conductivity is reduced upon increasing the magnetic field up to $B = 1$ T. In higher fields and below 1 K, the reduction of the phonon-magnon scattering rate reinforces the phonon conductivity and overcompensates this effect. At $B = 6$ T, the thermal conductivity at 0 T is recovered. The opening of a gap in the magnon-excitation spectrum is a possible explanation of this behavior. Above 1 K, the magnetic-field dependence of the thermal conductivity, $\kappa(B, T)$, is reduced upon increasing magnetic field. The scattering of the phonons by magnetic solitons could explain this effect.

The thermopower, $S(T)$, of the heavy-fermion system $\text{YbRh}_2(\text{Si}_{1-x}\text{Ge}_x)_2$ ($x = 0, 0.05$) presents negative values in the measured temperature range, as expected for an Yb compound. A logarithmic temperature dependence in $S(T)$ in a certain range of temperature is observed, as predicted by the model developed by Paul et al [213]. The temperature dependence of the thermal conductivity, $\kappa(T)$, shows striking deviations from the behavior expected for a simple metal, e.g., the Wiedemann-Franz law does not appear to be fulfilled. The thermal conductivity is dominated by the electronic part. The electronic contribution to the thermal conductivity is strongly temperature dependent and was found to have a logarithmic behavior in a certain range of temperature. A plausible explanation for the deviation from the Wiedemann-Franz law is the influence of spin fluctuations in the systems which can affect the thermal conductivity and the electrical resistivity in different ways. Further measurements will clarify this point.

The structurally disordered diamagnetic compound ThAsSe shows a thermal conductivity with a $T^{1.9}$ behavior. The electronic thermal conductivity is negligible with respect to the total thermal conductivity, as was estimated using electrical-resistivity measurements and the Wiedemann-Franz law. Thus, the thermal conductivity is phonon dominated: $\kappa = \kappa_{ph} \sim T^{1.9}$. From the Pippard ineffectiveness condition, it is possible to discard the phonon-electron scattering as the dominant scattering mechanism for the phonons, leaving phonons scattered by tunneling states as the most probable scattering mechanism.

The p -type clathrate $\text{Ba}_8\text{Ga}_{16}\text{Ge}_{30}$ shows a $T^{1.5}$ behavior below 1.5 K. The electronic contribution, calculated from the electrical resistivity using the Wiedemann-Franz law, is three orders of magnitude smaller than the total measured thermal conductivity over the whole range of temperature. Thus, the phonon contribution is the dominant contribution and shows a $T^{1.5}$ behavior. Since $\text{Ba}_8\text{Ga}_{16}\text{Ge}_{30}$ has a very low density of tunneling states, excluding those as possible scatterers of the phonons, we attribute the $T^{1.5}$ behavior to phonons scattered from electrons. We use a model developed for systems containing atoms which move differently from the host lattice, as it is the case for clathrates.

Bibliography

Bibliography

- [1] Proceedings of the International Conference on Strongly Correlated Electron Systems. *Physica B*, 359-361:Papers in this number, 2005.
- [2] P. J. Lee, editor. *Engineering Superconductivity*. Wiley-Interscience, John Wiley & Sons, Inc., 2001.
- [3] T. Chatterji, editor. *Colossal Magneto-Resistive Manganites*. Kluwer Academic Publisher, 2004.
- [4] G. D. Mahan. Good Thermoelectrics. *Solid State Physics*, 51:81, 1998.
- [5] R. Berman. *Thermal Conduction in Solids*. Clarendon Press, Oxford, 1976.
- [6] F. J. Blatt, P. A. Schroeder, C. L. Foiles and D. Greig. *Thermoelectric Power of Metals*. Plenum Press, New York, 1976.
- [7] A. V. Sologubenko, K. Giannó, H. R. Ott, U. Ammerahl and A. Revcolevschi. Thermal Conductivity of the Hole-Doped Spin Ladder System $\text{Sr}_{14-x}\text{Ca}_x\text{Cu}_{24}\text{O}_{41}$. *Phys. Rev. Lett.*, 84(12):2714, 2000.
- [8] D. L. Cox and A. Zawadowski. Exotic Kondo effects in metals: magnetic ions in a crystalline electric field and tunneling centers. *Adv. Phys.*, 47(5):599, 1998.
- [9] R. W. Hill, C. Proust, L. Taillefer, P. Fournier and R. L. Greene. Breakdown of Fermi-liquid theory in a copper-oxide superconductor. *Nature*, 414:711, 2001.

- [10] T. Saso and K. Urasaki. Seebeck Coefficient of Kondo Insulators. *J. Phys. Soc. Jpn.*, 71(Supp.):288, 2002.
- [11] Y. Isikawa, K. Mori, Y. Ogiso, K. Oyabe, and K. Sato. Thermal Conductivity of CeNiSn Single Crystals. *J. Phys. Soc. Jpn.*, 60(8):2514, 1991.
- [12] J. L. Cohn, G. S. Nolas, V. Fessatidis, T. H. Metcalf and G. A. Slack. Glasslike Heat Conduction in High-Mobility Crystalline Semiconductors. *Phys. Rev. Lett.*, 82(4):779, 1999.
- [13] N. W. Ashcroft and N. D. Mermin. *Solid State Physics*. Harcourt College Publisher, USA, 1976.
- [14] R. D. Barnard. *Thermoelectricity in Metals and Alloys*. Taylor and Francis Ltd, London, 1972.
- [15] D. K. C. MacDonald. *Thermoelectricity: an introduction to the principles*. John Wiley and Sons, Inc., New York, 1962.
- [16] F. Pobell. *Matter and Methods at Low Temperatures*. Springer-Verlag, Berlin Heidelberg, 1996.
- [17] B. Wand. *Untersuchungen zum Transport und zur spezifischen Wärme an elektronisch hochkorrelierten Systemen*. PhD thesis, TU Darmstadt, Germany, 1998.
- [18] J. Beyer Nielsen and H. Smith. Thermal Conductivity and Charge Relaxation in Strong-Coupling Superconductors. *Phys. Rev. Lett.*, 49(9):689, 1982.
- [19] J. Bardeen, G. Rickayzen and L. Tewordt. Theory of the Thermal Conductivity of Superconductors. *Phys. Rev.*, 113(4):982, 1959.
- [20] M. Odoni, P. Fuchs and, H. R. Ott. Size effect on the lattice thermal conductivity of lead single crystals. *Phys. Rev. B*, 28(3):1314, 1983.
- [21] J. M. Ziman. *Electrons and Phonons*. Oxford Science Publications, Oxford, 1960.

- [22] J. M. Ziman. The Effect of Free Electrons on Lattice Conduction. *Philos. Mag.*, 1:191, 1955.
- [23] A. B. Pippard. Ultrasonic Attenuation in Metals. *Philos. Mag.*, 46:1104, 1955.
- [24] A. Sergeev and V. Mitin. Breakdown of Pippard ineffectiveness condition for phonon-electron scattering in micro and nanostructures. *Europhys. Lett.*, 51(6):641, 2000.
- [25] H. Sato. On the Thermal Conductivity of Ferromagnetics. *Prog. Theor. Phys.*, 13:119, 1955.
- [26] Z. Fisk, J. L. Sarrao, S. L. Cooper, P. Nyhus, G. S. Boebinger, A. Passner, and P. C. Canfield. Kondo insulators. *Physica B*, 223&224:409, 1996.
- [27] G. Aeppli and Z. Fisk. Kondo Insulators. *Comments Condens. Matter Phys.*, 16(3):155, 1992.
- [28] M. Jaime, R. Movshovich, G. R. Stewart, W. P. Beyermann, M. Gomez Berisso, M. F. Hundley, P. C. Canfield and J. L. Sarrao. Closing the spin gap in the Kondo insulator $\text{Ce}_3\text{Bi}_4\text{Pt}_3$. *Nature*, 405:160, 2000.
- [29] Z. Fisk, J. L. Sarrao, J. D. Thompson, D. Mandrus, M. F. Hundley, A. Miglori, B. Bucher, Z. Schlesinger, G. Aeppli, E. Bucher, J. F. DiTusa, C. S. Oglesby, H.-R. Ott, P. C. Canfield and S. E. Brown. Kondo insulators. *Physica B*, 206&207:798, 1995.
- [30] T. Nishino and K. Ueda. Spin- and charge-excitation gaps in the one-dimensional periodic Anderson model. *Phys. Rev. B*, 47(19):12451, 1993.
- [31] H. Ikeda and K. Miyake. A theory of Anisotropic Semiconductor of Heavy Fermions. *J. Phys. Soc. Jpn.*, 65(6):1769, 1996.
- [32] T. Kasuya. Physical Mechanism in Kondo Insulator. *J. Phys. Soc. Jpn.*, 65(8):2548, 1996.

- [33] Y. Kagan, K. A. Kikoin and A. S. Mishchenko. Interplay between heavy fermions and crystal-field excitation in Kondo lattices: Low temperature thermodynamics and inelastic neutron scattering spectra of CeNiSn. *Phys. Rev. B*, 55(18):12348, 1997.
- [34] T. Saso and M. Itoh. Insulator-to-metal transition in Kondo insulators under a strong magnetic field. *Phys. Rev. B*, 53(11):6877, 1996.
- [35] N. A. de Oliveira, M. V. Tovar Costa, A. Troper, G. M. Japiassú and M. A. Continentino. Magnetic-field-driven metal-insulator transition in Kondo insulators. *Phys. Rev. B*, 60(3):1444, 1999.
- [36] M. V. Tovar Costa, A. Troper, N. A. de Oliveira, G. M. Japiassú, and M. A. Continentino. Metal-insulator transition in Kondo insulators: A functional-integral approach. *Phys. Rev. B*, 57(12):6943, 1998.
- [37] N. A. de Oliveira. Impurity effect on the metal-insulator transition in Kondo insulators. *Phys. Rev. B*, 61(23):15726, 2000.
- [38] L. Peche, E. V. Anda and C. A. Büsser. Transport properties of Kondo-insulator alloys. *Phys. Rev. B*, 68:245119, 2003.
- [39] L. D. Landau. The theory of a Fermi liquid. *Sov. Phys. JETP*, 3(6):920, 1957.
- [40] L. D. Landau. Oscillations in a Fermi liquid. *Sov. Phys. JETP*, 5(1):101, 1957.
- [41] L. D. Landau. On the theory of the Fermi liquid. *Sov. Phys. JETP*, 8(1):70, 1959.
- [42] R. Shankar. Renormalization-group approach to interacting fermions. *Rev. Mod. Phys.*, 66(1):129, 1994.
- [43] N. Grewe and F. Steglich. “Heavy fermions” in *Handbook on the physics and chemistry of rare earths.*, volume 14, chapter 97, page 343. Elsevier Science, The Netherlands, 1991.

- [44] S. Doniach. The Kondo lattice and weak antiferromagnetism. *Physica B*, 91:231, 1977.
- [45] G. R. Stewart. Heavy-fermion systems. *Rev. Mod. Phys.*, 56(4):755, 1984.
- [46] G. R. Stewart. Non-Fermi-liquid behavior in *d*- and *f*-electron metals. *Rev. Mod. Phys.*, 73:797, 2001.
- [47] A. J. Schofield. Non-Fermi-liquids. *Contemp. Phys.*, 40(2):95, 1999.
- [48] C. M. Varma, Z. Nussinov and W. v. Saarloos. Singular or non-Fermi liquids. *Phys. Rep.*, 361(5-6):267, 2002.
- [49] J. A. Hertz. Quantum critical phenomena. *Phys. Rev. B*, 14(3):1165, 1976.
- [50] A. J. Millis. Effect of a nonzero temperature on quantum critical points in itinerant fermion systems. *Phys. Rev. B*, 48(10):7183, 1993.
- [51] T. Moriya and, T. Takimoto. Anomalous Properties around Magnetic Instability in Heavy Electron System. *J. Phys. Soc. Jpn.*, 64(3):960, 1995.
- [52] G. G. Lonzarich. "The magnetic electron" in *Electron A centenary volume*, chapter 6, page 109. Cambridge University Press, Cambridge, 1997.
- [53] A. Rosch. Interplay of Disorder and Spin Fluctuations in the Resistivity near a Quantum Critical Point. *Phys. Rev. Lett.*, 82(21):4280, 1999.
- [54] H. v. Löhneysen, T. Pietrus, G. Portisch, H. G. Schlager, A. Schröder, M. Sieck and T. Trappmann. Non-Fermi-Liquid Behavior in a Heavy-Fermion Alloy at a Magnetic Instability. *Phys. Rev. Lett.*, 72(20):3262, 1994.
- [55] A. Schröder, G. Aeppli, R. Coldea, M. Adams, O. Stockert, H. v. Löhneysen, E. Bucher, R. Ramazashvili and P. Coleman. Onset of antiferromagnetism in heavy-fermion metals. *Nature*, 407:351, 2000.
- [56] O. Trovarelli, C. Geibel, S. Mederle, C. Langhammer, F. M. Grosche, P. Gegenwart, M. Lang, G. Sparn, and F. Steglich. YbRh₂Si₂: Pronounced

- Non-Fermi-Liquid Effects above a Low-Lying Magnetic Phase Transition. *Phys. Rev. Lett.*, 85(3):626, 2000.
- [57] P. Gegenwart, J. Custers, C. Geibel, K. Neumaier, T. Tayama, K. Tenya, O. Trovarelli, and F. Steglich. Magnetic-Field Induced Quantum Critical Point in YbRh_2Si_2 . *Phys. Rev. Lett.*, 89(5):056402, 2002.
- [58] Q. Si, S. Rabello, K. Ingersent, and J. L. Smith. Locally critical quantum phase transitions in strongly correlated metals. *Nature*, 413:804, 2001.
- [59] P. Coleman, C. Pépin, Q. Si, and R. Ramazashvili. How do Fermi liquids get heavy and die? *J. Phys.: Condens. Matter*, 13:R723, 2001.
- [60] P. Nozières and A. Blandin. Kondo effect in real metals. *J. Phys. (France)*, 41:193, 1980.
- [61] D. L. Cox and M. Jarrell. The two-channel Kondo route to non-Fermi-liquid metals. *J. Phys.: Condens. Matter.*, 8:9825, 1996.
- [62] P. S. Riseborough. Heavy fermion semiconductors. *Adv. Phys.*, 49(3):257, 2000.
- [63] T. Ekino, T. Takabatake, H. Tanaka, and H. Fujii. Tunneling Evidence for the Quasiparticle Gap in Kondo Semiconductors CeNiSn and CeRhSb . *Phys. Rev. Lett.*, 75(23):4262, 1995.
- [64] D. N. Davydov, S. Kambe, A. G. M. Jansen, P. Wyder, N. Wilson, G. Laperot and J. Flouquet. Anisotropic magnetic-field induced crossover from a pseudogap to a heavy-fermion state in CeNiSn . *Phys. Rev. B*, 55(12):R7299, 1997.
- [65] B. Bucher, Z. Schlesinger, P. C. Canfield and Z. Fisk. Kondo Coupling Induced Charge Gap in $\text{Ce}_3\text{Bi}_4\text{Pt}_3$. *Phys. Rev. Lett.*, 72(4):522, 1994.
- [66] M. F. Hundley, P. C. Canfield, J. D. Thompson, Z. Fisk, and J. M. Lawrence. Hybridization gap in $\text{Ce}_3\text{Bi}_4\text{Pt}_3$. *Phys. Rev. B*, 42(10):6842, 1990.

- [67] P. C. Canfield, A. Lacerda, J. D. Thompson, G. Sparn, W. P. Beyermann, M. F. Hundley and Z. Fisk. Doping and pressure study of $U_3Sb_4Pt_3$. *J. Alloys Compd.*, 181:77, 1992.
- [68] M. Kuriso, T. Takabatake and H. Fujiwara. Gap suppression in CeNiSn under hydrostatic pressure. *Solid State Commun.*, 68(7):595, 1988.
- [69] J. Beille, M. B. Maple, J. Wittig, Z. Fisk and L. E. DeLong. Suppression of the energy gap in SmB_6 under pressure. *Phys. Rev. Lett.*, 28(12):7397, 1983.
- [70] F. Iga, T. Suemitsu, S. Hiura, K. Takagi, K. Umeo, M. Sera and T. Takabatake. Thermoelectric properties of the Kondo semiconductor: $Yb_{1-x}Lu_xB_{12}$. *J. Magn. Magn. Mater.*, 226-230:137, 2001.
- [71] B. C. Sales, E. C. Jones, B. C. Chakoumakos, J. A. Fernandez-Baca, H. E. Harmon, J. W. Sharp and E. H. Volckmann. Magnetic, transport, and structural properties of $Fe_{1-x}Ir_xSi$. *Phys. Rev. B*, 50(12):8207, 1994.
- [72] A. Hiess, C. Geibel, G. Sparn, C.D. Bredl, F. Steglich, T. Takabatake and H. Fujii. Transport properties of CeNiSn at low temperatures and in high magnetic fields. *Physica B*, 199&200:437, 1994.
- [73] T. Ekino, T. Takabatake and H. Fujii. Break-junction measurements of CeNiSn under magnetic fields. *Physica B*, 230-232:635, 1997.
- [74] K. Sugiyama, F. Iga, M. Kasaya, T. Kasuya and M. Date. Field-Induced Metallic State in YbB_{12} under High Magnetic Field. *J. Phys. Soc. Jap.*, 57(11):3946, 1988.
- [75] T. Saso. Theory of Kondo insulators under strong magnetic field. *Physica B*, 281&-282:315, 2000.
- [76] J. C. Cooley, C. H. Mielke, W. L. Hults, J. D. Goettee, M. M. Honold, R. M. Modler, A. Lacerda, D. G. Rickel and J. L. Smith. High Field Gap Closure in the Kondo Insulator SmB_6 . *Journal of Superconductivity*, 12(1):171, 1999.

- [77] J. C. Cooley, M. C. Aronson and P. C. Canfield. High pressures and the Kondo gap in $\text{Ce}_3\text{Bi}_4\text{Pt}_3$. *Phys. Rev. B*, 55(12):7533, 1997.
- [78] M. Kasaya, F. Iga, M. Takigawa and T. Kasuya. Mixed valance properties of YbB_{12} . *J. Magn. Magn. Mater.*, 47&48:429, 1985.
- [79] M. Sera, S. Kobayashi, M. Hiroi, N. Kobayashi and S. Kunii. Thermal conductivity of RB_6 ($R = \text{Ce}, \text{Pr}, \text{Nd}, \text{Sm}, \text{Gd}$) single crystals. *Phys. Rev. B*, 54(8):R5207, 1996.
- [80] T. Takabatake, G. Nakamoto, T. Yoshino, H. Fujii, K. Izawa, S. Nishigori, H. Goshima, T. Suzuki, T. Fujita, K. Maezawa, T. Hiraoka, Y. Okayama, I. Oguro, A. A. Menovsky, K. Neumaier, A. Brückl and K. Andres. Localization effects in Kondo semimetals CeNiSn and CeRhSb . *Physica B*, 223&224:413, 1996.
- [81] F. Iga, N. Shimizu and T. Takabatabe. Single crystal growth and physical properties of Kondo insulator YbB_{12} . *J. Magn. Magn. Mater.*, 177-181:337, 1998.
- [82] T. Takabatake, F. Iga, T. Yoshino, Y. Echizen, K. Katoh, K. Kobayashi, M. Higa, N. Shimizu, Y. Bando, G. Nakamoto, H. Fujii, K. Izawa, T. Suzuki, T. Fujita, M. Sera, M. Hiroi, K. Maezawa, S. Mock, H. v. Löhneysen, A. Brückl, K. Neumaier and K. Andres. Ce- and Yb-based Kondo semiconductors. *J. Magn. Magn. Mater.*, 177-181:277, 1998.
- [83] K. Nakamura, Y. Kitaoka, K. Asayama, T. Takabatake, H. Tanaka, and H. Fujii. Low-Energy Excitation in Kondo Semiconductors CeNiSn and CeRhSb . *J. Phys. Soc. Jpn.*, 63(2):433, 1994.
- [84] A. P. Reyes, R. H. Heffner, P. C. Canfield, J. D. Thompson and Z. Fisk. ^{209}Bi NMR and NQR investigation of the small-gap semiconductor $\text{Ce}_3\text{Bi}_4\text{Pt}_3$. *Phys. Rev. B*, 49(23):16321, 1994.
- [85] M. Kyogaku, Y. Kitaoka, H. Nakamura, K. Asayama, T. Takabatake, F. Teshima and H. Fujii. NMR Investigation of the Energy Gap Forma-

- tion in the Valence Fluctuating Compound CeNiSn. *J. Phys. Soc. Jpn.*, 59(5):1728, 1990.
- [86] T. Yuen, C. L. Lin, P. Schlottmann, N. Bykovetz, P. Pernambuco-Wise and J. E. Crow. Anomalous thermodynamic, transport and Mössbauer properties of UNiSn: A half-metallic system. *Physica B*, 171:362, 1991.
- [87] T. T. M. Palstra, G. J. Nieuwenhuys, J. A. Mydosh and K. H. J. Buschow. Electrical transport properties of the ternary compounds UTSn, UTSb and ThTSn. *J. Magn. Magn. Matter.*, 54-57:549, 1986.
- [88] N. Bykovetz, W. N. Herman, T. Yuen, C. Jee, C. L. Lin and J. E. Crow. Unusual magnetic and lattice transformation in UNiSn, a possible half-metallic ferromagnetic system. *J. Appl. Phys.*, 63(8):4127, 1988.
- [89] P. S. Riseborough. Magnetic instability of Kondo insulators. *Physica B*, 246-247:378, 1998.
- [90] T. Takabatake, S. Miyata, H. Fujii, Y. Aoki, T. Suzuki, T. Fujita, J. Sakurai and T. Hiraoka. Heavy-Fermion and Semiconducting Properties of the Ternary Uranium Compounds $U_3T_3Sn_4$ and $U_3T_3Sb_4$ ($T = Ni, Cu, Pd, Pt$ and Au). *J. Phys. Soc. Jpn.*, 59(12):4412, 1990.
- [91] S. Paschen, V. H. Tran, N. Senthilkumaran, M. Baenitz, F. Steglich, A. M. Strydom, P. de V. du Plessis, G. Motoyama and N. K. Sato. First results on U_2Ru_2Sn single crystals. *Physica B*, 329-333:549, 2003.
- [92] M. Baenitz, A. Rabis, S. Paschen, N. Senthilkumaran, F. Steglich, V. H. Tran, P. de V. du Plessis and A. M. Strydom. Gap formation in the semimetal U_2Ru_2Sn : evidence from ^{119}Sn NMR investigations. *Physica B*, 329-333:545, 2003.
- [93] T. Takabatake, T. Sasakawa, J. Kitagawa, T. Suemitsu, Y. Echizen, K. Umeo, M. Sera and Y. Bando. Thermoelectric properties of Ce-based Kondo semimetals and semiconductors. *Physica B*, 328:53, 2003.

- [94] C. D. W. Jones, K. A. Regan and F. J. DiSalvo. Thermoelectric properties of the doped Kondo insulator: $\text{Nd}_x\text{Ce}_{3-x}\text{Pt}_3\text{Sb}_4$. *Phys. Rev. B*, 58(24):16057, 1998.
- [95] J. G. Park, M. Ocko and B. R. Cole. Thermopower studies of $(\text{Ce,U})\text{NiSn}$. *J. Phys.: Condens. Matter*, 6:L781, 1994.
- [96] T. Saso and K. Urasaki. Thermoelectric power of Kondo insulators. *J. Phys. Chem. Solids*, 63:1475, 2002.
- [97] J. Kitagawa, T. Sasakawa, T. Suemitsu, Y. Echizen and T. Takabatake. Effects of valance fluctuation and pseudogap formation on phonon thermal conductivity of Ce-based compounds with ϵ -TiNiSi-type structure. *Phys. Rev. B*, 66:224304, 2002.
- [98] M. Sera, N. Kobayashi, T. Yoshino, K. Kobayashi, T. Takabatake, G. Nakamoto and H. Fujii. Anisotropic pseudogap in CeNiSn and CeRhSb studied by a thermal-conductivity measurement. *Phys. Rev. B*, 55(10):6421, 1997.
- [99] U. Köhler, et al. PhD thesis in progress. Unpublished.
- [100] L. Menon, P. de V. du Plessis, and A. M. Strydom. Possible Kondo insulating behavior in $\text{U}_2\text{Ru}_2\text{Sn}$. *Solid State Commun.*, 106(8):519, 1998.
- [101] K. A. McEwen, D. T. Adroja, A. D. Hillier, J.-G. Park and R. I. Bewley. Inelastic neutron scattering study of the spin gap formation in the Kondo semiconductor $\text{U}_2\text{Ru}_2\text{Sn}$. To appear in *Physica B (Proc. SCES04)*.
- [102] M. F. Hundley, P. C. Canfield, J. D. Thompson and Z. Fisk. Substitutional effects on the electronic transport of the Kondo semiconductor $\text{Ce}_3\text{Bi}_4\text{Pt}_3$. *Phys. Rev. B*, 50(24):18142, 1994.
- [103] A. Severing, J. D. Thompson, P. C. Canfield, Z. Fisk and P. Riseborough. Gap in the magnetic excitation spectrum of $\text{Ce}_3\text{Bi}_4\text{Pt}_3$. *Phys. Rev. B*, 44(13):6832, 1991.

- [104] T. E. Mason, G. Aeppli, A. P. Ramirez, K. N. Clausen, C. Broholm, N. Stücheli, E. Bucher and T. T. M. Palstra. Spin Gap and Antiferromagnetic Correlations in the Kondo Insulator CeNiSn. *Phys. Rev. Lett.*, 69(3):490, 1992.
- [105] M. N. Peron, Y. Kergadallan, J. Rebizant, D. Meyer, J. M. Winand, S. Zwiner, L. Havela, H. Nakotte, J. C. Spirlet, G. M. Kalvius, E. Colineau, J. L. Oddou, C. Jeandey and J. P. Sanchez. A new family of actinide ternary intermetallic compounds. *J. Alloys Compd.*, 201:203, 1993.
- [106] S. Paschen, et al. Unpublished.
- [107] A. M. Strydom and R. Troć. Single-crystal magnetoresistivity and magnetic susceptibility of the Kondo semimetal U_2Ru_2Sn . *Solid State Commun.*, 126:207, 2003.
- [108] A. K. Rajarajan, A. Rabis, M. Baenitz, A. A. Gippius, E. N. Morozova, J. A. Mydosh and F. Steglich. NMR investigations on single crystals of U_2Ru_2Sn : A Kondo insulator. *Physica B*, 359-361:997, 2005.
- [109] V. H. Tran, S. Paschen, A. Rabis, N. Senthilkumaran, M. Baenitz, F. Steglich, P. de V. du Plessis, and A. M. Strydom. Magnetic, thermodynamic, NMR, and transport properties of the heavy-fermion semiconductor U_2Ru_2Sn . *Phys. Rev. B*, 67:075111, 2003.
- [110] E. F. Steigmeier and B. Abeles. Scattering of Phonons by Electrons in Germanium-Silicon Alloys. *Phys. Rev.*, 136(4A):A1149, 1964.
- [111] H. Anno, K. Matsubara, Y. Notohara, T. Sakakibara and H. Tashiro. Effect of doping on the transport properties of $CoSb_3$. *J. Appl. Phys.*, 86(7):3780, 1999.
- [112] P. W. Anderson. The Resonating Valance Bond State in La_2CuO_4 and Superconductivity. *Science*, 235:1196, 1987.
- [113] E. Manousakis. The spin 1/2 Heisenberg antiferromagnet on a square lattice and its application to the cuprous oxides. *Rev. Mod. Phys.*, 63(1):1, 1991.

- [114] E. Dagotto and T. M. Rice. Surprises on the Way from One- to Two-Dimensional Quantum Magnets: The ladder materials. *Science*, 271:618, 1996.
- [115] E. Dagotto. Experiments on ladders reveal a complex interplay between a spin-gapped normal state and superconductivity. *Rep. Prog. Phys.*, 62:1525, 1999.
- [116] P. Lemmens, G. Güntherodt and C. Gros. Magnetic light scattering in low-dimensional quantum spin system. *Phys. Rep.*, 375:1, 2003.
- [117] K. Kudo, S. Ishikawa, T. Noji, T. Adachi, Y. Koike, K. Maki, S. Tsuji and K. Kumagai. Spin gap and hole pairing of $\text{Sr}_{14-x}\text{A}_x\text{Cu}_{24}\text{O}_{41}$ (A= Ca and La) single crystals studied by the electrical resistivity and thermal conductivity. *J. Low. Temp. Phys.*, 117(5-6):1689, 1999.
- [118] S. Kurogi, K. Kudo, T. Noji, Y. Koike, T. Nishizaki and N. Kobayashi. Antiferromagnetic ordering in the one-dimensional edge-sharing CuO_2 chain system $\text{Ca}_{2+x}\text{Y}_{2-x}\text{Cu}_5\text{O}_{10}$. *J. Low Temp. Phys.*, 131(3-4):353, 2003.
- [119] E. Orignac, R. Chitra and R. Citro. Thermal transport in one-dimensional spin gap systems. *Phys. Rev. B*, 67:134426, 2003.
- [120] R. Jin, Y. Onose, Y. Tokura, D. Mandrus, P. Dai and B. C. Sales. In-Plane Thermal Conductivity of Nd_2CuO_4 : Evidence for Magnon Heat Transport. *Phys. Rev. Lett.*, 91(14):146601, 2003.
- [121] J. C. Bonner and M. E. Fisher. Linear Magnetic Chains with Anisotropic Coupling. *Phys. Rev.*, 135(3A):A640, 1964.
- [122] W. Heisenberg. Zur Theorie des Ferromagnetismus. *Z. Phys.*, 49:619, 1928.
- [123] H. Bethe. Zur Theorie der Metalle. I. Eigenwerte und Eigenfunktionen der linearen Atomkette. *Z. Phys.*, 71:205, 1931.
- [124] S. Sachdev. Quantum Criticality: Competing Ground States in Low Dimensions. *Science*, 288:475, 2000.

- [125] K. Kudo, T. Noji, Y. Koike, T. Nishizaki and N. Kobayashi. Thermal Conductivity of the Two-Dimensional Spin-Gap System $\text{SrCu}_2(\text{BO}_3)_2$ in Magnetic Field. *J. Phys. Soc. Jap.*, 70(6):1448, 2001.
- [126] B. C. Sales, M. D. Lumsden, S. E. Nagler, D. Mandrus and R. Jin. Magnetic Field Enhancement of Heat Transport in the 2D Heisenberg Antiferromagnet $\text{K}_2\text{V}_3\text{O}_8$. *Phys. Rev. Lett.*, 88(9):095901, 2002.
- [127] A. V. Sologubenko, K. Giannò, H. R. Ott, A. Vietkine and A. Revcolevschi. Heat transport by lattice and spin excitation in the spin-chain compounds SrCuO_2 and Sr_2CuO_3 . *Phys. Rev. B*, 64:054412, 2001.
- [128] X. Zotos, F. Naef and P. Prelovšek. Transport and conservation laws. *Phys. Rev. B*, 55(17):11029, 1997.
- [129] X. Zotos. High Temperature Thermal Conductivity of Two-Leg Spin-1/2 Ladders. *Phys. Rev. Lett*, 92(6):067202, 2004.
- [130] C. Hess, C. Baumann, U. Ammerahl, B. Büchner, F. Heidrich-Meisner, W. Brenig and A. Revcolevschi. Magnon heat transport in $(\text{Sr,Ca,La})_{14}\text{Cu}_{24}\text{O}_{41}$. *Phys. Rev. B*, 64:184305, 2001.
- [131] K. Saito, S. Takesue and S. Miyashita. Thermal conduction in a quantum system. *Phys. Rev. E*, 54(3):2404, 1996.
- [132] X. Zotos. Finite Temperature Drude Weight of the One-Dimensional Spin-1/2 Heisenberg Model. *Phys. Rev. Lett*, 82(8):1764, 1999.
- [133] F. Heidrich-Meisner, A. Honecker, D. C. Cabra, and W. Brenig. Thermal conductivity of anisotropic and frustrated spin-1/2 chains. *Phys. Rev. B*, 66:140406(R), 2002.
- [134] Y. Ando, J. Takeya, D. L. Sisson, S. G. Doettinger, I. Tanaka, R. S. Feigelson and A. Kapitulnik. Thermal conductivity of the spin-Peierls compound CuGeO_3 . *Phys. Rev. B*, 58(6):R2913, 1998.

- [135] J. Takeya, I. Tsukada, Y. Ando, T. Masuda, K. Uchinokura, I. Tanaka, R. S. Feigelson and A. Kapitulnik. Thermal conductivity of pure and Mg-doped CuGeO_3 in the incommensurate phase. *Phys. Rev. B*, 63:214407, 2001.
- [136] A. V. Sologubenko, E. Felder, K. Giannò, H. R. Ott, A. Vietkine and A. Revcolevschi. Thermal conductivity and specific heat of the linear chain cuprate Sr_2CuO_3 . Evidence for thermal transport via spinons. *Phys. Rev. B*, 62(10):R6108, 2000.
- [137] K. Kudo, T. Noji, Y. Koike, T. Nishizaki and N. Kobayashi. Thermal conductivity of the four-leg spin-ladder system $\text{La}_2\text{Cu}_2\text{O}_5$ single crystal. *J. Low. Temp. Phys.*, 131(3-4):725, 2003.
- [138] M. Hofmann, T. Lorentz, G. S. Uhrig, H. Kierspel, O. Zabara, A. Freimuth, H. Kageyama and Y. Ueda. Strong Damping of Phononic Heat Current by Magnetic Excitations in $\text{SrCu}_2(\text{BO}_3)_2$. *Phys. Rev. Lett.*, 87(4):047202, 2001.
- [139] J. L. Cohn, C. K. Lowe-Ma and T. A. Vanderah. Anomalous phonon damping and thermal conductivity in insulating cuprates. *Phys. Rev. B*, 52(18):R13134, 1995.
- [140] M. Hofmann, T. Lorentz, K. Berggold, M. Grüninger, A. Freimuth, G. S. Uhrig and E. Brück. Evidence for a large magnetic heat current in insulating cuprates. *cond-mat*, 0301093 v1, 2003.
- [141] C. Hess and B. Büchner. Thermal conductivity of doped La_2CuO_4 as example for heat transport by optical phonons in complex materials. *Eur. Phys. J. B*, 38:37, 2004.
- [142] B. Schmidt, H. Aoki, T. Cichorek, J. Custers, P. Gegenwart, M. Kohgi, M. Lang, C. Langhammer, A. Ochiai, S. Paschen, F. Steglich, T. Suzski, P. Thalmeier, B. Wand, and A. Yaresko. Low-energy excitations of the semimetallic one-dimensional $S = 1/2$ antiferromagnet Yb_4As_3 . *Physica B*, 300:121, 2001.

- [143] K. Iwasa, M. Kohgi, N. Nakajima, R. Yoshitake, Y. Hisazaki, H. Osumi, K. Tajima, N. Wakabayashi, Y. Haga, A. Ochiai, T. Suzuki and A. Uesawa. X-ray diffraction studies of lattice properties in CeX (X = P and As) and Yb₄As₃. *J. Magn. Magn. Mater.*, 177-181:393, 1998.
- [144] M. Kohgi, K. Iwasa, J.-M. Mignot, A. Ochiai and T. Suzuki. One-dimensional antiferromagnetic coupling in the low-carrier heavy-electron system: Yb₄As₃: The role of the charge ordering. *Phys. Rev. B*, 56(18):R11388, 1997.
- [145] P. Bonville, A. Ochiai, T. Suzuki and E. Vincent. Heterogeneous Yb³⁺ - Yb²⁺ mixed valency and unusual Kondo ground state in Yb₄As₃. *J. Phys. I France.*, 4:595, 1994.
- [146] A. Ochiai, T. Suzuki and, T. Kasuya. Heavy Fermion Behavior in Extremely Low Carrier Concentration System Yb₄As₃. *J. Phys. Soc. Jap.*, 59(11):4129, 1990.
- [147] O. Nakamura, N. Tomonaga, A. Ochiai, T. Suzuki and T. Kasuya. Specific heat in a magnetic field for the extremely low carrier system Yb₄As₃. *Physica B*, 171:377, 1991.
- [148] A. Ochiai, H. Aoki, T. Suzuki, R. Helfrich and F. Steglich. Strongly correlated electron system without free carrier Yb₄(As_{1-x}P_x)₃. *Physica B*, 230-232:708, 1997.
- [149] M. Rams, K. Królas, K. Tomala, A. Ochiai and T. Susuki. Charge segregation in Yb₄As₃ observed using ¹⁷²Yb PAC probe. *Hyperfine Interactions*, 97-98:125, 1996.
- [150] M. Kohgi, K. Iwasa, A. Ochiai, T. Suzuki, J.-M. Mignot, B. Gillon, A. Gukasov, J. Schweizer, K. Kakurai, M. Nishi, A. Dönni and T. Osakabe. Charge order and one-dimensional properties of Yb₄As₃. *Physica B*, 230-232:638, 1997.

- [151] K. Iwasa, M. Kohgi, A. Gukasov, J.-M. Mignot, A. Ochiai, H. Aoki and T. Suzuki. Magnetic states of Yb ions in the charge ordered phase of Yb_4As_3 determined by polarized-neutron scattering. *Physica B*, 281&282:460, 2000.
- [152] J. Des Cloizeaux and J. J. Pearson. Spin-Wave Spectrum of the Antiferromagnetic Linear Chain. *Phys. Rev.*, 128(5):2131, 1962.
- [153] H. Aoki, A. Ochiai, T. Susuki, R. Helfrich and F. Steglich. Systematic study in mixed valence system $\text{Yb}_4(\text{As}_{1-x}\text{Sb}_x)_3$. *Physica B*, 230-232:698, 1997.
- [154] R. Pittini, H. Nojiri, M. Motokawa, A. Ochiai and T. Suzuki. Cyclotron resonance experiments in $\text{Yb}_4(\text{As}_{0.6}\text{P}_{0.4})_3$ and $\text{Yb}_4(\text{As}_{0.71}\text{Sb}_{0.29})_3$. *Physica B*, 246-247:452, 1998.
- [155] S. Takagi, S. Furusawa, A. Kobayashi, H. Aoki and A. Ochiai. NMR and NQR studies of $\text{Yb}_4(\text{As}_{1-x}\text{P}_x)_3$. *Physica B*, 281&282:462, 2000.
- [156] M. Kohgi, K. Iwasa, J.-M. Mignot, N. Pyka, A. Ochiai, H. Aoki and T. Suzuki. Magnetic excitations in the charge ordered state of Yb_4As_3 and $\text{Yb}_4(\text{As}_{0.6}\text{P}_{0.4})_3$. *Physica B*, 259-261:269, 1999.
- [157] R. Helfrich, M. Köppen, M. Lang, F. Steglich and A. Ochiai. New observations concerning the low-temperature properties of the carrier-poor heavy-fermion system Yb_4As_3 . *J. Magn. Magn. Mater.*, 177-181:309, 1998.
- [158] B. Schmidt, P. Thalmeier and P. Fulde. Excitations in spin chains and specific-heat anomalies in Yb_4As_3 . *Europhys. Lett.*, 35(2):109, 1996.
- [159] G. Uimin, Y. Kudasov, P. Fulde and A. Ovchinnikov. Low-energy excitations of Yb_4As_3 in a magnetic field. *Eur. Phys. B*, 16:241, 2000.
- [160] M. Oshikawa, K. Ueda, H. Aoki, A. Ochiai and, M. Kohgi. Field-Induced Gap Formation in Yb_4As_3 . *J. Phys. Soc. Jap.*, 68(10):3181, 1999.
- [161] H. Aoki, A. Ochiai, M. Oshikawa and K. Ueda. Magnetic anisotropy in Yb_4As_3 with one-dimensional Yb^{3+} chains. *Physica B*, 281&282:465, 2000.
- [162] H. Shiba, K. Ueda and O. Sakai. Effective Hamiltonian for Charge-Ordered Yb_4As_3 . *J. Phys. Soc. Jpn.*, 69(5):1493, 2000.

- [163] M. Oshikawa and I. Affleck. Field-Induced Gap in $S = 1/2$ Antiferromagnetic Chains. *Phys. Rev. Lett.*, 79(15):2883, 1997.
- [164] I. Affleck and M. Oshikawa. Field-induced gap in Cu benzoate and other $S = 1/2$ antiferromagnetic chains. *Phys. Rev. B*, 60(2):1038, 1999.
- [165] M. Lang, M. Köppen, P. Gegenwart, T. Cichorek, P. Thalmeier, F. Steglich and A. Ochiai. Evidence for magnons and solitons in the one-dimensional $S = 1/2$ antiferromagnet Yb_4As_3 . *Physica B*, 281&282:458, 2000.
- [166] M. Köppen, M. Lang, R. Helfrich, F. Steglich, P. Thalmeier, B Schmidt, B Wand, D. Pankert, H. Benner, H. Aoki and A. Ochiai. Solitary Magnetic Excitations in the Low-Carrier Density One-Dimensional $S = 1/2$ Antiferromagnet Yb_4As_3 . *Phys. Rev. Lett.*, 82:4548, 1999.
- [167] M. Kohgi, K. Iwasa, J.-M. Mignot, B. Fåk, A. Hiess, P. Gegenwart, M. Lang, A. Ochiai, H. Aoki and T. Suzuki. Spin excitations of the one-dimensional $S = 1/2$ Heisenberg antiferromagnet Yb_4As_3 under magnetic field. *Physica B*, 312-313:359, 2002.
- [168] P. Gegenwart, H. Aoki, T. Cichorek, J. Custers, N. Harrison, M. Jaime, M. Lang, A. Ochiai and F. Steglich. Thermodynamic and transport properties of the one-dimensional $S = 1/2$ antiferromagnet Yb_4As_3 . *Physica B*, 312-313:315, 2002.
- [169] J. A. H. M. Buijs and W. J. M. de Jonge. Soliton-phonon scattering in TMMC and DMMC. *J. Phys.C: Solid State Phys.*, 15:6631, 1982.
- [170] C. L. Seaman, M. B. Maple, B. W. Lee, S. Ghamaty, M. Torikachvili, J.-S. Kang, L. Z. Lui, J. W. Allen and D. L. Cox. Evidence for Non-Fermi-Liquid Behavior in the Kondo Alloy $\text{Y}_{1-x}\text{U}_x\text{Pd}_3$. *Phys. Rev. Lett.*, 67(20):2882, 1991.
- [171] P. Coleman, B. Maple and A. Millis. "Institute for theoretical physics conference on non-Fermi liquid behaviour in metals". *J. Phys.:Condens. Matter.*, 8(48):Papers in this number, 1996.

- [172] M. B. Maple, C. L. Seaman, D. A. Gajewski, Y. Dalichaouch, V. B. Barbetta, M. C. de Andrade, H. A. Mook, H. G. Lukefahr, O. O. Bernal, and D. E. MacLaughlin. Non Fermi Liquid Behavior in Strongly Correlated f -Electron Materials. *J. Low Temp. Phys.*, 95(1-2):225, 1994.
- [173] B. Bogenberger and H. v. Löhneysen. Tuning of Non-Fermi-Liquid Behavior with Pressure. *Phys. Rev. Lett.*, 74(6):1016, 1995.
- [174] M. B. Maple, R. P. Dickey, J. Herrmann, M. C. de Andrade, E. J. Freeman, D. A. Gajewski and R. Chau. Single-ion scaling of the low-temperature properties of f -electron materials with non-Fermi-liquid groundstates. *J. Phys.: Condens. Matter.*, 8:9773, 1996.
- [175] K. Heuser, E.-W. Scheidt, T. Schreiner and G. R. Stewart. Inducement of non-Fermi-liquid behaviour with a magnetic field. *Phys. Rev. B*, 57(8):R4198, 1998.
- [176] H. v. Löhneysen. Fermi-liquid instability at magnetic-nonmagnetic quantum phase transitions. *J. Magn. Magn. Mater.*, 200:532, 1999.
- [177] E. Bauer, R. Hauser, A. Galatanu, H. Michor, G. Hilscher, J. Sereni, M. G. Berisso, P. Pedrazzini, M. Galli, F. Marabelli and P. Bonville. Non-Fermi-liquid behaviour of $\text{YbCu}_{5-x}\text{Al}_x$. *Phys. Rev. B*, 60(2):1238, 1999.
- [178] D. Jaccard, K. Behnia and J. Sierro. Pressure induced heavy fermion superconductivity of CeCu_2Ge_2 . *Phys. Lett. A*, 163:475, 1992.
- [179] N. D. Mathur, F. M. Grosche, S. R. Julian, I. R. Walker, D. M. Freye, R. K. W. Haselwimmer and G. G. Lonzarich. Magnetically mediated superconductivity in heavy fermion compounds. *Nature*, 394:39, 1998.
- [180] H. Hegger, C. Petrovic, E. G. Moshopoulou, M. F. Hundley, J. L. Sarrao, Z. Fisk and J. D. Thompson. Pressure-Induced Superconductivity in Quasi-2D CeRhIn_5 . *Phys. Rev. Lett.*, 84(21):4986, 2000.
- [181] H. v. Löhneysen. Non-Fermi-liquid behavior in the heavy-fermion system $\text{CeCu}_{6-x}\text{Au}_x$. *J. Phys.: Condens. Matter*, 8:9689, 1996.

- [182] K. Heuser, E.-W. Scheidt, T. Schreiner and G. R. Stewart. Disappearance of hyperscaling at low temperatures in non-Fermi-liquid $\text{CeCu}_{5.2}\text{Ag}_{0.8}$. *Phys. Rev. B*, 58(24):R15959, 1998.
- [183] B. Andraka and G. R. Stewart. Heavy-non-Fermi-liquid behavior in $\text{U}(\text{Cu},\text{Pd})_5$. *Phys. Rev. B*, 47(6):3208, 1993.
- [184] F. Steglich, P. Gegenwart, R. Helfrich, C. Langhammer, P. Hellmann, L. Donnevert, C. Geibel, M. Lang, G. Sparn, W. Assmus, G. R. Stewart and A. Ochiai. Are heavy-fermion metals Fermi liquids? *Z. Phys. B*, 103:235, 1997.
- [185] F. G. Aliev, H. El Mfarrej, S. Vieira and R. Villar. Anomalous ground state of $\text{U}_{0.9}\text{Th}_{0.1}\text{Be}_{13}$: Temperature dependence of the resistivity and magnetoresistance. *Solid State Commun.*, 91(10):775, 1994.
- [186] C. Sirvent, A. Izquierdo, J. L. Martinez, H. Noël, V. V. Pryadun, F. G. Aliev, R. Villar and S. Vieira. Ground-state crossover in $\text{U}_{1-x}\text{Th}_x\text{Be}_{13}$ ($0 \leq x \leq 0.15$). *J. Phys.: Condens. Matter*, 12:4187, 2000.
- [187] P. Gegenwart, C. Langhammer, R. Helfrich, N. Oeschler, M. Lang, J. S. Kim, G. R. Stewart and F. Steglich. Non-Fermi liquid normal state of the heavy-fermion superconductor UBe_{13} . *Physica C*, 408-410:157, 2004.
- [188] P. Gegenwart, F. Kromer, M. Lang, G. Sparn, C. Geibel and F. Steglich. Non-Fermi-Liquid Effects at Ambient Pressure in a Stoichiometric Heavy-Fermion Compound with Very Low Disorder: CeNi_2Ge_2 . *Phys. Rev. Lett.*, 82(6):1293, 1999.
- [189] P. Gegenwart, P. Hinze, C. Geibel, M. Lang and F. Steglich. Incipient superconductivity and NFL behavior in off-stoichiometric $\text{Ce}_{1+x}\text{Ni}_{2+y}\text{Ge}_{2+z}$ polycrystals. *Physica B*, 281&282:5, 2000.
- [190] T. Fukuhara, S. Akamaru, H. Ito, T. Kuwai, J. Sakurai and K. Maezawa. Magnetism and phase-diagram of $\text{Ce}(\text{Ni}_{1-x}\text{Pd}_x)_2\text{Ge}_2$. *Physica B*, 259-261:81, 1999.

- [191] G. Knebel, M. Brando, J. Hemberger, M. Nicklas, W. Trinkl and A. Loidl. Magnetic, calorimetric, and transport properties of $\text{Ce}(\text{Pd}_{1-x}\text{Ni}_x)_2\text{Ge}_2$ and $\text{CeNi}_2(\text{Ge}_{1-y}\text{Si}_y)_2$. *Phys. Rev. B*, 59(19):12390, 1999.
- [192] T. Fukuhara, H. Kadowaki, N. Aso, T. Takeuchi, T. Kuwai, J. Sakurai and K. Maezawa. Magnetic Structure of $\text{Ce}(\text{Ni}_{1-x}\text{Pd}_x)_2\text{Ge}_2$ Proximate to the Magnetic Instability. *J. Phys. Soc. Jpn.*, 71(5):1360, 2002.
- [193] P. Gegenwart, C. Langhammer, C. Geibel, R. Helfrich, M. Lang, G. Sparn, F. Steglich, R. Horn, L. Donnevert, A. Link and W. Assmus. Breakup of Heavy Fermions on the Brink of “Phase A” in CeCu_2Si_2 . *Phys. Rev. Lett.*, 81(7):1501, 1998.
- [194] M. Gómez Berisso, P. Pedrazzini, M. Deppe, O. Trovarelli, C. Geibel and J. G. Sereni. Composition dependence of the magnetic properties of Ge-doped CeCu_2Si_2 . *Physica B*, 320:380, 2002.
- [195] I. R. Walker, F. M. Grosche, D. M. Freye and G. G. Lonzarich. The Normal and Superconducting States of CeIn_3 Near the Border of Antiferromagnetic Order. *Physica C*, 282-287:303, 1997.
- [196] F. M. Grosche, S. R. Julian, N. D. Mathur, F. V. Carter and G. G. Lonzarich. Quantum-phase transitions in CePd_2Si_2 and CeRh_2Si_2 . *Physica B*, 237-238:197, 1997.
- [197] A. V. Sologubenko, J. Jun, S. M. Kazakov, J. Karpinski and H. R. Ott. Anomalous low-temperature thermal conductivity of MgB_2 . *Physica C*, 388-389:133, 2003.
- [198] R. Bel, K. Behnia, C. Proust, P. v. d. Linden, D. Maude and S. I. Vedeneev. Test of the Wiedemann-Franz Law in an Optimally Doped Cuprate. *Phys. Rev. Lett.*, 92(17):177003, 2004.
- [199] M. Sutherland, D. G. Hawthorn, R. W. Hill, F. Ronning, S. Wakimoto, H. Zhang, C. Proust, E. Boaknin, C. Lupien, L. Taillefer, R. Liang, D. A. Bonn, W. N. Hardy, R. Gagnon, N. E. Hussey, T. Kimura, M. Hohara and H. Takagi. Thermal conductivity across the phase diagram of cuprates:

- Low-energy quasiparticles and doping dependence of the superconducting gap. *Phys. Rev. B*, 67:174520, 2003.
- [200] H. R. Ott, O. Marti and F. Hulliger. Low temperature thermal conductivity of CeAl₃. *Solid State Commun.*, 49(12):1129, 1984.
- [201] D. Jaccard and J. Flouquet. The normal phase of heavy fermion compounds. *J. Magn. Magn. Mater.*, 47&48:45, 1985.
- [202] C. Marcenat, D. Jaccard, J. Sierro, J. Flouquet, Y. Onuki and T. Komatsubahara. Extended Transport Measurements on High-Purity CeB₆. *J. Low Temp. Phys.*, 78(5-6):261, 1990.
- [203] M. Sera, S. Kobayashi, M. Hiroi, N. Kobayashi, H. Ohkuni and Y. Onuki. Thermal conductivity of single-crystalline CeRu₂Si₂. *Phys. Rev. B*, 56(21):13689, 1997.
- [204] Y. Isikawa, F. Taniguchi, Y. Ogiso, T. Mizushima, J. Sakurai and K. Mori. Thermal conductivity and thermoelectric power of dense-Kondo compound CeNi₂Al₅. *Physica B*, 206&207:240, 1995.
- [205] Y. Peysson, B. Salce, C. Ayache and E. Bauer. Thermal conductivity of CeCu₆ and LaCu₆. *J. Magn. Magn. Mater.*, 54-57:423, 1986.
- [206] I. A. Smirnov and V. S. Oskotski. *Thermal conductivity of rare earth compounds in Handbook on the physics and chemistry of rare earths*, volume 16, chapter 106, page 107. Elsevier Science, The Netherlands, 1993.
- [207] S. Kambe, H. Suderow, T. Fukuhara, J. Flouquet, and T. Takimoto. Spin-Fluctuation Mediated Thermal Conductivity Around Magnetic Instability of CeNi₂Ge₂. *J. Low Temp. Phys.*, 117(1/2):101, 1999.
- [208] D. R. Niven and R. Smith. Electron-electron interaction corrections to the thermal conductivity in disordered conductors. *Phys. Rev. B*, 71:035106, 2005.
- [209] R. Raimondi, G. Savona, P. Schwab and T. Lück. Electronic thermal conductivity of disordered metals. *Phys. Rev. B*, 70:155109, 2004.

- [210] E. G. Mishchenko. Nonlinear Voltage Dependence of the Shot Noise in Mesoscopic Degenerate Conductors with Strong Electron-Electron Scattering. *Phys. Rev. Lett.*, 85(19):4144, 2000.
- [211] T. Senthil, S. Sachdev and M. Vojta. Fractionalized Fermi Liquids. *Phys. Rev. Lett.*, 90(21):216403, 2003.
- [212] T. Senthil, M. Vojta and S. Sachdev. Weak magnetism and non-Fermi liquids near heavy-fermion critical points. *Phys. Rev. B*, 69:035111, 2004.
- [213] I. Paul and G. Kotliar. Thermoelectric behavior near the magnetic quantum critical point. *Phys. Rev. B*, 64:184414, 2001.
- [214] J. Benz, C. Pfleiderer, O. Stockert and H. v. Löhneysen. Low-temperature thermal conductivity and thermopower of $\text{CeCu}_{6-x}\text{Au}_x$ near the magnetic quantum phase transition. *Physica B*, 259-261:380, 1999.
- [215] O. Trovarelli, et al. Unpublished.
- [216] J. Custers, P. Gegenwart, H. Wilhelm, K. Neumaier, Y. Tokiwa, O. Trovarelli, C. Geibel, F. Steglich, C. Pépin and P. Coleman. The break-up of heavy electrons at a quantum critical point. *Nature*, 424:524, 2003.
- [217] P. Gegenwart, J. Custers, T. Tamaya, K. Tenya, C. Geibel, O. Trovarelli, F. Steglich and K. Neumaier. Divergence of the heavy quasiparticles mass at the antiferromagnetic quantum critical point in YbRh_2Si_2 . *Acta Physica Polonica B*, 34(2):323, 2003.
- [218] K. Ishida, D. E. MacLaughlin, Ben-Li Young, K. Okamoto, Y. Kawasaki, Y. Kitaoka, G. J. Nieuwenhuys, R. H. Heffner, O. O. Bernal, W. Higemoto, A. Koda, R. Kadono, O. Trovarelli, C. Geibel and F. Steglich. Low-temperature magnetic order and spin dynamics in YbRh_2Si_2 . *Phys. Rev. B*, 68:184401, 2003.
- [219] K. Ishida, K. Okamoto, Y. Kawasaki, Y. Kitaoka, O. Trovarelli, C. Geibel and F. Steglich. YbRh_2Si_2 : Spin Fluctuations in the Vicinity of a Quantum Critical Point at Low Magnetic Field. *Phys. Rev. Lett.*, 89(10):107202, 2002.

- [220] R. KÜchler, F. Weickert, P. Gegenwart, N. Oeschler, J. Ferstl, C. Geibel and F. Steglich. Low-temperature thermal expansion and magnetostriction of $\text{YbRh}_2(\text{Si}_{1-x}\text{Ge}_x)_2$ ($x = 0$ and 0.05). *J. Magn. Magn. Mater.*, 272-276:229, 2004.
- [221] S. Mederle, R. Borth, C. Geibel, F. M. Grosche, G. Sparn, O. Trovarelli, and F. Steglich. An unconventional metallic state in $\text{YbRh}_2(\text{Si}_{1-x}\text{Ge}_x)_2$ – a high pressure study. *J. Phys.: Condens. Matter.*, 14:10731, 2002.
- [222] K. Alami-Yadri, D. Jaccard and D. Andreica . Thermopower of Yb Heavy Fermion Compounds at High Pressure. *J. Low Temp. Phys.*, 114(1-2):135, 1999.
- [223] R. KÜchler, N. Oeschler, P. Gegenwart, T. Cichorek, K. Neumaier, O. Tegus, C. Geibel, J. A. Mydosh, F. Steglich, L. Zhu and Q. Si. Divergence of the Grüneisen Ratio at Quantum Critical Point in Heavy Fermion Metals. *Phys. Rev. Lett.*, 91(6):066405, 2003.
- [224] J. Paglione, M. A. Tanatar, D. G. Hawthorn, R. W. Hill, F. Ronning, M. Sutherland, L. Taillefer, C. Petrovic and P. C. Canfield. Heat Transport as a Probe of Electron Scattering by Spin Fluctuations: the Case of Antiferromagnetic CeRhIn_5 . *Phys. Rev. Lett.*, 94:216602, 2005.
- [225] R. Bel, K. Behnia, Y. Nakajima, K. Izawa, Y. Matsuda, H. Shishido, R. Settai and Y. Onuki. Giant Nernst Effect in CeCoIn_5 . *Phys. Rev. Lett.*, 92(21):217002, 2004.
- [226] W. A. Phillips. Tunneling States in Amorphous Solids. *J. Low Temp. Phys.*, 7(3-4):351, 1972.
- [227] J. L. Black. “Low-Energy Excitations in Metallic Glasses” in *Glassy Metals I*. Springer-Verlag, Berlin Heidelberg, 1981.
- [228] A. Zawadowski. Kondo-like State in a Simple Model for Metallic Glasses. *Phys. Rev. Lett.*, 45(3):211, 1980.

- [229] K. Vladár and A. Zawadowski. Theory of the interaction between electrons and the two-level system in amorphous metals. I. Noncommutative model Hamiltonian and scaling of first order. *Phys. Rev. B*, 28(3):1564, 1983.
- [230] K. Vladár and A. Zawadowski. Theory of the interaction between electrons and the two-level system in amorphous metals. II. Second-order scaling equations. *Phys. Rev. B*, 28(3):1582, 1983.
- [231] K. Vladár and A. Zawadowski. Theory of the interaction between electrons and the two-level system in amorphous metals. III. Experimentally observable quantities. *Phys. Rev. B*, 28(3):1596, 1983.
- [232] P. D. Sacramento and P. Schlottmann. Low-temperature properties of a two-level system interacting with conduction electrons: An application of the overcompensated multichannel Kondo model. *Phys. Rev. B*, 43(16):13294, 1991.
- [233] G. Zaránd, T. Costi, A. Jerez and N. Andrei. Thermodynamics of the anisotropic two-channel Kondo problem. *Phys. Rev. B*, 65:134416, 2002.
- [234] Z. Henkie, T. Cichorek, A. Pietraszko, R. Fabrowski, A. Wojakowski, B. S. Kuzhel, L. Kępiński, L. Krajczyk, A. Gukasov and P. Wiśniewski. On the origin of the impurity Kondo-like resistivity component of UAsSe ferromagnets. *J. Phys. Chem. Solids*, 59(3):385, 1998.
- [235] Z. Henkie, A. Wojakowski, T. Cichorek, R. Wawryk, M. B. Maple, E. D. Bauer and F. Steglich. On evaluation of Kondo-like electron transport characteristics of TLS-Kondo ferromagnets; uranium pnictochalcogenides. *Physica C*, 387:113, 2003.
- [236] T. Cichorek, R. Wawryk, A. Wojakowski, Z. Henkie and F. Steglich. Non-magnetic Kondo-like scattering in UPS and UAsSe ferromagnets. *Acta Physica Polonica B*, 34(2):1339, 2003.
- [237] Z. Henkie, R. Fabrowski and A. Wojakowski. Anisotropies of the electrical resistivity and Hall effect in UAsSe. *J. Alloys Comp.*, 219:248, 1995.

- [238] T. Cichorek, Z. Henkie, P. Gegenwart, M. Lang, A. Wojakowski, M. Dischner and F. Steglich. A non-magnetic Kondo effect in UAsSe ferromagnet? *J. Magn. Magn. Mater.*, 226-230:189, 2001.
- [239] Z. Henkie, R. Wawryk, A. Wojakowski, A. Pietraszko, T. Cichorek and F. Steglich. Transport properties of $UX_{1-x}Y_{1+x}$ ($X = P, As, Sb$; $Y = S, Se, Te$) ferromagnet: Is there an analogy between the nonmagnetic Kondo-like system and the classical heavy fermion one? *Acta Physica Polonica B*, 34(2):1323, 2003.
- [240] R. C. Zeller and R. O. Pohl. Thermal Conductivity and Specific Heat of Noncrystalline Solids. *Phys. Rev. B*, 4(6):2029, 1971.
- [241] R. B. Stephens. Low-Temperature Specific Heat and Thermal Conductivity of Noncrystalline Dielectric Solids. *Phys. Rev. B*, 8(6):2896, 1973.
- [242] M. W. Klein. Density of states for interacting tunneling units in the absence of long-range order. *Phys. Rev. B*, 29(10):5825, 1984.
- [243] F. J. Walker and A. C. Anderson. Low-energy excitations in yttria-stabilized zirconia. *Phys. Rev. B*, 29(10):5881, 1984.
- [244] T. Cichorek, H. Aoki, J. Custers, P. Gegenwart, F. Steglich, Z. Henkie, E. D. Bauer and M. B. Maple. ThAsSe diamagnet: Evidence for a Kondo effect derived from structural two-level systems. *Phys. Rev. B*, 68:144411, 2003.
- [245] T. Cichorek, Z. Henkie, J. Custers, P. Gegenwart and F. Steglich. TLS Kondo effect in structurally disordered ThAsSe. *J. Magn. Magn. Mater.*, 272-276:66, 2004.
- [246] J. Schoenes, W. Bacsa and F. Hulliger. Anomalous transport properties of UAsSe and ThAsSe single crystals. *Solid State Commun.*, 68(3):287, 1988.
- [247] T. Cichorek, A. Sanchez, P. Gegenwart, F. Weickert, A. Wojakowski, Z. Henkie, G. Auffermann, S. Paschen, R. Knip and F. Steglich. Two-Channel Kondo Effect in Glass-Like ThAsSe. *Phys. Rev. Lett.*, 94:236603, 2005.

- [248] S. Paschen. “*Thermoelectric aspects of strongly correlated electron systems*” in *Thermoelectrics Handbook: Macro to Nano-Structured materials*. CRC Press, Boca Raton, Book in preparation.
- [249] G. A. Slack. *CRC Handbook of Thermoelectrics*, chapter 34. edited by D.M. Rowe, Chemical Rubber, Boca Raton, FL, 1995.
- [250] V. L. Kuznetsov, L. A. Kuznetsova, A. E. Kaliazin and D. M. Rowe. Preparation and thermoelectric properties of $A_8^{II}B_{16}^{III}B_{30}^{IV}$ clathrate compounds. *J. Appl. Phys.*, 87(11):7871, 2000.
- [251] S. E. Lattner, J. D. Bryan, N. Blake, H. Metiu, and G. D. Stucky. Siting of Antimony Dopants and Gallium in $Ba_8Ga_{16}Ge_{30}$ Clathrates. *Inorg. Chem.*, 41:3956, 2002.
- [252] A. Bentien, M. Christensen, J. D. Bryan, A. Sanchez, S. Paschen, F. Steglich, G. D. Stucky and B. B. Iversen. Thermal conductivity of thermoelectric clathrates. *Phys. Rev. B*, 69:045107, 2004.
- [253] G. S. Nolas, T. J. R. Weakley, J. L. Cohn, and R. Sharma. Structural properties and thermal conductivity of crystalline Ge clathrates. *Phys. Rev. B*, 61(6):3845, 2000.
- [254] S. Paschen, W. Carrillo-Cabrera, A. Bentien, V.H. Tran, M. Baenitz, Yu. Grin, and F. Steglich. Structural, transport, magnetic, and thermal properties of $Eu_8Ga_{16}Ge_{30}$. *Phys. Rev. B*, 64:214404, 2001.
- [255] J. S. Tse, K. Uehara, R. Rousseau, A. Ker, C. I Ratcliffe, M. A. White and G. MacKay. Structural Principles and Amorphouslike Thermal Conductivity of Na-doped Si Clathrates. *Phys. Rev. Lett.*, 85(1):114, 2000.
- [256] G. S. Nolas, B. C. Chakoumakos, B. Mahieu, G. J. Long and T. J. R. Weakley. Structural Characterization and Thermal Conductivity of Type-I Tin Clathrates. *Chem. Mater.*, 12:1947, 2000.
- [257] G. S. Nolas, J. L. Cohn, J. S. Dyck, C. Uher and J. Yang. Transport properties of polycrystalline type-I Sn clathrates. *Phys. Rev. B*, 65:165201, 2002.

- [258] A. Bentien. *Transport and magnetic properties of rare-earth containing clathrates and clathrate-like compounds*. PhD thesis, TU Dresden, Germany, 2004.
- [259] B. C. Sales, B. C. Chakoumakos, R. Jin, J. R. Thompson and D. Mandrus. Structural, magnetic, thermal, and transport properties of $X_8\text{Ga}_{16}\text{Ge}_{30}$ ($X = \text{Eu}, \text{Sr}, \text{Ba}$) single crystals. *Phys. Rev. B*, 63:245113, 2001.
- [260] C. R. Crosby and C. G. Grenier. Thermal Conductivity of Heavily Doped p -Type InSb at Liquid-Helium Temperatures. *Phys. Rev. B*, 4(4):1258, 1971.

List of symbols

| Symbol | Definition |
|-----------|------------------------------------------|
| a, b, c | Lattice parameters |
| A | Cross section |
| B | Magnetic field |
| c_e | Heat capacity per electron |
| C | Specific heat |
| C_e | Electronic heat capacity per unit volume |
| C_m | Magnetic heat capacity |
| C_{ph} | Phonon specific heat |
| e | Electron charge |
| E_{def} | Deformation potential |
| E_F | Fermi energy |
| f_0 | Fermi Dirac distribution |
| F_0^a | Antisymmetric Landau parameter |
| \hbar | Plank constant divide by 2π |
| H | Magnetic field |
| I | Electrical current |
| J | Magnetic coupling |
| \vec{k} | Wave vector |
| k_B | Boltzmann constant |
| k_F | Fermi wave number |

| | |
|--------------------|------------------------------------------------------------------------------|
| l_e | Electronic mean free path |
| l_m | Magnon mean free path |
| l_{ph} | Phonon mean free path |
| $l_{ph-Casimir}$ | Phonon mean free path for the boundary scattering |
| l_{ph-e} | Phonon mean free path for the phonon charge scattering |
| L | Distance |
| L | Electron mean free path with respect to the quasistatic potential scattering |
| L_0 | Lorentz number |
| m_e | Electron mass |
| m_0 | Free electron mass |
| m^* | Effective mass |
| n | Charge carrier concentration |
| N | Number of atoms per unit cell |
| $N(E_F)$ | Density of states at the Fermi energy |
| $N(\varepsilon)$ | Density of states |
| $P(z)$ | Cutoff function |
| q | Phonon wave number |
| q_{dom} | Dominant phonon wave number |
| \dot{Q} | Heat rate |
| \vec{r} | Position |
| R | Resistance |
| R_H | Hall coefficient |
| \vec{s}, \vec{S} | Spin |
| S | Thermopower |
| S_d | Diffusion thermopower |
| t | Time |
| T | Temperature |

| | |
|-------------------------|----------------------------------------------------------------------------|
| T_c | Critical temperature of a superconductor |
| T_K | Kondo temperature |
| T_N | Néel temperature |
| T_{RKKY} | Characteristic temperature of the RKKY interaction |
| $1/T_1$ | Spin-lattice relaxation time |
| $v(\varepsilon)$ | Group velocity |
| v_e | Mean velocity of the electrons |
| v_F | Fermi velocity |
| v_m | Magnon velocity |
| v_{ph} | Mean phonon velocity |
| V | Electrical potential |
| W_e | Thermal resistivity |
| γ | Electronic specific heat coefficient |
| ΔT | Difference of temperature |
| ΔV_{th} | Thermal voltage |
| ε | Energy |
| θ_D | Debye temperature |
| κ | Thermal conductivity |
| κ_e | Electronic thermal conductivity |
| κ_e^{WF} | Electronic thermal conductivity estimated using the Wiedemann-Franz law |
| κ_m | Magnon thermal conductivity |
| κ_{ph} | Phonon thermal conductivity |
| $\kappa_{ph}^{Casimir}$ | Phonon thermal conductivity due to boundary scattering |
| μ | Chemical potential |
| μ_B | Bohr magneton |
| μ_H | Hall mobility |

| | |
|-----------------------|---------------------------------|
| μ_0 | Induction constant in vacuum |
| ν_{dom} | Dominant phonon frequency |
| ξ | Correlation length |
| ϕ | Diameter |
| ρ | Electrical resistivity |
| ρ_m | Mass density |
| ρ_0 | Residual resistivity |
| σ | Electrical conductivity |
| $\Sigma(\varepsilon)$ | Transport distribution function |
| τ | Correlation time |
| τ_{ph} | Phonon relaxation time |
| $\tau(\varepsilon)$ | lifetime |
| χ | Magnetic susceptibility |

Acknowledgements

First of all, I would like to express my sincere gratitude to Professor Frank Steglich for invaluable suggestions and help.

I am indebted to Dr. Silke Paschen for her support and for valuable discussions. Her suggestions and comments have helped me in the development of this thesis.

A very special thanks to Professor Joachim Wosnitza who allowed me to work in his lab and to use his dilution refrigerator at the Technical University Dresden during one year. I am grateful to Dr. Manfred Jäckel and Dr. Bernd Kluge for teaching me how to use of the dilution refrigerator and for having so much patience during my work at the TU.

I would like to thank Professor Ana Celia Mota and Dr. Christoph Geibel for their interest in my work, for the encouragement they have given me and for the fruitful discussions we have had.

I am very thankful to Dr. Phillip Gegenwart and the low-temperature group for accepting me in their group meetings. I have learned a lot of physics and about low-temperature techniques with them. Especially, I wish to thank Dr. Thomas Lühmann for his infinite patience, his invaluable advice and help during my work at the institute.

I also give a special thanks to Gabriel Dionicio for the resistivity measurements on YbRh_2Si_2 . I am grateful to Dr. Raul Cardoso for helping me to understand the crystal structures of some of the compounds studied in this thesis.

I would like to thank Professor John Mydosh, Professor Akira Ochiai, Dr Octavio Trovarelli, Dr. Zygmunt Henkie, Dr. Andrzej Wojakowski and Dr. B. Iversen for providing me interesting samples.

A special acknowledgment is made to Professor Ana Celia Mota, Dr. Silke

Paschen, Dr. Michael Baenitz, Dr. Oliver Stocker, Dr. Tomasz Cichorek, Gabriel Dionicio, Matthias Dischner and Enrique Kaul for their reading on sections or all of my thesis, for their stimulating discussions and for their valuable comments on the thesis.

Special thanks goes to Mr. Robert Borth, Mrs. Heike Rave, Mrs. Nubia Caroca Canales, Mr. Andreas Schwoboda and the people of the mechanics workshop, as well as to the people of the electronic workshop. Their technical support was important for many experiments.

The administration of our institute, particularly Mrs Petra Nowak, Mrs. Uta Prautzsch, Mrs. Carmen Kratochwil, Mrs. Katarina Klein, Mrs. Katrin Demian and Mrs. Claudia Strohbach are thanked for their kindness and for making things work out.

I am also grateful to the PhD students at the institute for their warm friendship. Especially, I would like to thank to my roommates Anders, Vladimir and Jan for the nice chats and continuous support during my PhD.

I am very thankful to my family (mi mami, Patricia, Margarita, Danilo, Nicolas y los mellizos) and friends in Colombia, as well as to Liliana in USA, Diana and my brother Pedrito in Spain and Saadia in Germany for the constant emails and calls which make my life very happy.

I wish to give my thanks to my friends who I have met in Dresden, Julia, Gabriel, Juan Diego, Javier, Edward, and many others for making my life more interesting.

Special thanks to Matthias for his infinite patience and for his invaluable help, understanding and support during the difficult moments of my PhD work.

To all who in some way or another have helped to realize this thesis thank you very much.

Finally, I acknowledge the scholarship from the Max Planck Society.

List of publications

- S. Paschen, V. Pacheco, A. Bentien, A. Sanchez, W. Carrillo-Cabrera, M. Baenitz, B. B. Iversen, Y. Grin, F. Steglich;
Are type-I clathrates Zintl phases and 'phonon glasses and electron single crystals' ?
Physica B, **328**, 39-43 (2003)
- A. Bentien, M. Christensen, J. D. Bryan, A. Sanchez, S. Paschen , F. Steglich, G. D. Stucky, B. B. Iversen;
Thermal conductivity of thermoelectric clathrates.
Phys. Rev. B **69**, 45107-1-5 (2004)
- A. Sanchez, S. Paschen, B. Wand, H. Aoki, A. Ochiai and F. Steglich;
Thermal conductivity of the one-dimensional $S = 1/2$ antiferromagnet $\text{Yb}_4(\text{As}_{1-x}\text{P}_x)_3$ ($x = 0$ and 0.3).
J. Magn. Magn. Mater. **272-276**, E703-E705 (2004)
- A. Sanchez, S. Paschen, J. Wosnitza, J. A. Mydosh, A. M. Strydom, P. de V. du Plessis and F. Steglich;
Thermal transport properties of $\text{U}_2\text{Ru}_2\text{Sn}$ at low temperatures.
Physica B **359-361**, 1015-1017 (2005)
- T. Cichorek, A. Sanchez, P. Gegenwart, F. Weickert, A. Wojakowski, Z. Henkie, G. Auffermann, S. Paschen, R. Kniep and F. Steglich
Two-channel Kondo effect in glass-like ThAsSe .
Phys. Rev. Lett. **94**, 236603-1-4 (2005)

Author's declaration

I declare that the work in this dissertation was carried out in accordance with the regulations of the Technische Universität Dresden. No part of this work has been submitted previously for a degree or other qualification at this or any other university. The research reported herein is original, except where specific reference is acknowledged to the work of others. All the research was carried out under the supervision of Prof. Frank Steglich and Dr. Silke Paschen in Max-Planck-Institute for Chemical Physics of Solids between September 2000 to February 2005.

Adriana Mercedes Sánchez Lotero
Dresden, Germany

Versicherung

Hiermit versichere ich, dass ich die vorliegende Arbeit ohne unzulässige Hilfe Dritter und ohne Benutzung anderer als der angegebenen Hilfsmittel angefertigt habe; die aus fremden Quellen direkt oder indirekt übernommenen Gedanken sind als solche kenntlich gemacht. Die Arbeit wurde bisher weder im Inland noch im Ausland in gleicher oder ähnlicher Form einer anderen Prüfungsbehörde vorgelegt.

Die vorliegende Dissertation wurde unter der Betreuung von Prof. Dr. Frank Steglich und Frau Dr. Silke Paschen am Max-Planck-Institut für Chemische Physik fester Stoffe in Dresden angefertigt. Ich erkenne die Promotionsordnung an.

Adriana Mercedes Sánchez Lotero
Dresden, Germany